REPLICATION OF GEOMEMBRANE INTERFACES USING 3D PRINTING (FUSED DEPOSITION MODELLING) TECHNIQUE

A THESIS SUBMITTED TO
THE GRADUATE SCHOOL OF NATURAL AND APPLIED SCIENCES
OF
MIDDLE EAST TECHNICAL UNIVERSITY

BY

SEMKAN URAGAN

IN PARTIAL FULFILLMENT OF THE REQUIREMENTS
FOR
THE DEGREE OF MASTER OF SCIENCE
IN
CIVIL ENGINEERING

DECEMBER 2020

Approval of the thesis:

REPLICATION OF GEOMEMBRANE INTERFACES USING 3D PRINTING (FUSED DEPOSITION MODELLING) TECHNIQUE

submitted by **SEMKAN URAGAN** in partial fulfillment of the requirements for the degree of **Master of Science** i**n Civil Engineering, Middle East Technical University** by,

Prof. Dr. Halil Kalıpçılar
Dean, Graduate School of **Natural and Applied Sciences** _____

Prof. Dr. Ahmet Türer
Head of the Department, **Civil Engineering** _____

Assoc. Prof. Dr. Nejan Huvaj Sarıhan
Supervisor, **Civil Engineering, METU** _____

Examining Committee Members:

Assoc. Prof. Dr. Nabi Kartal Toker
Civil Engineering, METU _____

Assoc. Prof. Dr. Nejan Huvaj Sarıhan
Civil Engineering, METU _____

Prof. Dr. Berna Unutmaz
Civil Engineering, Hacettepe University _____

Prof. Dr. Bahadır Sadık Bakır
Civil Engineering., METU _____

Prof. Dr. Zeynep Gülerce
Civil Engineering, METU _____

Date: 22.12.2020

I hereby declare that all information in this document has been obtained and presented in accordance with academic rules and ethical conduct. I also declare that, as required by these rules and conduct, I have fully cited and referenced all material and results that are not original to this work.

Name, Last name : Semkan, Uragan

Signature :

ABSTRACT

REPLICATION OF GEOMEMBRANE INTERFACES USING 3D PRINTING (FUSED DEPOSITION MODELLING) TECHNIQUE

Uragan, Semkan
Master of Science, Civil Engineering
Supervisor: Assoc. Prof. Dr. Nejan Huvaj Sarıhan

December 2020, 106 pages

Geomembrane – soil interface is a critical consideration in geotechnical engineering applications such as liners and covers in landfills, canals or mine tailing dams. In some cases, lack of sufficient shear strength in these interfaces leads to poor performance, uneconomical design (such as requiring a longer geomembrane in an anchor trench), or may even lead to failure. To eliminate such problems, geometrical features known as asperities (or protrusions) are used on the geomembrane's interfacing faces. These asperities improve the interface shear strength by providing a surface that rakes through the soil rather than slipping. Research involving the optimization of these asperities requires rapid manufacturing of variety of these prototype geomembranes used as samples for interface shear tests. In this study, commercially available HDPE geomembrane samples are compared to 3D printed geomembrane samples in terms of their tensile strength and interface shear characteristics.

Firstly, Polypropylene (PP) is selected among other thermoplastics namely PLA, ABS and re-PETG to replicate High Density Poly Ethylene (HDPE) using the data obtained from tensile strength tests. Three soil samples are prepared (containing 0%, 12% and 40% fines content) using Çine sand and non-plastic silt and the index properties for these soil samples are determined. Finally, using the selected prototyping material PP, 3D printed geomembrane samples are compared to HDPE geomembrane samples in interface with these soil samples under 20, 100, and 200

kPa vertical pressures using 60 x 60 mm direct shear tests. Seventy-two direct shear tests are conducted for geomembrane-soil interface shear strength using three different soil mixtures, where each soil sample is prepared at two different densities (loose and dense condition). To simplify the comparison of the similarity between HDPE and FDM-manufactures PP specimens, three comparison indexes are calculated, namely, Asperity Similarity (AS), Smooth Similarity (SS), and Improvement Similarity (IS). As a result of these tests, while FDM-manufactures PP showed promising and comparable results in replication of HDPE samples for all soil mixtures interfaced with geomembranes with asperities, some amount of deviation is observed in soil mixture A, which consists only of sub-angular Çine sand, interfaced with smooth PP geomembrane especially under higher normal loads. This deviation is attributed to the elevated effect of the raking mechanism provided by sub-angular sand coupled with the rougher surface profile that is a known characteristic defect of FDM manufactured parts. Finally, the use of FDM technique in optimization of geomembrane interfaces was recommended and discussed.

Keywords: Geomembrane, 3D Printing, Interface Shear Strength, Direct Shear, Asperity Optimization, Fused Deposition Modelling

ÖZ

GEOMEMBRAN ARAYÜZLERİNİN 3B YAZMA (ERİYİK YIĞMA MODELLEMESİ TEKNİĞİ) KULLANILARAK REPLİKASYONU

Uragan, Semkan
Yüksek Lisans, İnşaat Mühendisliği
Tez Yöneticisi: Doç. Dr. Nejan Huvaj Sarıhan

Aralık 2020, 106 sayfa

Katı atık veya maden atıkları depolama sahalarında taban veya örtü kaplaması gibi çeşitli geoteknik mühendisliği uygulamalarında geomembran - zemin arayüzü oldukça önemli bir tasarım faktörü olarak önümüze çıkmaktadır. Bazı örneklerde, bu arayüzlerdeki kesme mukavemetinin yetersizliği nedeniyle kötü performans, ekonomik olmayan tasarım (geomembranı bir hendek içine sabitlemek için daha uzun membran gerekmesi gibi) veya kimi zaman yenilmeler görülmektedir. Bu yenilme davranışına karşı, çıkıntı (veya pürüz) olarak bilinen geometrik değişiklikler zemin - geomembran arayüzlerinde uygulanmaktadır. Bu çıkıntılar arayüz kesme mukavemetini kayma yerine kazıma özelliği gösteren bir yüzey sağlayarak arttırmaktadır. Bu çıkıntıların geometrik optimizasyonu üzerine yapılan çalışmalar için hızlı prototipleme yöntemlerine gerek duyulmaktadır. Bu çalışmada, piyasada bulunan HDPE geomembran örnekleri 3D yazıcılardan üretilmiş örnekler ile çekme dayanımı ve yüzey sürtünme özellikleri açısından karşılaştırılmıştır. İlk olarak, HDPE, PP, PLA, ABS ve re-PETG malzemeleri üzerinde yapılan çekme deneyleri ile prototiplenecek malzeme Polipropilen (PP) olarak belirlenmiştir. 3 tip zemin örneği, artan ince dane yüzdesi göz önünde bulunarak, Çine kumu ve plastik olmayan silt kullanılarak hazırlanmış ve zemin özellikleri belirlenmiştir. Son olarak, seçilen prototipleme malzemesi PP kullanılarak üretilen geomembran örnekleri HDPE

geomembran örnekleri ile belirtilen zemin örnekleri ile, 20, 100 ve 200 kPa'lık düşey yük altında 60 x 60 mm direk kesme kutusunu deneyleri ile karşılaştırılmıştır. Yetmiş iki adet geomembran – zemin arayüzüde direkt kesme kutusu deneyi planlanmış, bu deneylerde üç farklı zemin tipi(%0, %12 ve %40 ince dane yüzdesi) gevşek ve sıkı koşullarda olmak üzere piyasadan temin edilen HDPE ve FDM tekniği ile üretilmiş PP geomembran numuneleri ile karşılaştırılmıştır. Bu karşılaştırmayı kolaylaştırmak adına üç adet karşılaştırma indisi, Çıkıntı Benzerliği (AS), Düz Yüzey Benzerliği (SS) ve Güçlendirme Benzerliği (IS) hesaplanmıştır. Bu deneyler sonucunda HDPE ve PP numuneler zemin A dışında oldukça yüksek benzerlik göstermiştir. Yalnızca yuvarlak köşeli danecik yapısına sahip kum içeren zemin A numunelerinde ise bir miktar sapma, özellikle düz yüzeyli numunelerde ve yüksek normal yük altında gözlemlenmiştir. Bu sapma danecik yapısına bağlı olarak artan kazıma etkisine ve FDM tekniğinin karakteristik hatası olan daha yüksek yüzey pürüzlülüğünün etkisine bağlandığı düşünülmektedir. Son olarak, bu tekniğin geomembran arayüzlerinin geliştirilmesinde kullanılması önerilmiş ve tartışılmıştır.

Anahtar Kelimeler: Geomembran, 3B Yazıcı, Arayüz Sürtünme Dayanımı, Direkt Kesme, Çıkıntı Optimizasyonu, Eriyik Yığma Modellemesi

Dedicated to the loving memory of my father, Seyit Uragan.

ACKNOWLEDGMENTS

I wish to express my profound and deepest gratitude for my supervisor Assoc. Prof. Dr. Nejan Huvaj Sarıhan for her invaluable guidance, support, criticism and consultancy throughout my graduate studies.

I like to thank Assoc. Prof. Dr. Nabi Kartal Toker for his treasured guidance and comments.

I would like to thank all my co-workers and professors at METU Design Factory, Müge Kruşa Yemişcioğlu, Gizem Yetiş, Murat Akın, Asst. Prof. Dr. Arsev Umur Aydınoğlu, Dr. Barış Yazıcı, Dr. Serkan Alkan, Dr. Arda Bülben Yazıcı, Prof. Dr. İlhan Konukseven and Prof. Dr. Arzu Gönenç Sorguç for their endless support, invaluable mentorship and kindness.

I also would like to thank all the staff members and fellows of METU Geotechnical Engineering Laboratory including Kamber Bilgen, Ulaş Nacar, Berkan Söylemez, Melih Kenanoğlu, Anıl Ekici, Can Şimşek, Arda Yazıcı, Emre Duman and Yılmaz Emre Sarıçiçek for their personal and professional help and support throughout my studies.

I would like to thank Geoplas for providing the HDPE geomembrane specimens.

Lastly, I would like to thank my friends and family that never abstained from supporting me my whole life. Mürvet Uragan, Venüs Uragan, Habibe Mutlu, Kıymet Mutlu, Merve Tuncay, Soner Ünsal, Ege Soydemir, Hakan Güneş, Özgün Şen, Türker Şengöz and Ömercan Yılmaz. I express my sincerest gratitude towards their efforts.

TABLE OF CONTENTS

LIST OF TABLES

TABLES

LIST OF FIGURES

FIGURES

LIST OF ABBREVIATIONS

ABBREVIATIONS

ABS: Acrylonitrile Butadiene Styrene

AM: Additive Manufacturing

AS: Asperity Similarity

CGI: Course Grained Interface

CNC: Computer Numerical Control

FC: Fines Content

FCI: Filament-Continuum Interface

FDM: Fused Deposition Modelling

FESEM: Field Emission Scanning Electron Microscope

FGI: Fine Grained Interface

HDPE: High Density Polyethylene

IR: Improvement Ratio

IS: Improvement Similarity

LDPE: Low Density Polyethylene

MJP: Multi-Jet Printing

PA: Polyamide

PLA:Polyactic Acid

PP: Polypropylene

PVC: Polyvinyl Chloride

re-PETG: Recycled Polyethlene Terephthalate Glycol

SLA: Stereolithography

SLS: Selective Laser Sintering

SMP: Silyl Modified Polymer

SS: Smooth Similarity

UV: Ultraviolet

LIST OF SYMBOLS

SYMBOLS

R_n : Normalized Roughness

$R_{max(L= D_{50})}$: Absolute vertical distance between highest and lowest points along a profile distance specified as the D_{50} of the soil.

D_{50}: The particle size that cumulative 50% of the particles in the sample by mass is greater or lesser than.

E: Efficiency

δ: Interface Friction Angle

Φ: Internal Friction Angle

τ_u : Ultimate Shear Strength, Peak Shear Strength

σ_n : Normal Stress

G_S: Specific Gravity

R^2: Coefficient of Determination

E_0: Initial Modulus of Elasticity, calculated as a secant modulus at %1 strain.

σ_y: Tensile Yield Strenght

ε_y: Elongation at Yield

CHAPTER 1

INTRODUCTION

Geosynthetics are one of the critical materials in geotechnical engineering field. They exhibit essential functions such as drainage, filtration, containment, reinforcement, and separation. Far superior ability to perform these functions compared to more traditional solutions led the geosynthetic industry in a 10% growth per year since the first installment of geosynthetic products back in the 1970s. Geosynthetics are being manufactured in factories by massive amounts using thermoplastic polymeric materials (Koerner, 2005) such as HDPE (High-Density Poly Ethylene), LDPE (Low-Density Polyethylene), PP (Polypropylene), and PVC (Polyvinyl Chloride), among others.

The aforementioned growth of the geosynthetic industry has driven research to develop novel uses and types of geosynthetics. While some of those include mixing polymers with other materials such as bentonite clay to create impermeable barriers named geocomposites, some novel geosynthetics was born out of optimizing or developing new materials and geometrical design approaches. Many examples show how the development of novel geosynthetics affects the geotechnical engineering field in various ways, such as strength, function, reliability, and efficiency. On the other hand, while mass production and alteration of chemical properties of the polymers used in the geosynthetics industry are well known, prototyping and testing of new ideas related to these novel geosynthetics lack mainly because of manufacturing setbacks. Huge production lines prove to be costly and not-feasible to alter for a small-batched R&D production run.

Geosynthetic interfaces with soil and other geosynthetics is a field that is of paramount importance in geotechnical engineering. Some examples of applications evaluate the interface friction of geomembranes with soil and with geotextiles when used as part of a liner system for a landfill or mine waste storage facility (Figure 1b). Poor interface shear strength properties may lead to failure or unsatisfactory performance in terms of sliding of geosynthetics on a slope, or pull-out type failure of a geomembrane out of an anchor trench (Figure 1.1(a)), or unacceptable amount of deformations.

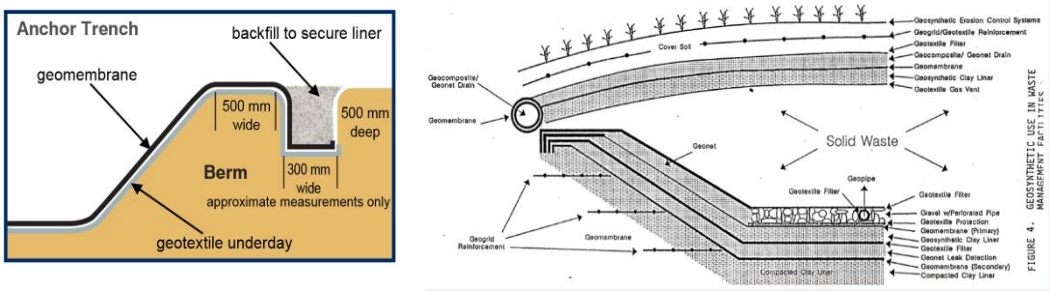

Figure 1.1- Cross-sections of :(a) anchor trench ; (b) landfill or mine waste storage.

Images downloaded from *https://poolblanket.wordpress.com/2015/03/13/dam-liners-installing-them-yourself/* and *http://www.sdobor.com/Rough-Geomembrane.html* respectively.

To enhance interface shear strength properties, especially in geomembranes, different geometric features are used on the geomembrane's surface to produce roughened / textured surfaces having more friction compared to a smooth surface. These features are called asperities (or protrusions) and can be found mainly in two forms in commercially available HDPE geomembranes. One is a thin layer of rough texture formed on the smooth geomembrane. The others are geometrical features pressed on while manufacturing the geomembrane, as seen in Figures 1.2(a) and 1.2(b). In geogrids, the use of surface asperities is not a common practice simply because granular fill is utilized; therefore, interlocking action becomes much more dominant for the mobilization of surface friction.

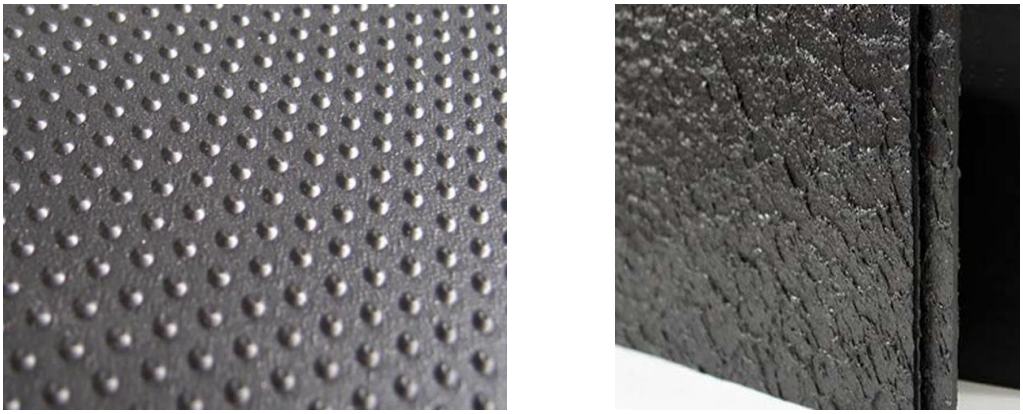

Figure 1.2 - : (a) Point-textured geomembrane ; (b) Rough textured geomembrane.

Images downloaded from *https://dzhongxiang.en.made-in-china.com/product/nvMxytFPgQYK/China-HDPE-Point-Textured-Geomembrane-for-Landfill.html* and *http://www.sdobor.com/Rough-Geomembrane.html* respectively.

Additionally, scaled model tests involving geosynthetics prove costly and challenging due to the necessity of massive centrifuge equipment and requirements resulting from the scaling laws. These scaling laws for these model tests dictate that geometrical and mechanical properties of the model geosynthetics must be scaled accordingly (Viswanadham & König, 2004), as seen in Table 1.1. The scaling requirements for the model tests are generally not met, or partially met, simply because of the difficulties regarding manufacturing the model with the required mechanical and geometrical properties.

Table 1.1. - Scaling factors used in model tests (Viswanadham & König, 2004)

Parameters	Scale factors	
	$1g$ model	Ng model
Geosynthetic strain ε_g (%)	1	1
Length a, b, t (m)[a]	$1/N$	$1/N$
Displacement δ (mm)	$1/N$	$1/N$
Cross-section area of rib A (m^2)[b]	$1/N^2$	$1/N^{2c}$
Cross-section area of rib/unit length A' (m)[b]	$1/N$	$1/N$
Tensile strength T_g (kN/m)	$1/N^2$	$1/N^c$
Secant modulus J_g (kN/m)	$1/N^2$	$1/N$
Pull-out force P (kN)	$1/N^3$	$1/N^2$
Bond stress τ_b (kN/m^2)	$1/N$	1
Soil–geosynthetic friction angle ϕ_{sg} (deg)	1	1

[a] a, b, t: Geometric dimensions in longitudinal and transverse directions for geogrid and in the case of geogrid t thickness of rib or thickness of geotextile (see Fig. 2).
[b] Not valid for geotextiles.
[c] $A_m/A_p = 1/N^2$; $(T_g)_m/(T_g)_p = 1/N$.

Additive manufacturing (commonly referred to by the public as `3D printing`) is a trending method used in scientific and industrial development cycles utilizing the aforementioned small batched R&D production runs. Developed and patented in the 1980's by Charles W. Hull (Hull, 1984), Stereolithography (SLA) and Fused Deposition Modeling (FDM) methods were the pioneers of the additive manufacturing field. Additive manufacturing is a manufacturing methodology that mainly operates by depositing desired materials on top of each other layer by layer. Various additive manufacturing methods have been developed and continue to be developed, allowing users to rapidly and precisely manufacture parts using materials ranging from thermoplastic and thermoset polymers, composites, ceramics, metals, and organic materials. Manufacturing of parts with challenging geometries is also possible using additive manufacturing methods.

1.1 Problem Statement

Challenges involved in the geotechnical engineering field require more optimized novel geosynthetics to be developed. One of these challenges is the improvement of the efficiency of geosynthetic interfaces. Efficiency, in terms of interface shear strength, is defined as the ratio of the tangents of the interface friction angle to the soil's internal friction angle. A geosynthetic interface's efficiency varies greatly with parameters such as soil type, gradation, grain topography, angularity, geosynthetic type and geometry, and arrangement (density) of asperities used in textured geosynthetics as seen in Table 1.2. However, optimization of geomembrane texturing asperities that targets higher efficiency values for a broad range of soils is required for critical applications. The development of novel geosynthetics requires prototyping and testing, as described previously. While traditional manufacturing methods of these geosynthetics could not provide the required flexibility, speed, and accuracy to successfully prototype and test, additive manufacturing methods prove to be useful regarding these requirements. Additive manufacturing is a method that is used widely across fields involving research, production, and even among hobbyists. Applications of additive manufacturing in the geotechnical engineering field are blooming and promising, yet a limited number of researchers contributed to this subject. Additionally, most of the laboratory tests in the geotechnical engineering field require special supporting equipment to be manufactured according to the test equipment's particular needs, specimen type, and testing conditions such as tampers, fixtures, and soil distribution tools. Therefore, studying interaction mechanisms, especially concerning interface properties between additive manufactured parts and soil particles of different types, prove to be beneficial for future researchers.

Table 1.2. Soil to Geomembrane Friction Angle Values of Various Interfaces (Koerner, 2005)

(a) Soil-to-Geomembrane Friction Angles

Geomembrane	Soil type					
	Concrete Sand ($\phi = 30°$)		Ottawa Sand ($\phi = 28°$)		Mica Schist Sand ($\phi = 26°$)	
HDPE						
Textured	30°	(100%)	26°	(92%)	22°	(83%)
Smooth	18°	(56%)	18°	(61%)	17°	(63%)
PVC						
Rough	27°	(88%)	—	—	25°	(96%)
Smooth	25°	(81%)	—	—	21°	(79%)
CSPE-R	25°	(81%)	21°	(72%)	23°	(87%)

1.2 Research Objectives

This study's main objective is to test and discuss the usability of the Fused Deposition Modelling (FDM) additive manufacturing technique in the optimization of interface shear strength properties of geomembrane – soil interfaces. A geomembrane interface with soil will be considered in this study. Soil type with varying densities and fines content values are considered factors/variables. Three different laboratory-mixed sand samples with increasing silt percentages are interfaced with prototype and commercially available HDPE geomembranes. The prototype geomembranes are manufactured using an additive manufacturing called Fused Deposition Modelling (FDM). Commercially available HDPE geomembranes are supplied from the industry and cut using a laser cutter. A detailed comparison of FDM manufactured geomembrane samples and commercially available HDPE geomembranes are made in terms of shear response using 60mm x 60mm direct shear test setup, in order to asses the afformentioned usability of FDM method. Other objectives are;

1. Contribution to the future researchers that will use additively manufactured parts and tools and require data in terms of interface properties with different soil types. This study also aims to compare the tensile strength

characteristics of thermoplastics that are commonly used in geosynthetics literature to thermoplastics generally used in FDM manufacturing.

2. Conduct a brief literature review on the use cases of additive manufacturing in geotechnical engineering research.
3. Discuss the similarity and usability of geomembrane specimens manufactured using Fused Deposition Modelling (FDM) techniques for future research involving geomembrane asperity geometry optimization for different soils.
4. Discuss the usability and limitations of the Fused Deposition Modelling (FDM) method in geotechnical engineering and geosynthetics-related research.

1.3 Scope

The investigation area and the scope for this study are to evaluate, test, and compare the surface asperity geometries in geomembranes by using the Fused Deposition Modelling (FDM) additive manufacturing technique. In Chapter 2, a brief literature review is presented on the relevant topics. In Chapter 3, the methodology and the materials that were used to conduct the research are detailed. In Chapter 4, the results of the conducted tests are presented, and these results are discussed in detail. In Chapter 5, the study is concluded with further discussions.

CHAPTER 2

LITERATURE REVIEW

In this chapter, a literature review on the topics within the scope of this study is presented. Firstly, a brief overview of geosynthetics and novel geosynthetics, followed by studies on soil-geosynthetic interfaces, are detailed. Afterward, additive manufacturing methodology is reviewed concisely within the scope of this study, followed by a review detailing the studies on the literature about the applications of this methodology in geotechnical engineering.

2.1 Geosynthetics & Novel Geosynthetics

Geosynthetics, defined by ASTM D4439 (ASTM International, 2018), are planar products manufactured from polymeric materials used in geotechnical engineering applications. These geosynthetic products mainly provide essential functions such as drainage, reinforcement, separation, filtration, and containment. That being said, by looking at the definition of geosynthetics alone, it can be seen that geosynthetic products are not limited to these functions and bare the potential for novelty. Manufacturing of these geosynthetics is made in controlled factories that produce vast amounts of geosynthetic products. This mass production provides reduced costs while maintaining standardized material quality and reliability. The reliability of geosynthetic products is ensured using well-developed testing methodologies specified in ISO, EN, ASTM, and other national standards. There are around 159 standards in the context of geosynthetics in the American Society for Testing and Materials (ASTM) as of 2020 (ASTM International, 2020a). Followed by this elaborate testing methodology, geosynthetics are mainly produced using polymer

products that can be re-shaped using heat, known as thermoplastics. A variety of thermoplastics as listed in Table 2.1 are used in the geosynthetics industry for different applications, frequently coupled with additives and stabilizers such as carbon black for UV resistance in geomembranes (Shukla, 2012). It is no coincidence that development and growth in the geosynthetics industry coincide with widespread usage of these thermoplastic polymers after the second world war during the 1950's (Gilbert, 2017). After this period, the earliest known academic paper on geosynthetics is published by Agerschou in 1961 (Agerschou, 1961), followed by an increasing interest that led to the first geosynthetics conference held in Paris in 1977. Afterward, the establishment of the International Geosynthetics Society in 1983 ensured that geosynthetics and polymer materials are materials of paramount importance in geotechnical engineering.

Table 2.1 - Various types of polymers used in the geosynthetic industry (Shukla, 2012)

Geosynthetics	Raw materials
Geotextiles	PP, PET, PA, PE
Geogrids	PET, PP, HDPE
Geonets	MDPE, HDPE
Geomembranes	HDPE, LLDPE, VLDPE, PVC, CPE, CSPE, PP
Geofoams	EPS, XPS
Geopipes	HDPE, PVC, PP

Today, geosynthetic products are being used throughout the globe and reached US$5 billion in annual sales (Blond et al., 2019). In 2018 global plastics production almost reached 360 million tonnes according to research by PlasticsEurope Institution (*Plastics – the Facts 2019*, 2019). While the geosynthetic industry feeds off this global supply surplus in terms of manufacturing cost, the accumulation of waste plastics throughout the globe dictates better and sustainable usage of these materials. The recycling schemes for these polymers are well understood and widely applied within other industries. Unfortunately, the use of recycled polymers within the geosynthetics industry remains limited due to concerns about inhomogeneity in

material properties of the geosynthetic products made of recycled polymers and possible service life limits. On the other hand, developing more efficient and durable geosynthetics is well within the scope of geosynthetic research in literature, leading to a reduction of plastic waste generated by the geosynthetic industry.

The aforementioned efficiency in the use of geosynthetics is made possible with novel geosynthetics developed. There are currently nine different geosynthetic classifications recognized by the International Geosynthetics Society (IGS). These are geotextiles, geogrids, geonets, geomembranes, geocomposites, geosynthetic clay liners, geopipes, geocells, and geofoams. Each one of the listed geosynthetics serves unique function/functions within the scope of geotechnical engineering. These classifications can also be sub-divided to different types under the same branch based on geometrical features, manufacturing material, and manufacturing method. Novel geosynthetic research aims to broaden these classifications. One of the latest examples of this novel geosynthetics is patented under TENSAR Co. in 2017 (Shelton & Tyagi, 2017), as seen in Figure 2.1. By optimizing the planar geometry of the conventional geogrids and inventing a new approach in the manufacturing method, inventors of this patent achieved a more efficient geosynthetic in terms of strength and stiffness.

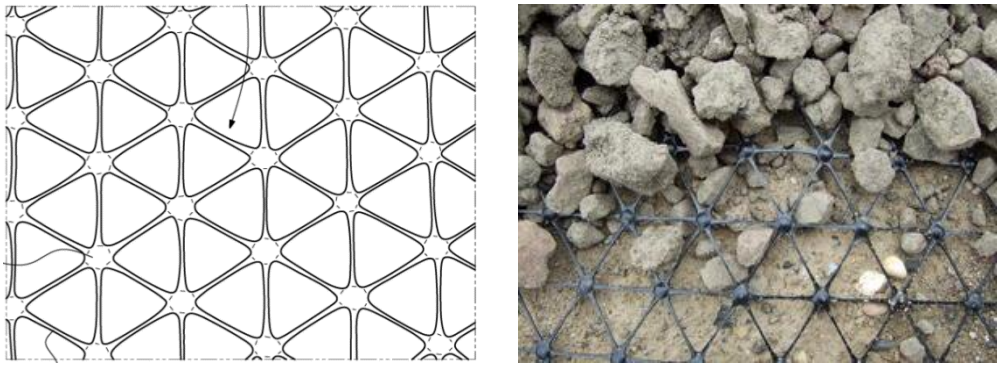

Figure 2.1 - Triaxial HDPE geogrid developed by TENSAR Co.

Another example is known as electrokinetic geosynthetics, patented in 1998 by J.F. Colin Jones and Colin Robert Pugh (J. F. C. Jones & Pugh, 1998). This geosynthetic applies the electrokinetic phenomena by using electrically conductive geosynthetics as electrodes in cohesive soil to force drainage of water through electro-osmosis. While dissipation of water in cohesive soils using electro-osmosis is applied in the field before the electrically conductive geosynthetics, this novel geosynthetic provided a material that is not prone to corrosion, unlike its former counterparts. The application of this novel geosynthetic in water, food, mining, civil engineering, and sports industries is now well-understood, and some examples are shown in Figure 2.2 (C. Jones et al., 2017).

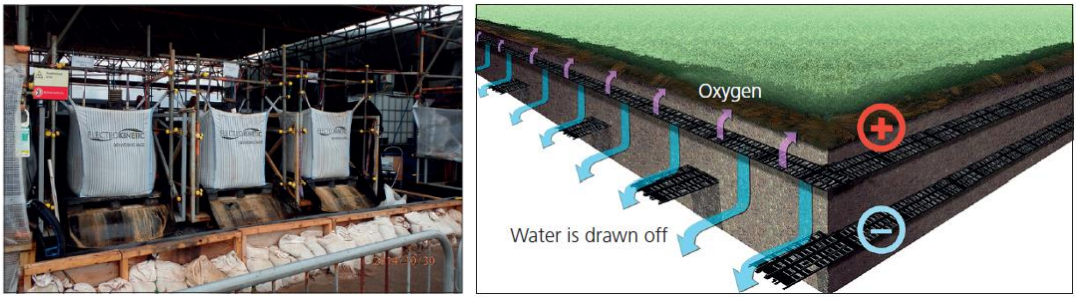

Figure 2.2 - Example pictures utilizing electrokinetic geosynthetics : (a) A dewatering bag ; (b) Drainage control on a sports turf (C. Jones et al., 2017)

2.2 Soil-Geosynthetic Interfaces

The interface behavior of geosynthetics is a critical consideration and field of study within geotechnical engineering. All main functions of geosynthetics namely, drainage, reinforcement, separation, filtration, and containment, are directly related to physical or chemical interface mechanisms with the neighboring media of the geosynthetic and therefore must be carefully studied according to the needs of any engineering project (Gregory L Hebeler, 2005)(K. et al., 1990). Within the scope of

this study, the physical interfacing mechanism of geosynthetics is considered. This physical interfacing can then be further sub-divided into interlocking and friction behavior of the interface. Identifying the main contributing physical interfacing mechanism of the interface is critical consideration since any effort to optimize or improve the properties of that interface depends on this identification. For example, while the main contributing physical interfacing mechanism between a geogrid and a coarse-grained soil is interlocking, the main contributor for an interface between a smooth geomembrane and a non-cohesive soil would be surface-related friction. This friction behavior of continuous interfacing surfaces is principally studied under the field called tribology. In geotechnical engineering applications, granular media is interfaced with continuous surfaces such as geosynthetics. In the current literature, geomaterials interfacing with common materials regarding geotechnical engineering applications are divided into three main categories. These are coarse-grained interfaces (CGI), such as sands and gravels, fine-grained interfaces (FGI), such as silts, clays, and organic materials, and finally, filament-continuum interfaces (FCI), such as geotextiles and geonets. A detailed summary of prominent factors influencing the behavior of these interface types are collected and reported by Hebeler in 2005 and can be seen in Table 2.2 (Gregory L Hebeler, 2005).

In the study by Dove & Frost (Dove & Frost, 1999), the CGI type interface's internal mechanisms are investigated on a single and multiple grain scale. Researchers further discuss the interface friction mechanisms of geomembranes and sand particles by referring to tribology studies performed by other researchers, most notably (Briscoe, 1992). The main contributors to this mechanism are defined as adhesion (also described as sliding) and plowing, as seen in Figure 2.3.

.

Table 2.2 - A summary of prominent factors influencing the behavior of interface types CGI, FGI and FCI (Gregory L Hebeler, 2005)

Factors and Properties Affecting Particulate - Continuum Interface Behavior

Type	Factor	CGI Significance		FGI Significance		FCI Significance		Remarks
		Peak	Residual	Peak	Residual	Peak	Residual	
Particulate	Macro Shape	H	H	H	H	L	M	Angularity / Length / Eccentricity
	Micro Shape	L	L	L	L	L	L	e.g. Particle Roughness
	Cementation / Diagenesis / Calendering	M	L	M	L	L	M	Any strengthening of inter particulate bonds
	Density \ Void Ratio	M	L	M	L	M	L	
	Initial structure	L	L	M	L	L	L	Homogeniety of particulate structure (Floc / Disp)
	Mean particle size (D_{50})	H	H	M	M	H	M	Specific surface for Fine Grained material…
	Mineral / Chemical composition	H	H	H	H	L	M	
	Uniformity coefficient (Cu)	L	M	L	L	---	---	*At this time all geotechnical fabrics have Cu = 1
	Stress History	M/L	M/L	H	H	M	L	OCR, etc.
	Strain History	M/L	M/L	H	M	H	M	
	Plasticity	---	---	H	H	---	---	
	Individual particle strength	H	H	L	L	M	H	Effect of particle crushing / tearing
	Water content / Degree of Saturation	L	L	H	H	L	L	
Continuum	Surface hardness	H	H	L	L	M	H	
	Micro surface roughness	H	H	H	H	H	H	On the order of Rmax < 30 mm
	Macro surface roughness	H	H	M	M	H	H	On the order of Rmax > 100 mm
	Texture Geometry / Manufacturing Process	M	M	L	L	H	H	Directionality and Shape of Textural Asperities
Boundary Conditions	Normal stress	H	H	H	H	H	H	Influence on behavior and τ not just δ
	Current State of Stress	M	M	M	M	M	M	
	Strain Rate	L	L	M	M	L	L	Velocity of Shear
	Drainage	L	L	M	M	L	L	
	Test Geometry	M	M	M	M	M	M	Direct, Simple, Ring, Axisymmetric modes
	Confinement Condition / Media	M	H	M	H	M	M	Physical boundary condition, e.g. CNS vs. CNL
	1-way cycling	H	M	H	M	M	L	Cycling without crossing zero stress
	2-way cycling	H	H	H	M	H	M	Cycling crossing the stress axis

* All catergories are described for ideal properties (e.g. Particulate mixtures of coarse and fine grained materials are not considered)
* CGI - Coarse Grained Interface; FGI - Fine Grained Interface; FCI - Filament Continuum Interface
* FCI - An interface consisting of a needle punched nonwoven geotextile is representative of a geotechnical filament material.

L - Likely to have limited effect on interface behavior
M - Likely to have some effect on interface behavior
H - Likely to have a dominant effect on interface behavior

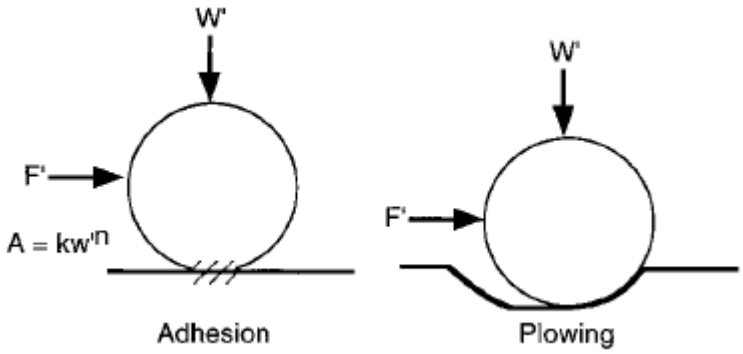

Figure 2.3 – Main contributing factors in interface friction mechanics according to Briscoe (Briscoe, 1992)(Dove & Frost, 1999)

In their study, Dove & Frost states that for a smooth HDPE – dense Ottawa 20/30 sand (relative density ranging between 74-82%) interface, the adhesion component of the interfacing mechanism dominates between a normal load range up to 50 kPa. The deformations during this phase of the shearing are stated to be elastic, and no scarring of the counterface is observed. Increasing the normal load further than 50 kPa leads to grain penetration, and plowing starts to influence the interface mechanism. Plowing occurs as a result of plastic shear deformations on the counterface caused by the local yielding of the polymer. The peak secant friction coefficient – normal stress plot visualizing this behavior can be seen in Figure 2.4. This transition between the governing mechanisms is closely related to the surface hardness, particle geometry, and particle contact area (which is a function of particle properties and relative density of the soil).

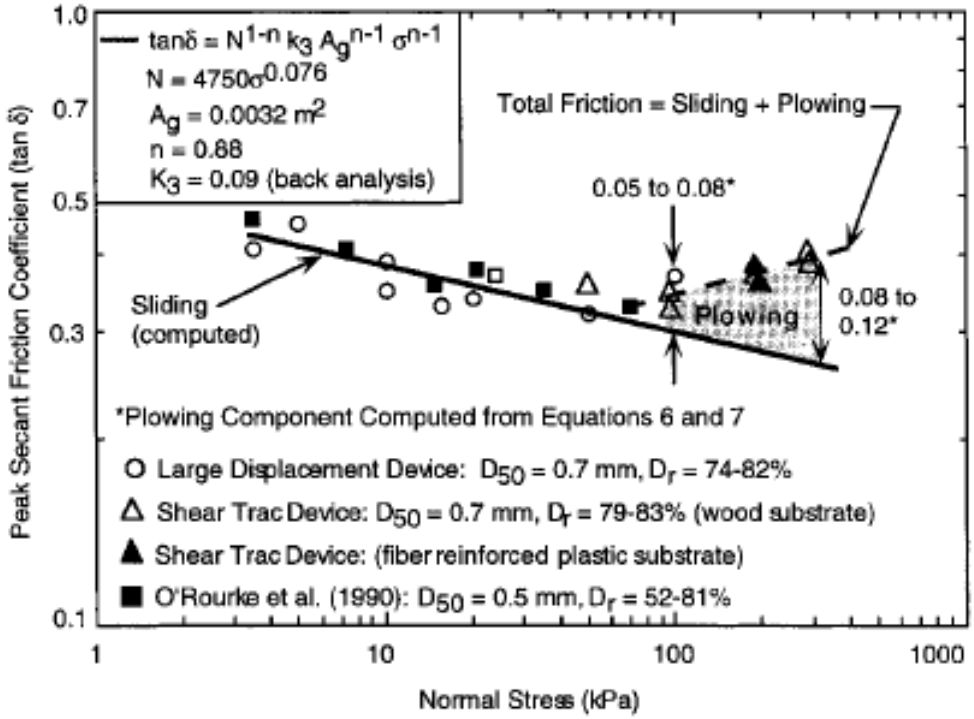

Figure 2.4 - Interfacing mechanism between smooth HDPE geomembrane - dense Ottawa 20/30 sand interface (Dove & Frost, 1999)

The effect of particle geometry is further studied by Zettler et al. (Zettler et al., 2000). 4 different types of sand with different particle angularities (glass beads, Ottowa sand 20/30, Ottawa sand 50/70, and blasting sand) are sheared against smooth HDPE geomembrane specimens using a circular direct shear device under 25, 50, 100, 300 and 500 kPa normal pressures. Surface roughness measurements were conducted using a surface profilometer before and after the tests. It is shown in Figure 2.5 that under the same normal stress value, particles with higher angularities cause more deformations on the geomembrane surface; thus plowing mechanism is utilized even more, especially for blasting sand, which has the highest particle angularity among all other particles tested in this study. Figure 2.7 clearly shows the effect of particle angularity as it compares peak interface shear strength values of conducted direct shear tests, as the increase in normal stress results in a dramatic increase in peak interface shear strength for particles with higher angularities, namely Ottawa sands and blasting sand.

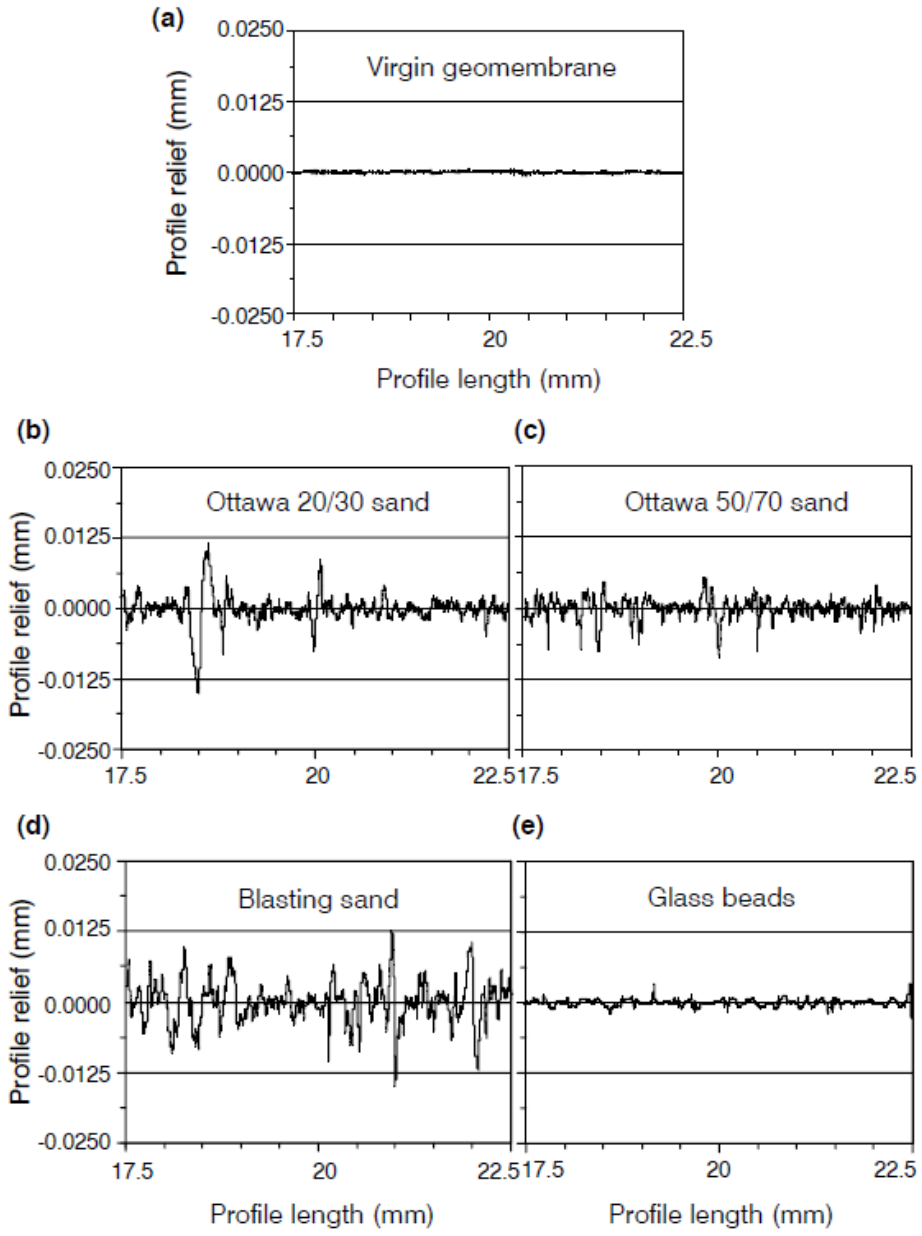

Figure 2.5 - Smooth HDPE surface profilometer results under 500 kPa normal load for : (a) virgin geomembrane; (b) after shearing with Ottawa 20/30 sand; (c) Ottawa 50/70 sand; (d) blasting sand; (e) glass beads. (Zettler et al., 2000)

The plowing caused by sand particles interfacing with an HDPE geomembrane can be seen in the images captured by a Field Emission Scanning Electron Microscope (FESEM) used in the study conducted by Punetha et al. (Punetha et al., 2017) in Figure 2.6.

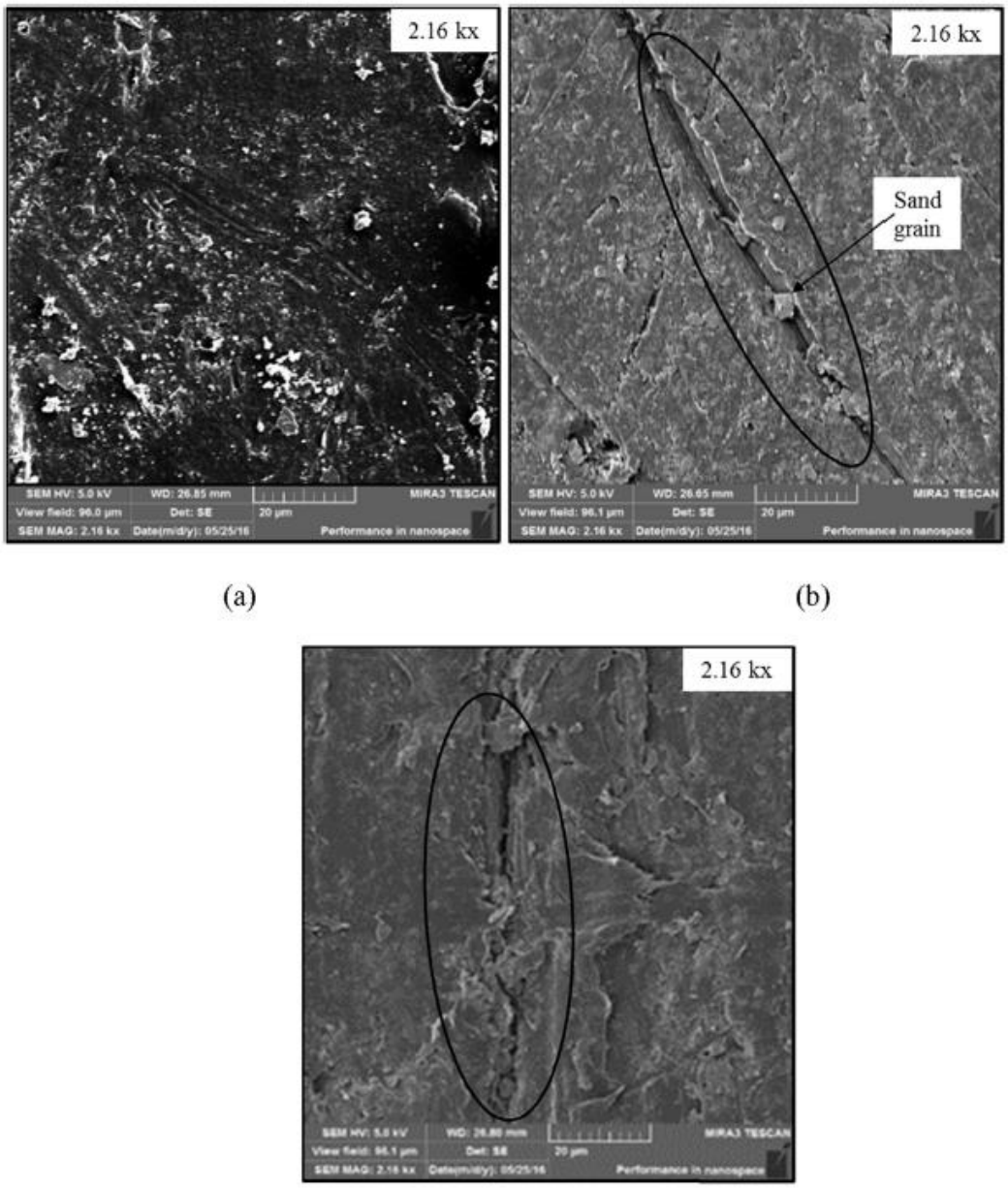

Figure 2.6 - FESEM images captured of an HDPE geomembrane after direct shear box tests interfacing with sand under: (a) 50 kPa; (b) 100 kPa and; (c) 150 kPa normal stress

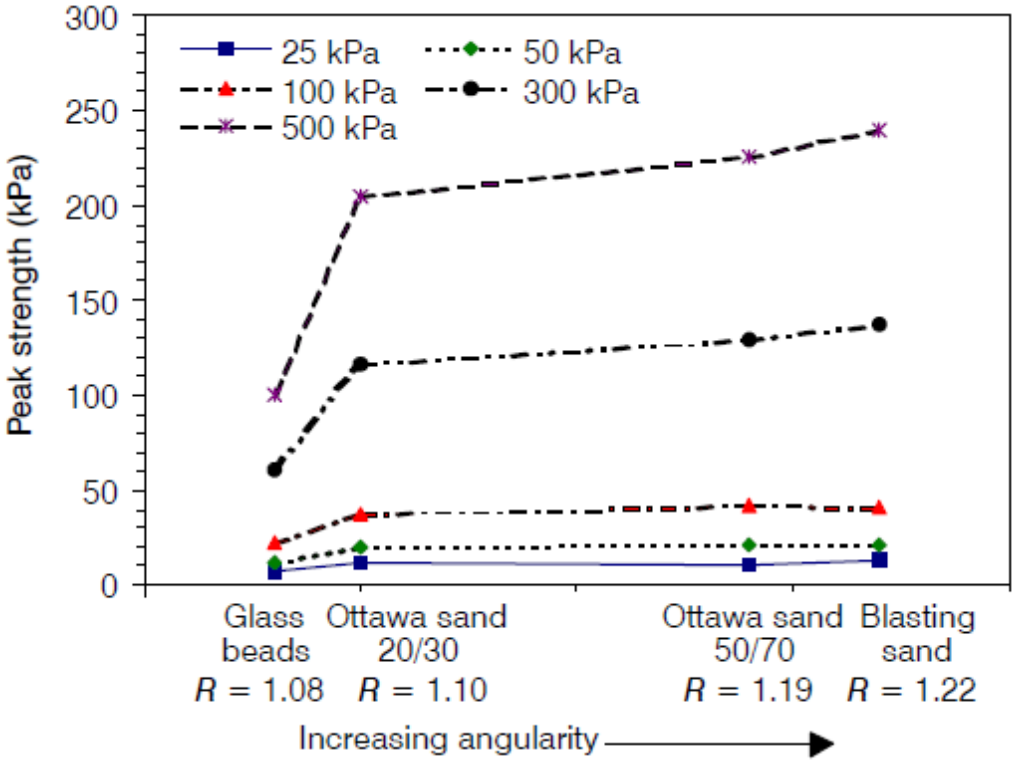

Figure 2.7 - Effect of particle angularity on peak interface shear strength in HDPE geomembrane - particle interfaces under different normal loads. (Zettler et al., 2000)

The other critical parameter that is crucial in interface shear strength of CGI type interfaces is the surface roughness of the counterface. The relationship between the coefficient of friction and normalized roughness for sand-steel interfaces is, as seen in Figure 2.7 is stated by Uesugi & Kishida in 1986 (Uesugi & Kishida, 1986). Normalized roughness is defined by the researchers as,

$$R_n = {R_{max(L=D_{50})}}/{D_{50}} \tag{2.1}$$

Where, R_n is the normalized roughness of the interface, $R_{max(L=D_{50})}$ is the absolute vertical distance between highest and lowest points along a profile distance specified as the D_{50} of the soil.

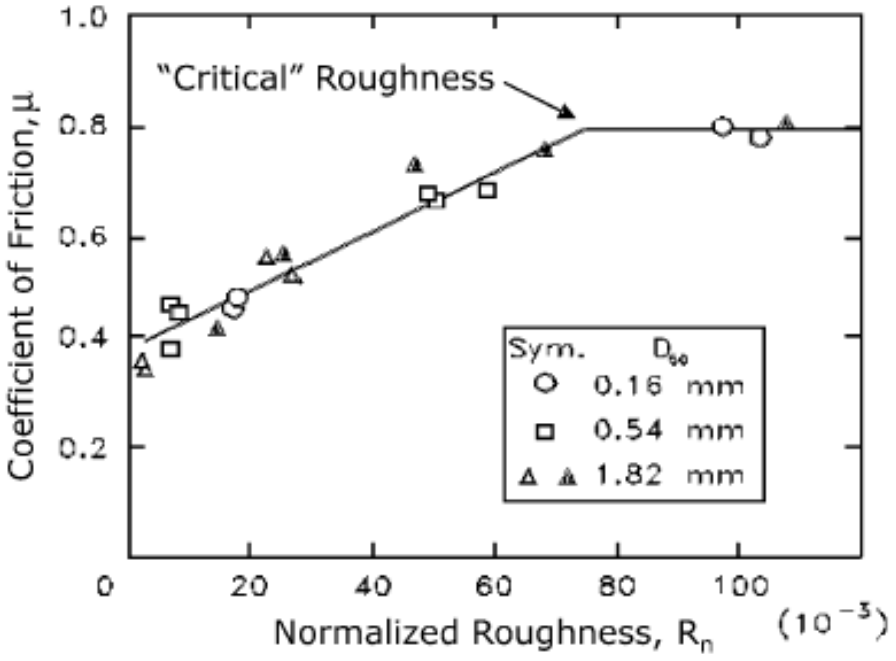

Figure 2.8 - Normalized interface roughness versus coefficient of friction relationship (Uesugi & Kishida, 1986).

The relationship shown in Figure 2.8 dictates a bilinear relationship between these two values for surfaces where plowing cannot occur because of the interfacing material of the counterface. The coefficient of friction increases as the normalized roughness of the interface increases under the same normal load until a critical roughness state is reached, and no improvement on the coefficient of friction is seen after that value.

The coupled effect of counterface hardness and roughness is investigated in further research by Frost, DeJong & Recalde (Frost et al., 2002). Researchers conducted direct shear tests using Ottawa 20/30 sand and counterface materials with varying hardness and roughness values, as shown in the three-dimensional plot shown in Figure 2.9

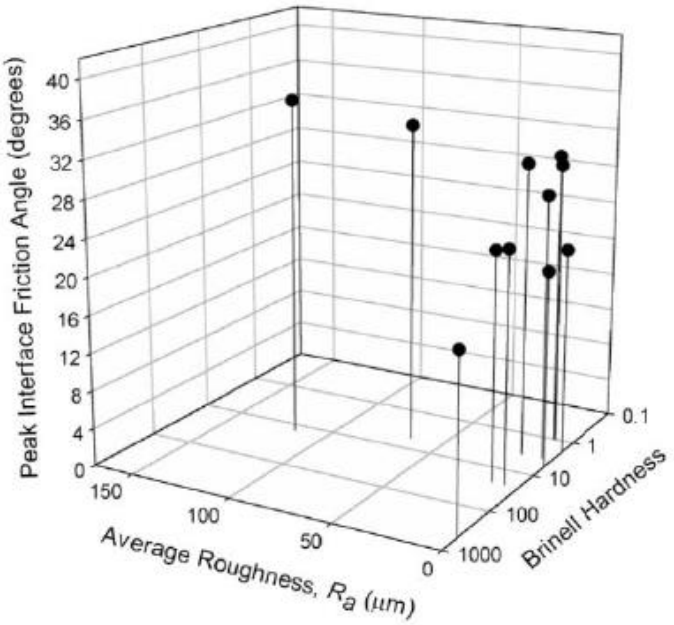

Figure 2.9 - Coupled effect of counterface roughness and hardness using Ottawa 20/30 sand

For the interface shear strength of fine-grained particles, properties such as water content, plasticity, stress history, and rate of shearing become important factors affecting the performance of the interface.

Interface research involving silty sands and geomembranes in the literature (Fleming et al., 2006)(Zabielska-Adamska, 2006) concluded that an increase in placement water content for silty sand mixtures results in a reduction of the plowing component of the interfacing mechanism as shown in the data obtained from surface profilometry in Figure 2.10. The reduction in the mobilization of the plowing mechanism leads to a decrease in interface shear strength and efficiency, especially in higher normal load values. Efficiency, as defined by the geotechnical engineering literature (R M Koerner et al., 1986), is:

$$E = {tan\delta}/{tan\Phi} \tag{2.2}$$

Where, E is the efficiency, δ, and Φ are the interface friction angle between soil and geosynthetic and internal friction angle of the soil, respectively.

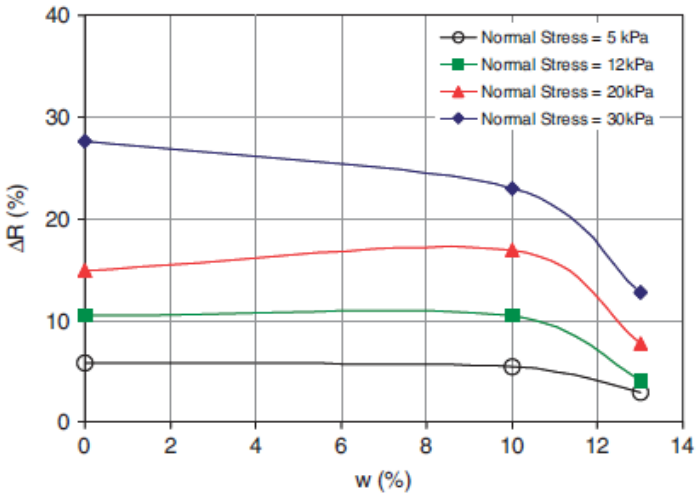

Figure 2.10 - Water content effect on the post-shear surface roughness silty sand - smooth HDPE geomembrane interfaces obtained by surface profilometry (Fleming et al., 2006).

In a more recent study by Markou et al. (Markou & Evangelou, 2018), the efficiency values for seven different types of geomembranes versus two sands with varying particle angularities and a silty-clayey cohesive soil is investigated using a 100 x 100 mm direct shear box. The efficiency values obtained from tests with sands are seen in Figure 2.11. By looking at these values, it can be seen that with a surface texturing of 0.25 mm, only a %10 increase in efficiency for an HDPE geomembrane – sand interface is achieved.

By reviewing the current literature on soil – geomembrane interfaces, it is evident that for interfaces where the plowing mechanism could not be as effective as other material types due to material hardness such as HDPE, increase efficiency for that interface type can be achieved through optimized surface texturing. While some research is conducted in the literature on optimizing steel surfaces interfacing with soils (Feligha et al., 2016; Punetha et al., 2017) and on quantifying hook-type asperities for geotextile interfaces (G L Hebeler et al., 2005), future research in this subject remains promising.

Table 2.3 - Friction coefficient and efficiency values obtained from direct shear tests on different geomembrane-sand interfaces (Markou & Evangelou, 2018).

Geomembrane	Rounded sand		Sub-angular sand	
	tanδ	E_{φ} (%)	tanδ	E_{φ} (%)
PVC+PET	0.596	82.1	0.865	80.7
PVC	0.535	73.7	0.833	77.7
EPDM	0.562	77.4	0.926	86.4
TPO/FPA	0.495	68.2	0.669	62.4
VLDPE	0.430	59.2	0.665	62.0
HDPE-S	0.305	42.0	0.636	59.3
HDPE-T	0.479	66.0	0.744	69.4

A new approach to the optimization of geosynthetic interface optimization was led by Fowmes et al. in their subsequent studies in 2016 and 2017 (Gary J Fowmes et al., 2016; Gary John Fowmes et al., 2017). Researchers analyzed and manufactured optimized prototype geomembrane specimens to be evaluated using additive manufacturing methods, which will be discussed later in this chapter in more detail.

2.3 Additive Manufacturing

Additive manufacturing (AM), as defined by ASTM (ASTM International, 2015), is "the process of joining materials to make parts from 3D model data, usually layer upon layer, as opposed to subtractive manufacturing and formative manufacturing methodologies." This technique, patented by Stratasys in the 1980's, has evolved and been adopted by many different industries over the years, such as aerospace, medical, military, education, architecture, consumer products, and research. This rapid adaptation is of no coincidence because of the fact that AM tools offer; fast and reliable prototype manufacturing using a wide array of material and finishing options can manufacture complex geometries that cannot be manufactured using traditional methods and shorten the supply-chain for specialty parts such as custom tools, parts, and fixtures. In their review, Bikas et al. (Bikas et al., 2016) generally categorized the AM processes as seen in Table 2.4. While some of these AM

processes require sophisticated equipment and high machinery and material costs, Stereolithography (SLA) and Fused Deposition Modelling (FDM) techniques are broadly being used and implemented by, because of low equipment and material costs, many different industries and companies, even hobbyists.

Table 2.4 - Categorization of AM processes (Bikas et al., 2016).

Additive Manufacturing (AM) Processes													
Process	Laser Based AM Processes						Extrusion Thermal		Material Jetting		Material Adhesion		Electron Beam	
	Laser Melting				*Laser Polymerization*									
Process Schematic	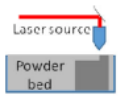		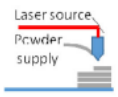		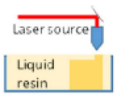		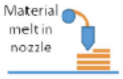		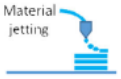				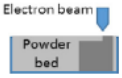	
Name / Material	SLS		DMD		SLA		FDM		3DP		LOM		EBM	
	SLM		LENS		SGC		Robocasting		IJP		SFP			
	DMLS		SLC		LTP				MJM					
			LPD		BIS				BPM					
					HIS				Thermojet					
Bulk Material Type			Powder		Liquid		Solid							

2.3.1 Fused Deposition Modelling (FDM)

Fused Deposition Modelling (FDM) is an additive manufacturing technique that utilizes CNC controlled heated liquifying chamber and a deposition nozzle fitted on a movement system, as seen in Figure 2.11.

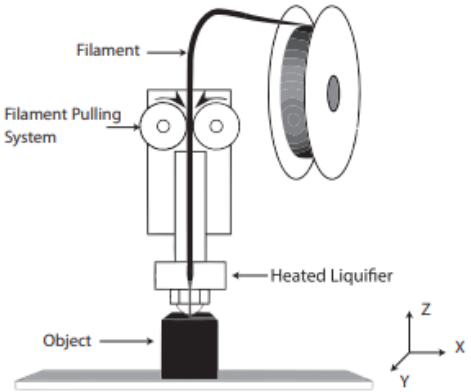

Figure 2.11 - Schematic drawing of the FDM AM technique.(Carneiro et al., 2015)

By depositing liquified thermoplastic polymer layers on top of each other in a controlled manner, an object is formed in the 3D space. An FDM manufacturing equipment basically consists of a movement system, a build plate, an extrusion component that includes the plastic filament path known as the "cold-end" and plastic liquifying zone known as the "hot-end", electronics and casing. This simplified yet capable design enables the FDM technique to be a versatile and inexpensive alternative to other more complex AM techniques.

Technically, all of the thermoplastic polymers can be manufactured using this process, including thermoplastics containing carbon fiber or fiberglass additives, even though in practice, some of the thermoplastics such as HDPE, PP, ABS, and PA requires special care because of their tendency to deform during the cooling process. This thermal induced deformation is known as warping and happens due to uneven cooling of the extruded layers, as seen in Figure 2.12.

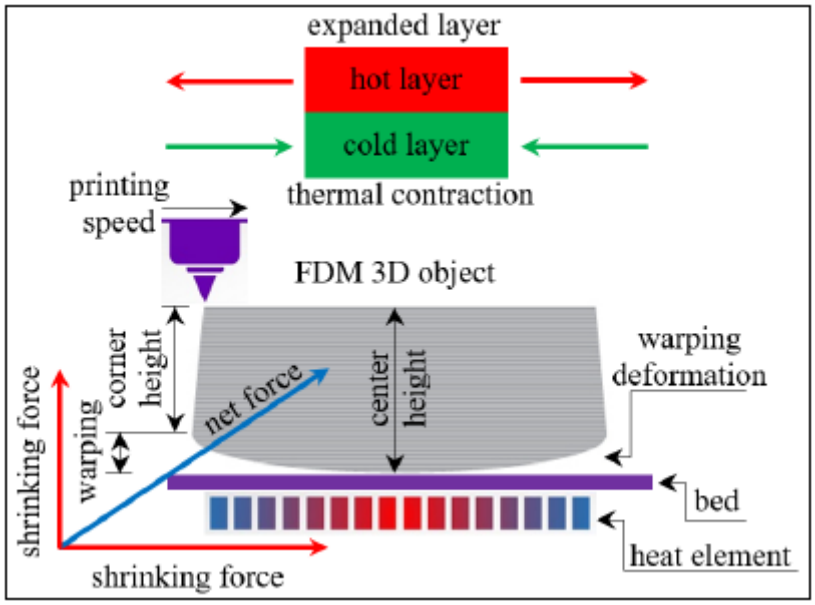

Figure 2.12 - Schematic drawing of the warping phenomenon (Alsoufi & El-Sayed, 2017).

To counteract this deformation, various methods, including; improving the adhesion between the build plate and the printed part, improving the distribution of heat around the FDM equipment, or applying structural modifications to the model, are advised (Singh, 2018).

For semi-crystalline polyolefin thermoplastics such as polyethylene (PE) and polypropylene (PP), which concerns the scope of this study, this warping effect becomes much more drastic. To overcome this problem, researchers suggested several methods (Bachhar et al., 2020; Chong et al., 2017; Schirmeister et al., 2019; Spoerk et al., 2020). For PE, the most effective method for warp prevention as of 2020 is to use a SEBS, Kraton FG1901 G build plate, a copolymer based on styrene and ethylene/butylene with a polystyrene content of 30% (Kraton Corporation, 2019). For PP based FDM manufacturing applications, the most common and practical approach is to use PP based tapes and geometrical printing approaches such as increasing the surface area of the base of the part. A suitable adhesion of the warp-countering material to the build plate is also necessary since analysis in the literature shows for a small PP part with 100% infill can generate contact stresses up to 70 MPa as seen in Figure 2.13.

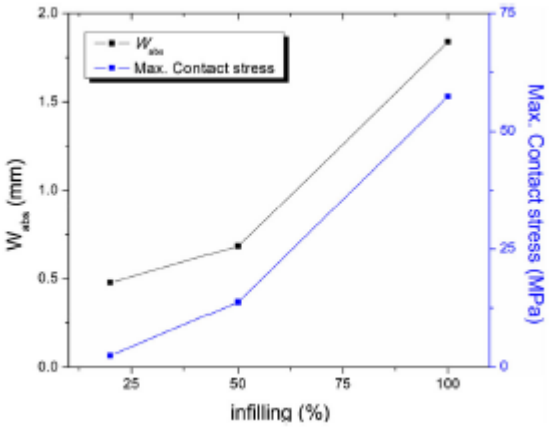

Figure 2.13 - Warpage and maximum contact stress values with increasing infill ratios for an FDM manufactured PP part (Bachhar et al., 2020).

2.4 Applications of Additive Manufacturing in Geotechnical Engineering

Applications of AM in the geotechnical engineering domain in literature is relatively new but novel and promising field of research. The use of AM for the analysis of granular morphology was first demonstrated by Miskin & Jager in 2013 (Miskin & Jaeger, 2013). Following this novel technique, the first application of AM in geotechnical engineering literature was published by Hanaor et al. in 2016 (Hanaor et al., 2016). In their study, by using a material jet type additive manufacturing equipment, researchers manufactured pseudo-sand particles generated with an algorithm named "contour rotation interpolation (CRI)" which utilizes 2D grain contours obtained through electron microscopy or optical methods. Additively manufactured pseudo-sand particles are shown with their respective 3D model images are shown in Figure 2.14.

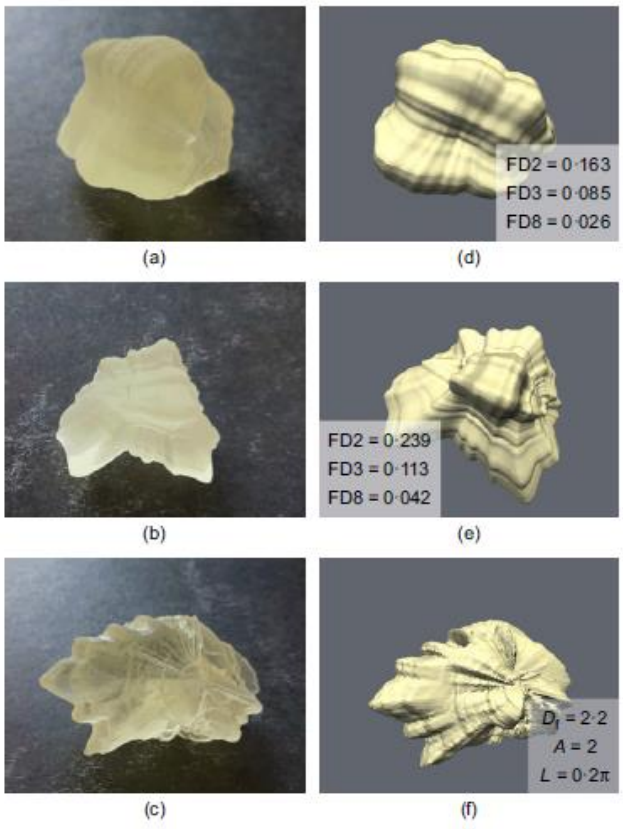

Figure 2.14 - Comparison of (a), (b), (c) Additively manufactured and; (d), (e), (f) 3D model files of pseudo-sand particles (Hanaor et al., 2016).

In the same study, researchers manufactured 8000 grains using Fullcure 720 resin supplied by Stratasys, with a mean diameter of 2 mm to form a triaxial test specimen. The resin is reported to have a specific gravity of 1.19 and an elastic modulus of 2.87 GPa, which differs from typical quartz sand significantly. They reported a manufacturing time of around two weeks. After performing the consolidated & drained (CU) triaxial test, researchers reported a typical stress response of sand but noted time-dependent compressibility due to material properties of the manufactured material. Stress ratio and volumetric strain plots reported by the researchers are presented in Figure 2.15.

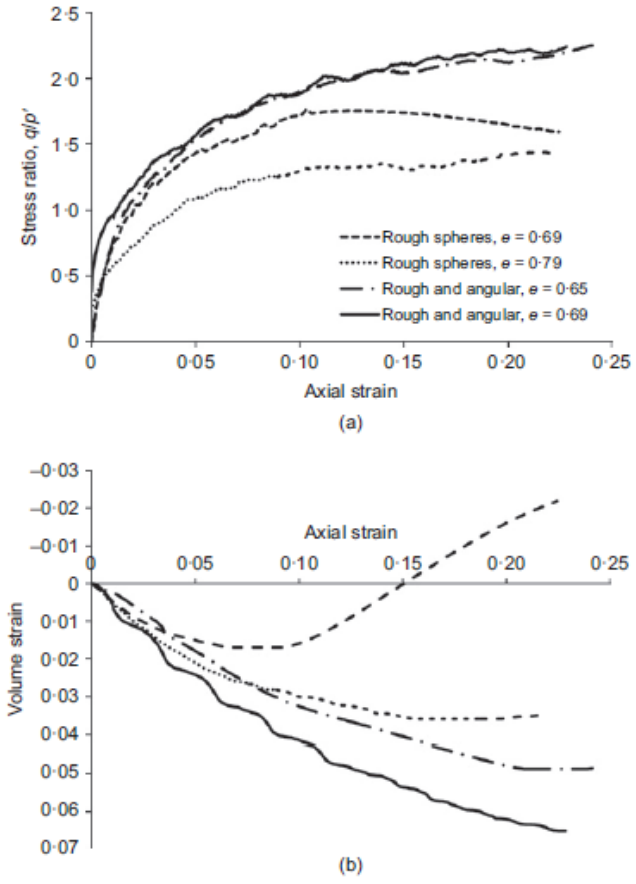

Figure 2.15 - Triaxial shear behavior of pseudo-sand particles: (a) stress ratio; (b) volumetric strain vs. axial strain (Hanaor et al., 2016).

Following this study, other researchers used additive manufacturing tools to replicate sand particles for morphological studies. Adamidis et al. (Adamidis et al., 2020) investigated the response of additively manufactured pseudo-sand particles using hydraulic conductivity tests and drained triaxial tests. Manufacturing of the particles was also made using a material jet additive manufacturing equipment. The comparison between the shear response of additively manufactured particles and benchmark sand can be seen in Figure 2.16. Researchers reported the similarity in shear response and confirmed the reusability of the manufactured particles using repeated tests and μCT scanning.

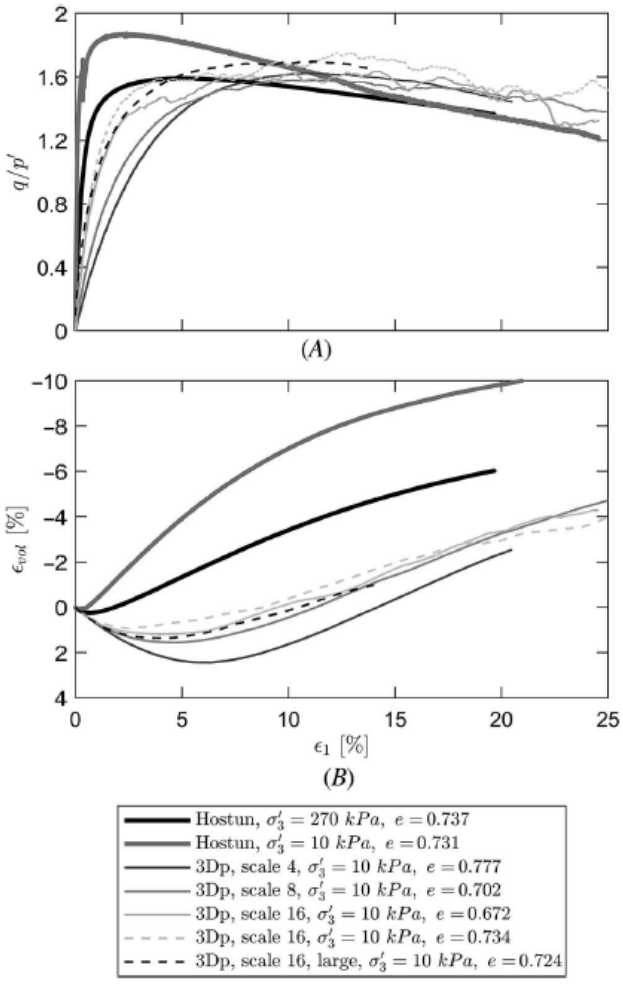

Figure 2.16 - Comparison between additively manufactured particles and benchmark sand using drained triaxial test results: (a) stress ratio; (b) volumetric strain vs. axial strain (Adamidis et al., 2020).

Another study investigation of morphological properties of sand particles using additive manufacturing is conducted by Su et al. (Su et al., 2020). In their study, researchers generated different particle geometries with controlled morphological parameters and additively manufactured them using the SLA technique. Researchers used these particles in a direct shear test setup to determine the internal friction angle of the specimens.

Starting with consecutive studies by Fowmes et al. (Gary J Fowmes et al., 2016; Gary John Fowmes et al., 2017), additively manufactured geosynthetics can be seen in geotechnical engineering literature. While some researchers, most notably Fowmes et al. and Palumbo(Palumbo, 2018), focused primarily on improving interface geometries, other researchers such as Stathas et al. (Stathas et al., 2017), Amurane et al. (Amurane et al., 2019), Mallett et al. (Mallett et al., 2018) and, Arab et al. (Arab et al., 2020) focused on replication and developing novel approaches in the field.

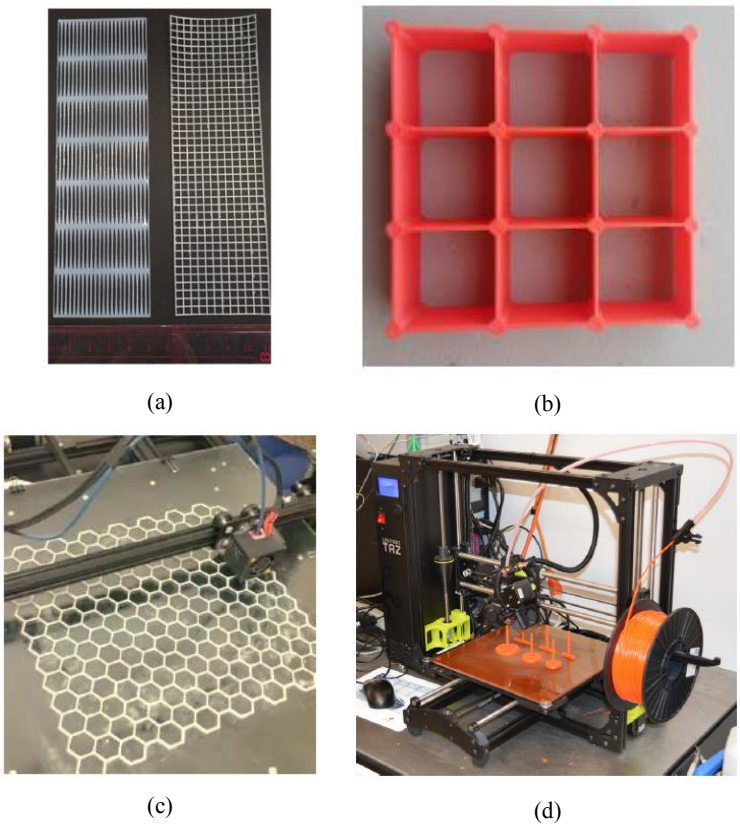

Figure 2.17 - Research involving geosynthetics and additive manufacturing in recent years: (a) MJP manufactured geogrids for scaled model tests (Stathas et al., 2017); (b) FDM manufactured geocells (Amurane et al., 2019); (c) FDM manufactured geogrids (Arab et al., 2020); (d) Bio-inspired FDM manufactured anchorage model (Mallett et al., 2018).

Contributions made by Fowmes and Palumbo are the most important ones within the scope of this thesis.

The study conducted by Fowmes et al. in 2017 aims to replicate and improve textured geomembrane surfaces by using additive manufacturing tools. In the first part of their study, researchers additively manufactured geomembranes using Selective Laser Sintering (SLS), an additive manufacturing process that utilizes a laser that sinters and joins the polymer powder and FDM (referred to as FFF in this research) techniques by referencing a commercially available HDPE geomembrane with

"spike" asperities. FDM parts were manufactured using polylactic acid (PLA), which is a much stiffer polymer compared to HDPE. It should be noted that researchers discussed using PP or HDPE for FDM parts but refrained from using these polymers due to their problems, as also discussed in this thesis. SLS parts were manufactured using a form of polyamide (PA), namely PA2200, which is also a significantly stiffer polymer compared to HDPE and PP. Researchers compared the behavior of the reference, SLS and FDM manufactured geomembranes interfacing with a non-woven needle-punched geotextile using a 100 x 100 mm direct shear test setup. This comparison can be seen in Figure 2.18.

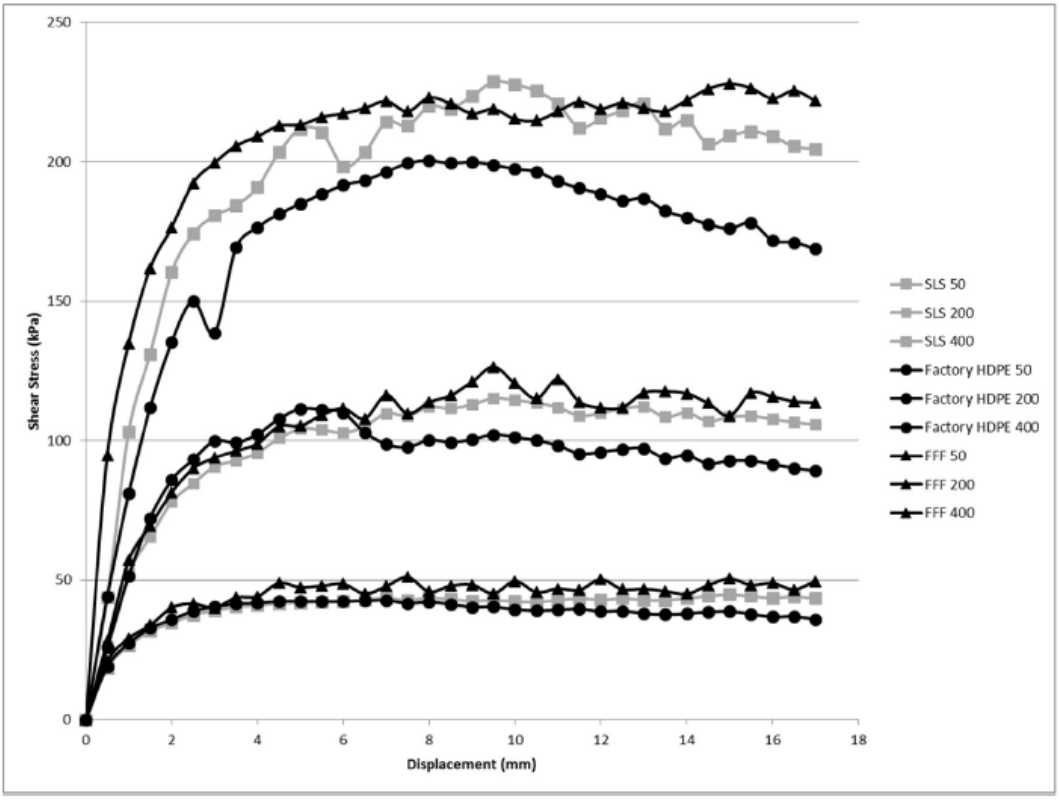

Figure 2.18 - Comparison of reference HDPE, SLS, and FDM manufactured geomembranes interfaced with a geotextile (Gary John Fowmes et al., 2017)

In the following chapters of the same research by Fowmes et al., researchers investigated replicability of the reference HDPE compared to SLS manufactured geomembranes using sand and clay interfaces. They concluded a remarkably similar behavior at 50 kPa normal pressure but a higher peak strength by 10.0% and 11.1%

for 200 and 400 kPa normal pressure values for the sand interface as seen in Figure. For the clay interface, they reported very similar peak shear strength values for every normal load value.

In the subsequent chapters of the study, researchers discuss the shape, height, and spacing parameters of the asperities to be used with clay and geotextile interfaces.

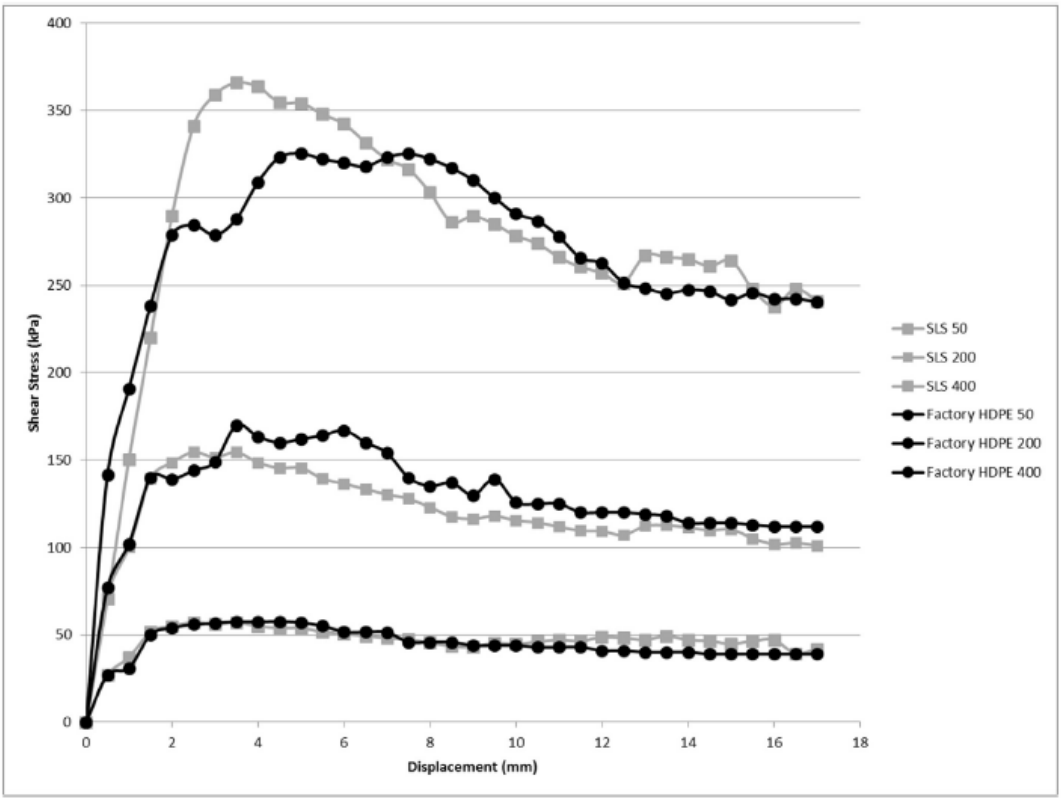

Figure 2.19 - Comparison of reference HDPE and SLS manufactured geomembranes interfaced with sand(Gary John Fowmes et al., 2017).

In 2018 Palumbo (Palumbo, 2018) used additive manufacturing in her study. The researcher used surface properties bio-inspired from thirty snake species to improve interface shear strength against Ottawa 20/30 and Ottawa F-65 sub-rounded sand particles. SLA additive manufacturing technique using a UV curable resin was utilized to manufacture these surfaces. The development workflow of these surfaces developed by the same researchers in an earlier can be seen in Figure 2.20.

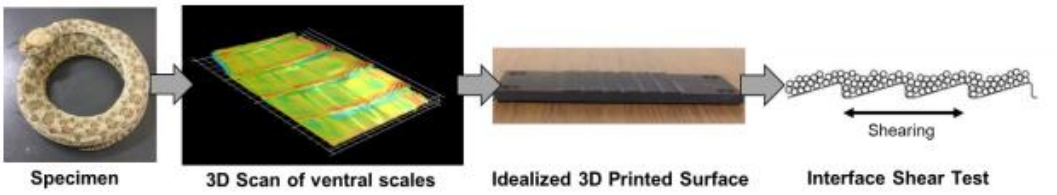

Figure 2.20 - Development workflow of snake-inspired surfaces (Martinez & Palumbo, 2018)

After numerous trials to optimize the geometric structure, researchers accomplished significant improvements in the interface shear strength. The anisotropic nature of this asperity type was also discussed to contribute to applications requiring different interface properties for opposing directions.

By reviewing the literature, it is evident that research using additive manufacturing for interface and geosynthetic research is a promising, exciting, and scientifically uncharted field. For interface and asperity studies related to geomembranes, an exact replication methodology is yet to be established. While other researchers experimented with MJP, SLA, and SLS additive manufacturing techniques, this equipment generally has expensive material and machinery costs and can only mimic the properties of the original thermoplastic in certain situations. This mimicry can be advantageous for the researchers in scaled model tests where specific scaling laws need to be applied to the mechanical properties of the material, as seen in the research by Stathas et al. (Stathas et al., 2017). While some effort was directed towards FDM printing in the current literature, additively manufacturing the geomembrane interface with the original material is yet to be studied as of 2020. While HDPE still being a challenging material to be used in FDM manufacturing, recent techniques discussed in this chapter allows PP to be used to replicate the shear behavior of geomembranes. In the following chapters, the use of PP as an HDPE geomembrane prototyping replicant will be justified, and test results will be shared.

CHAPTER 3

MATERIALS & METHOD

In order to analyze the usability of FDM manufactured geomembranes, a series of tests are performed. Firstly, in order to obtain three soil mixtures with increasing fines content values, Çine Sand and non-plastic silt are mixed with varying amounts. To obtain and ensure the index characteristics, a series of soil index tests, including wet sieving, specific gravity, and direct shear tests, are performed. Secondly, to evaluate and compare the mechanical behavior of mostly used FDM materials to HDPE, 40 axial tensile tests are conducted. An FDM available material is selected after these tests with regards to the similarity of mechanical behavior to HDPE. Finally, commercially available smooth and asperity samples are compared to their geometrically identical FDM manufactured counterparts utilizing 60 x 60mm direct shear tests using three different soils with increasing fines contents and densities. Details regarding these tests are discussed in this chapter.

3.1 Soil Preparation and Soil Index Tests

In this study, three soils are prepared with increasing target fines content values of 0%, 12%, and 40%. In all these three soil mixtures, as granular base Çine Sand is used, which is classified as a sub-angular to angular sand as seen in Figure 3.1. Non-plastic silt, as seen in Figure 3.2, is mixed accordingly in order to reach these target fines content values. Particle size distribution and specific gravity properties of these base soils were predetermined and presented in Figure 3.3. For 0%, 12% and, 40%, fines content soil mixtures, namely Mixture A, B, and C, 0%, 9.6% and, 40.3% non-plastic silt is mixed respectively by dry weight with Çine Sand. These soils, as seen

in Figure 3.4, are kept in sealed containers and mixed thoroughly before each sampling.

To determine the particle-size distributions of these soil mixtures, wet sieve analyses are performed according to ASTM D6913/D6913M-17(ASTM International, 2017). As seen in the resulting particle-size distribution curves in Figure 3.5, an increasing amount of particles under sieve #200 (0.075mm) is achieved. The final fines content values of soils A, B, and C are 1.36%, 11.5%, and 37.9%, respectively.

Figure 3.1 - Detailed photograph of Çine Sand particles. (Simsek, 2017)

The specific gravity of the soil samples is determined using a water pycnometer as described in ASTM D854-14(*Standard Test Methods for Specific Gravity of Soil Solids by Water Pycnometer*, n.d.) using three different samples for each soil type. Specific gravity values for A, B, and C are determined to be 2.66, 2.68, and 2.67, respectively. 103.37,196.35, and 220.03 grams of representative soil samples were collected from soils A, B, and C, respectively, to determine the water content of soils. After drying the samples in a 105°C oven for 72 hours, water content values of the soils were measured to be 0.12%, 0.10% and, 0.10% for soils A, B, and, C respectively. Following this measurement all soil samples used in these thesis are assumed to be in dry condition.

Figure 3.2 - Non-plastic silt used in the soil mixtures.

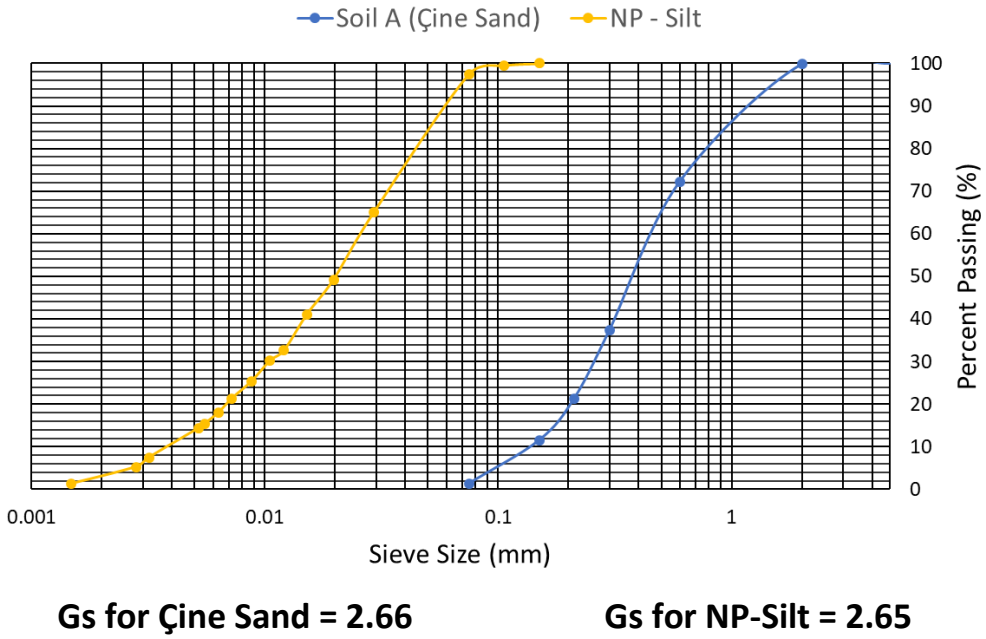

Figure 3.3 - Particle size distributions and specific gravity values of base soils Çine Sand and non-plastic silt

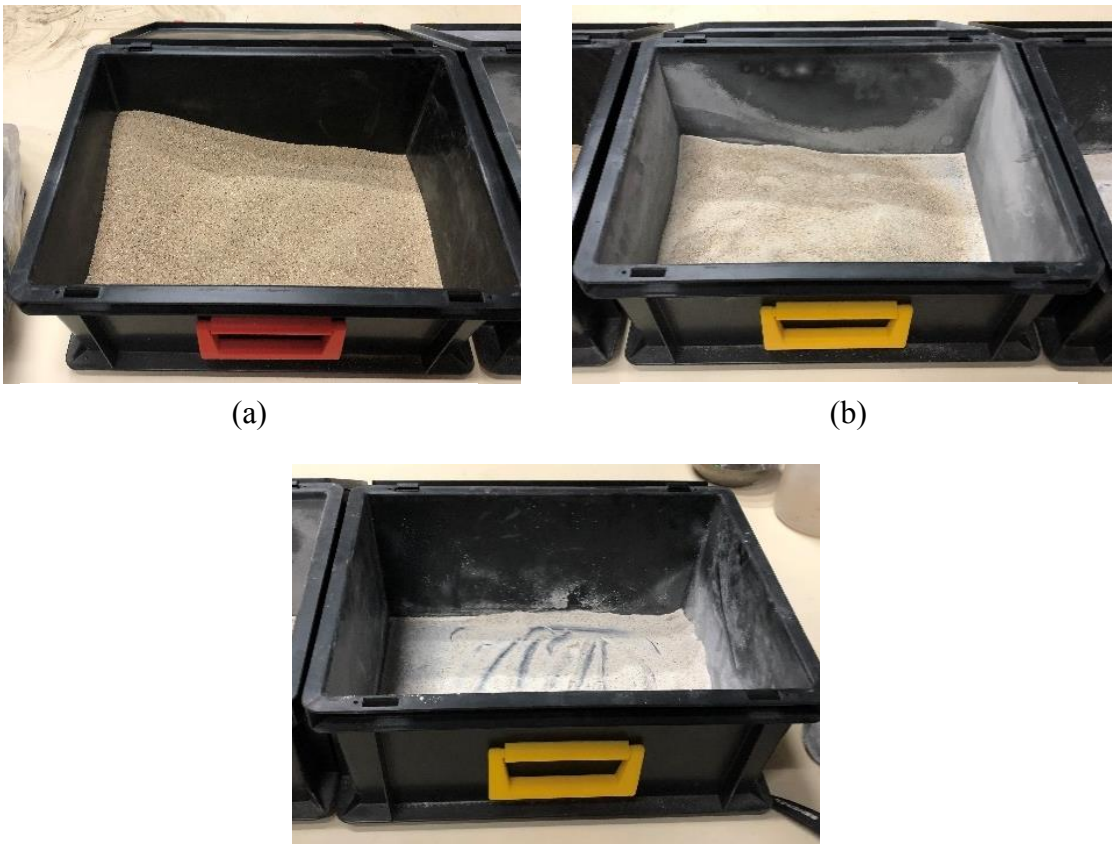

(a) (b)

(c)

Figure 3.4 - Soil mixtures, (a) Soil A (%0 F.C), (b) Soil B (%12 F.C), (c) Soil C (%40 F.C)

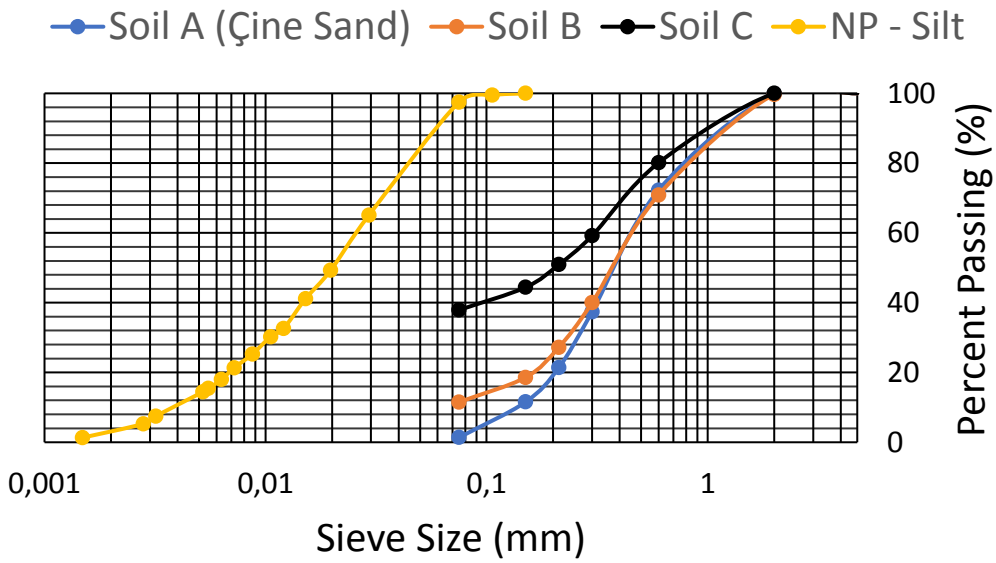

Figure 3.5 - Particle size distributions of soil mixtures A, B, and C

Additionally, to determine the internal shear strength characteristics of soils A, B, and C, a total of 18 60 x 60 mm direct shear box tests are performed according to ASTM D3080-04 (ASTM International, 2004). Two different void ratios are determined for soils A, B, and C to represent loose and dense conditions. The goal was not to achieve the loosest and densest possible conditions, but, rather, to generate two different density conditions. Values of density and void ratio can be seen in Figure 3.15 for all tests. Direct shear tests were carried out regarding these void ratios and under 20, 100, and 200 kPa vertical loads to ensure a proper representation of the Mohr-Coulomb failure envelope of the internal shear resistance of the soils. These Mohr-Coulomb failure envelopes accompanied by their respective internal friction angle values are presented in Figure 3.6. (a), (b) and (c) for the loose and dense conditions of soils A, B, and C, respectively.

Loose %0FC Sand			Dense %0FC Sand		
Normal Stress (kPa)	Shear Stress (kPa)	Internal Friction Angle (°)	Normal Stress (kPa)	Shear Stress (kPa)	Internal Friction Angle (°)
21.07	13.39		20.52	15.93	
108.25	65.35	**32.54**	105.82	82.59	**37.71**
218.50	141.25		210.70	162.50	

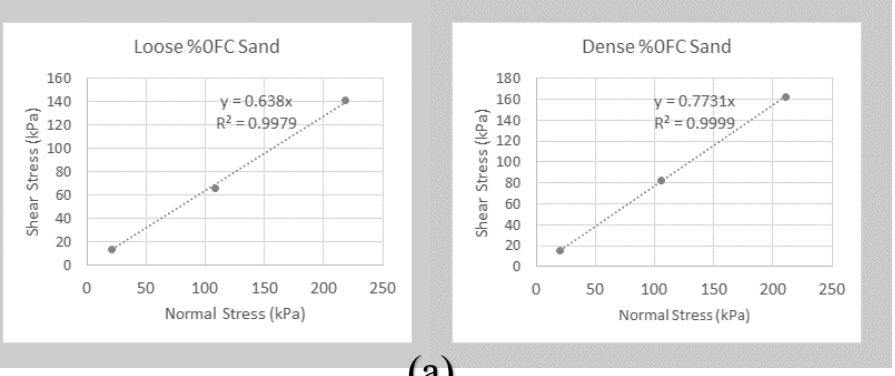

(a)

Loose %12FC Sand				Dense %12FC Sand			
Normal Stress (kPa)	Shear Stress (kPa)	Cohesion (kPa)	Internal Friction Angle (°)	Normal Stress (kPa)	Shear Stress (kPa)	Cohesion (kPa)	Internal Friction Angle (°)
21.70	16.93			20.48	24.14		
109.55	75.63	**0.00**	**34.27**	105.16	100.24	**0.00**	**44.05**
215.53	146.15			209.72	203.20		

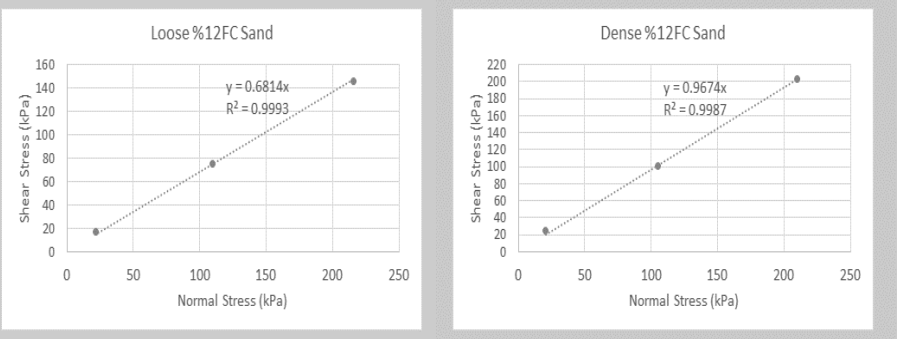

(b)

Loose %40FC Sand				Dense %40FC Sand			
Normal Stress (kPa)	Shear Stress (kPa)	Cohesion (kPa)	Internal Friction Angle (°)	Normal Stress (kPa)	Shear Stress (kPa)	Cohesion (kPa)	Internal Friction Angle (°)
21.91	16.77			20.39	23.68		
109.55	75.94	**0.00**	**34.90**	103.77	102.39	**0.00**	**43.10**
205.84	143.66			197.60	181.65		

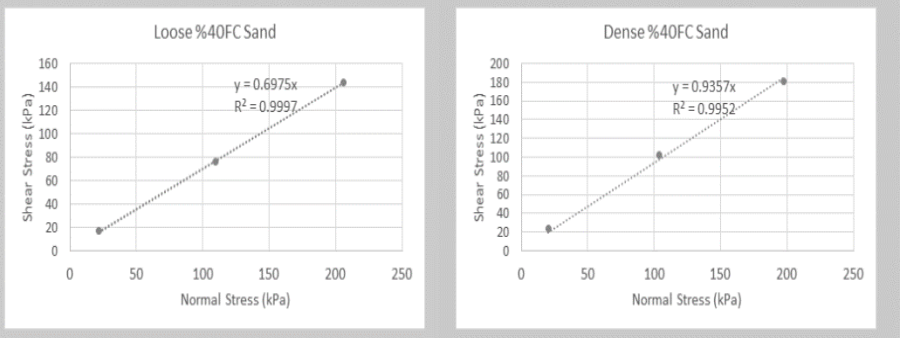

(c)

Figure 3.6 - Internal shear behavior Mohr-Coulomb failure envelopes for loose and dense conditions of (a) Soil A; (b) Soil B; (c) Soil C

3.2 Tensile Strength Tests

To evaluate and quantify the best matching FDM material to represent the mechanical behavior of HDPE geomembranes, tensile strength tests were performed. For this purpose, four candidate materials that are being used in FDM manufacturing is selected. These are, namely, Polylactic Acid (PLA), Acrylonitrile butadiene styrene (ABS), Recycled polyethylene terephthalate glycol-modified (re-PETG), and Polypropylene (PP). Also, 20 benchmark smooth and with asperity HDPE geomembrane specimens are cut out using a hydraulic press mold. 3D model of the specimen geometry described in ASTM D 6693 is constructed using Autodesk Fusion 360 software, as seen in Figure 3.7.

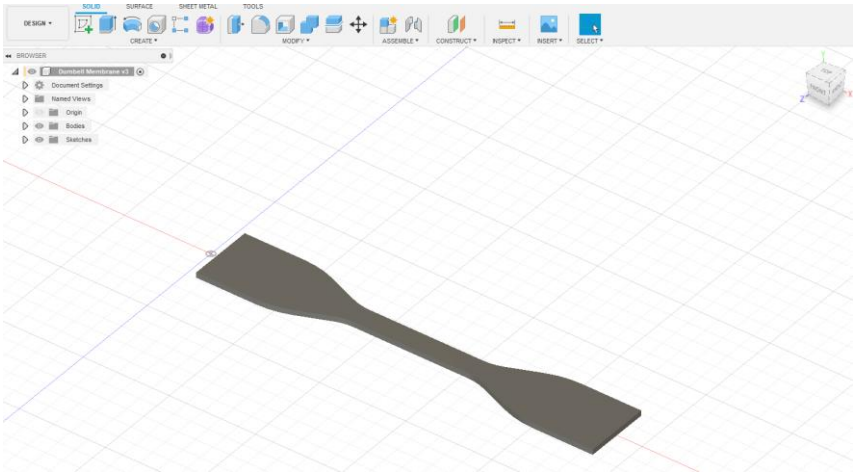

Figure 3.7 Modeled ASTM D6693 Specimen

After modeling, FDM manufactured specimens were prepared for manufacturing in the PrusaSlicer software using the parameters listed in Table 3.1. The parts are oriented to be at a 45-degree angle to the X-Y plane of the 3D printer, as seen in Figure 3.8. For all the specimens, plastic extrusion lines are calibrated to be parallel to the loading axis and fully filled with a 0.40 mm nozzle.

Manufacturing files are then transferred to the Prusa MK3 3D printer to be manufactured for each material in batches of 5. PLA, ABS, and re-PETG samples are manufactured using a Polyethyleneimine (PEI) coated steel sheet to ensure

adhesion between manufactured parts and printer bed. For the PP parts, another bed is coated with PP tape since adhesion between PEI and PP is not sufficient. This process in manufacturing can be seen in Figure 3.9.

Table 3.1 - Manufacturing parameters for tensile test specimens

Material	Filament Manufacturer	Layer Height	Printing Temperature	Print Bed Temperature	Print Speed	Average Thickness (mm)	Average Minimum Width (mm)	Average Length (mm)
PLA	Porima	0.2 mm	210	60	80mm/s	2.0646	6.126	114.78108
ABS	Porima	0.2 mm	255	110	80mm/s	2.1568	6.0202	114.41002
re-PET	BASF	0.2 mm	240	85	55mm/s	2.1836	5.9988	114.48446
PP	BASF	0.2 mm	230	70	50mm/s	2.1454	6.4336	113.95862

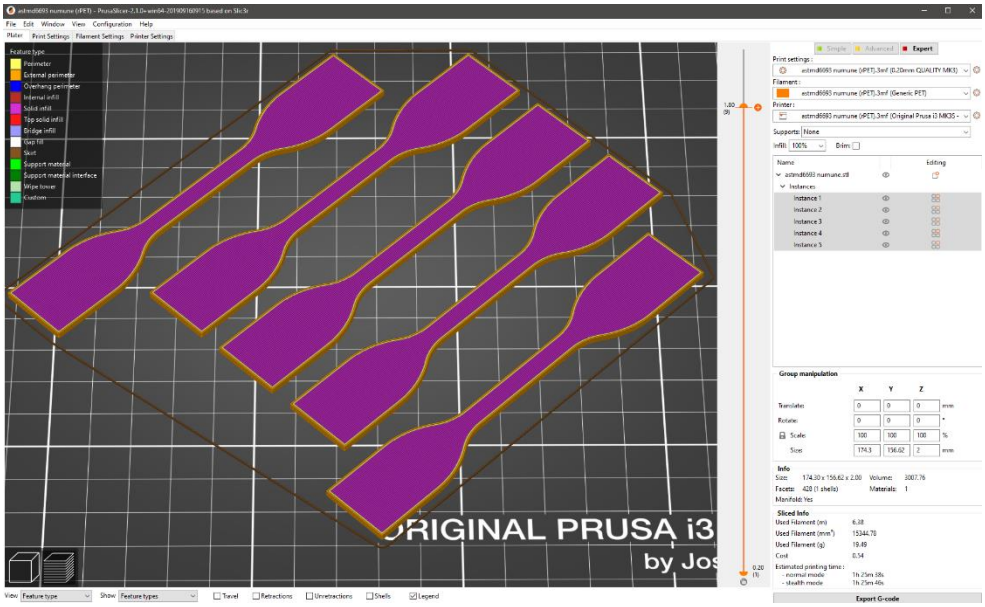

Figure 3.8 Pre-manufacturing preparation of ASTM D6693 Specimens

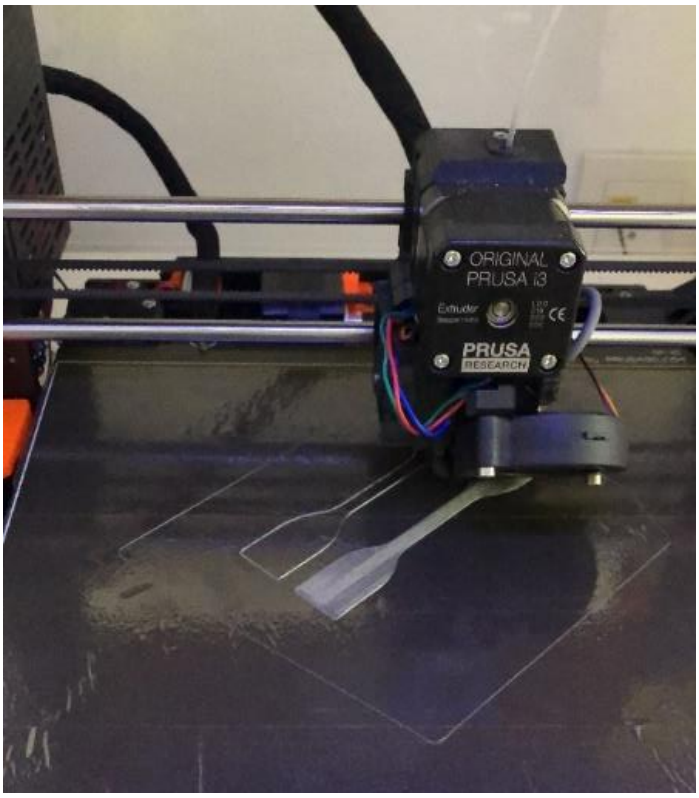

Figure 3.9 - 3D Printing of PP Tensile Strength Specimens

For the asperity and smooth HDPE geomembrane specimens, a hydraulic press and a cut-out mold are used. Ten ASTM D6693 tensile test specimens are cut out for each type of HDPE geomembrane. Out of these ten specimens, six specimens are cut out perpendicular to the extrusion direction, two are cut out to be at a 45-degree angle, and the last two is cut out parallel to the extrusion direction of the geomembrane. Cut and labeled specimens can be seen in Figure 3.11.

Figure 3.10 - Length measurement of tensile test specimens using linear height gauge and datum planes

Figure 3.11 – Cut out HDPE ASTM D6693 tensile test specimens using a hydraulic press cut-out mold.

After the preparation, the minimum width and length of all the specimens were measured using a Mitutoyo LH-600E linear height gauge and micrometer. The thickness and minimum width measurements are made using a micrometer. Length measurements are made using a linear height gauge by orienting the specimens between horizontal datum plates and a granite base plate, as seen in Figure 3.10. Mean and standard deviation values for thickness, minimum width, and specimen length readings are presented in Table 3.2

Table 3.2 - Thickness, minimum width, and length measurements of tensile test specimens

Material	Manufacturing Method	Mean Thickness (mm)	Std. Deviation (mm)	Mean Minimum Width (mm)	Std. Deviation (mm)	Mean Length (mm)	Std. Deviation (mm)
HDPE	Factory Extruded	2,0601	0,0124762	6,0042	0,010368756	115,10079	0,070976967
HDPE-A	Factory Extruded	2,063	0,023720596	6,0266	0,017212399	115,16085	0,137235598
PLA	3D Printed	2,0646	0,015355781	6,126	0,056182738	114,78108	0,064586043
ABS	3D Printed	2,1568	0,027417148	6,0202	0,041306174	114,41002	0,163678441
re-PETG	3D Printed	2,1836	0,007056912	5,9988	0,030621888	114,48446	0,088306642
PP	3D Printed	2,1454	0,020947554	6,4336	0,054738469	113,95862	0,289002936

Tensile strength tests were conducted in METU Central Laboratory using a Zwick/Roell Z250 tester, as seen in Figure 3.12. A total of 40 specimens were tested according to ASTM D6693 (ASTM International, 2020b). ASTM D6693 dictates a 50 mm/min load rate for HDPE specimens; therefore, 16 out of 20 HDPE specimens were tested using a 50 mm/min load rate. The remaining four specimens were tested using a 5 mm/min load rate. There is no recommendation in ASTM D6693 for FDM manufactured specimens, therefore by considering the brittle nature of these specimens, a 5 mm/min load rate is considered for 3 out of 5 specimens manufactured in PLA, ABS, re-PETG, and PP. The remaining two specimens were tested using a 50 mm/min load rate.

Specimens are placed on the device while maintaining an initial grip to grip separation of 65 mm and preloaded to 1 N before loading. An extensometer is utilized, and a gauge length of 33 mm is utilized as specified by ASTM D6693 for gauge length for yield.

Figure 3.12 - Zwick/Roell Z250 Tensile Test Device

3.3 Interface Shear Strength Tests using Direct Shear Apparatus

To determine the shear strength properties of geomembrane – soil interfaces, a total of 72, 60 x 60 mm direct shear box tests are conducted. For each soil type, namely soil A, B, and C, two different density values are determined to be at loose and dense soil conditions. Direct shear tests under 20,100 and 200 kPa normal pressures were performed for each soil condition. The test plan is shown as a flow chart in Figure 3.15. Counterface surfaces were prepared using commercially available smooth and textured HDPE geomembrane and smooth and textured PP geomembranes, which were additively manufactured using the FDM technique. PP geomembranes are 3D modeled to be exact geometric counterparts of the HDPE geomembranes. Figure 3.14 shows a schematic drawing of the direct shear test setup. It should be noted that for each of these tests, a new geomembrane specimen was placed in the shear box due to possible surface deformations on the geomembrane specimens.

Three repeatability tests were performed on asperity PP – dense soil, A test set under 20, 50, and 100 kPa normal pressures. Repeatability of individual tests is calculated in terms of normalized difference as:

$$Normalized\ Difference = 100 \times \frac{\left|\tau_{u,test1} - \tau_{u,test2}\right|}{MAX\left(\tau_{u,test1}, \tau_{u,test2}\right)} \tag{3.1}$$

Where $\tau_{u,test1}$ and $\tau_{u,test2}$ are the ultimate shear strength for repeatability tests 1 and 2, respectively. The Mohr-Coulomb failure envelops, comparison between individual tests, and the difference between calculated friction angle can be seen in Figure 3.13.

Asperity PP - Dense 0% FC Soil A - Test 1			Comparison	Asperity PP - Dense 0% FC Soil A - Test 2		
Normal Stress (kPa)	Shear Stress (kPa)	Interface Friction Angle (°)	Normalized Difference (%)	Normal Stress (kPa)	Shear Stress (kPa)	Interface Friction Angle (°)
20.32	13.96		5.859375	20.32	14.83	
100.02	67.07	**28.84**	5.008635579	100.02	63.71	**33.09**
198.66	103.09		20.71269488	198.66	130.02	
			Friction Angle Difference (°)			
			4.25			

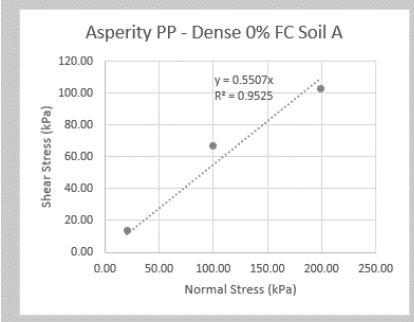

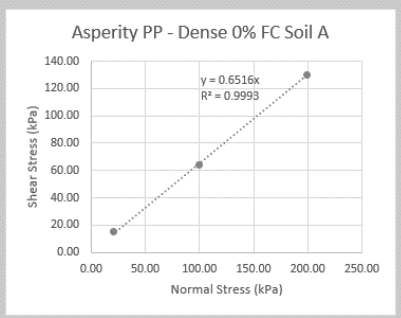

Figure 3.13 – Repeatability comparison between repeated tests involving asperity PP – dense soil A interface type.

This test is specifically selected to be checked for repeatability since the maximum effect of the interface and soil density is expected due to possible particle geometry effects on the surface and surface asperities. 5%, 5%, and 20.71% difference in these separate test sets were observed for 20, 50, and 100 kPa normal load, respectively. While tests under 20 and 100kPa of normal load are within reasonable repeatability limits, the test under 200kPa of normal load showed great deviation for this case.Evidently, the friction angle difference between these tests is calculated to be

4.25°. It should be noted that since the coefficient of determination (R^2) for test 2 is significantly greater than test 1, values corresponding to test 2 was used in the final comparative evaluation of interface shear strengths. All R^2 values are reported throughout this study and test sets that showed R^2 values under 0.99 were repeated.That being said, this fluctuation in this test is considered in the evaluation.

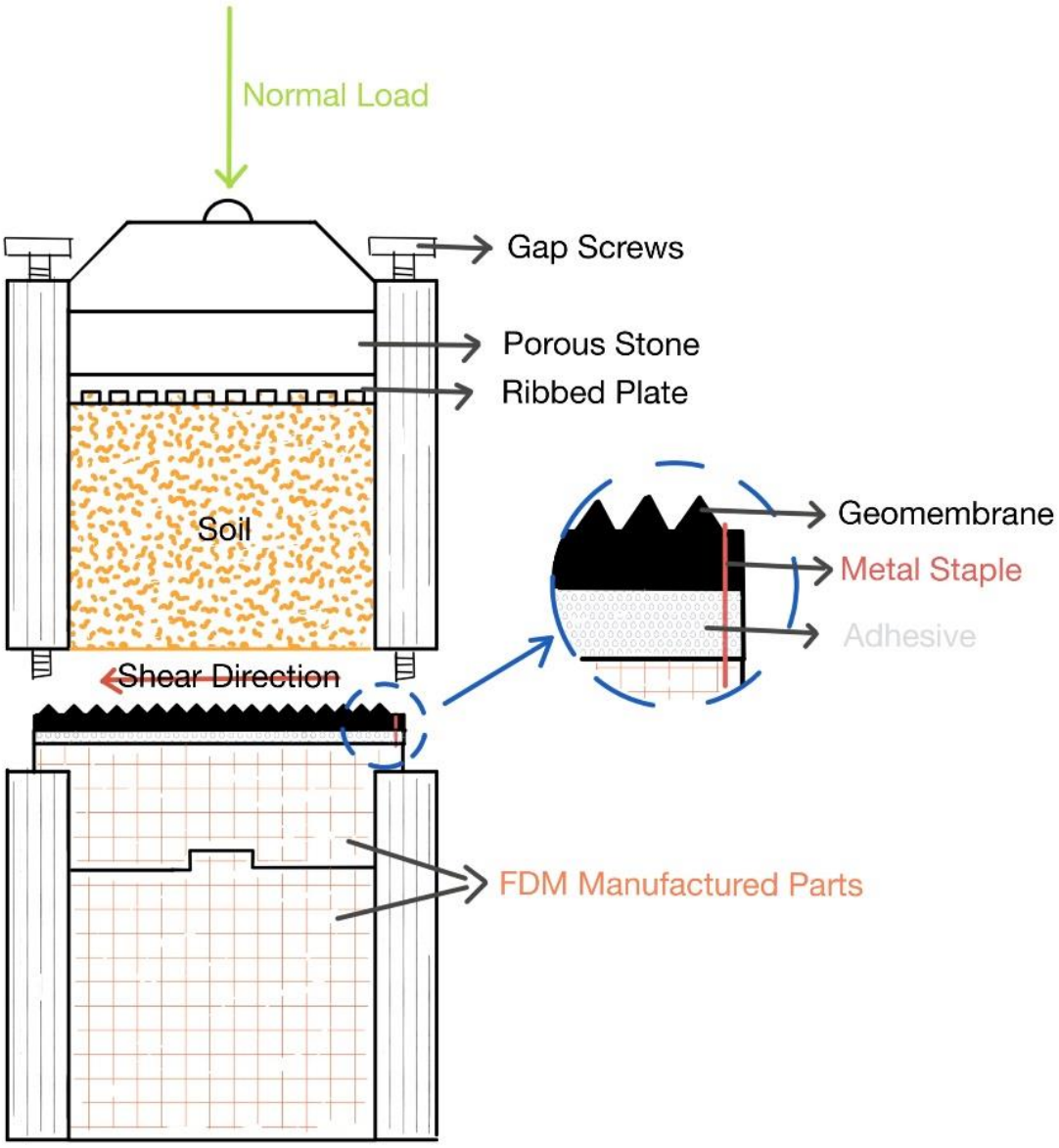

Figure 3.14 - Schematic drawing of the direct shear test setup (not to scale).

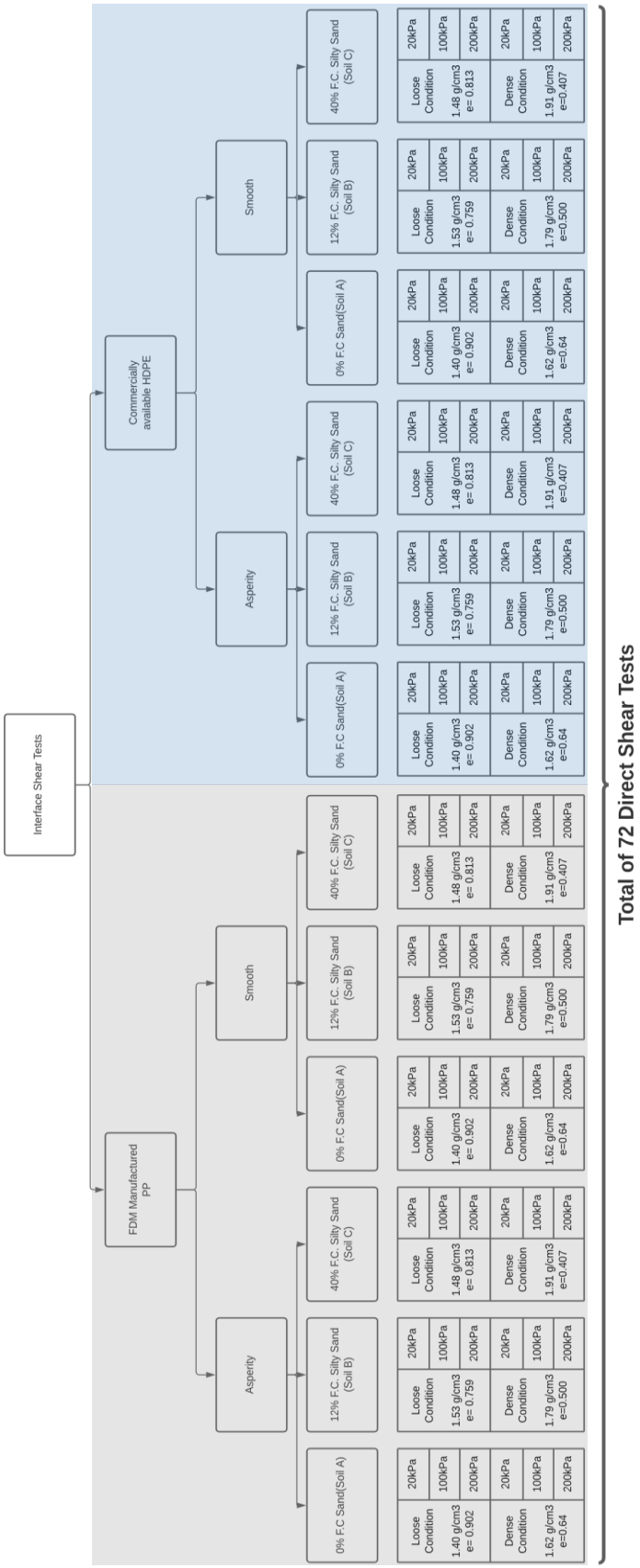

Figure 3.15 -Interface shear strenght tests.

For the preparation of the samples before the shear tests, the following steps were followed. Firstly, a two-part assembly that speeds up the specimen replacement process between tests is designed and manufactured using FDM additive manufacturing. This assembly can be seen in Figure 3.16.

Figure 3.16 - Additively manufactured two-part assembly mounted on the direct shear setup.

Next, HDPE geomembranes were cut using a laser cutter according to desired dimensions (88 x 68.5 mm). The specimen was over-fitted to the shearing box in both directions to ensure a constant shear area and minimize particle outflow. For the additively manufactured PP geomembrane specimens, a Prusa MK3 FDM manufacturing machine is used. For this purpose, a 3D model of the replicated geomembrane is generated according to dimensional measurements of the geomembrane. A schematic drawing showing these dimensions can be seen in Figure 3.17. A total asperity count of n=59 is achieved in a 3D model and additively manufactured PP geomembranes. Reference HDPE geomembrane and PP

geomembrane is compared visually in Figure 3.18. It should be noted that a slight deviation in asperity numbers due to cutting of the HDPE membrane was neglected.

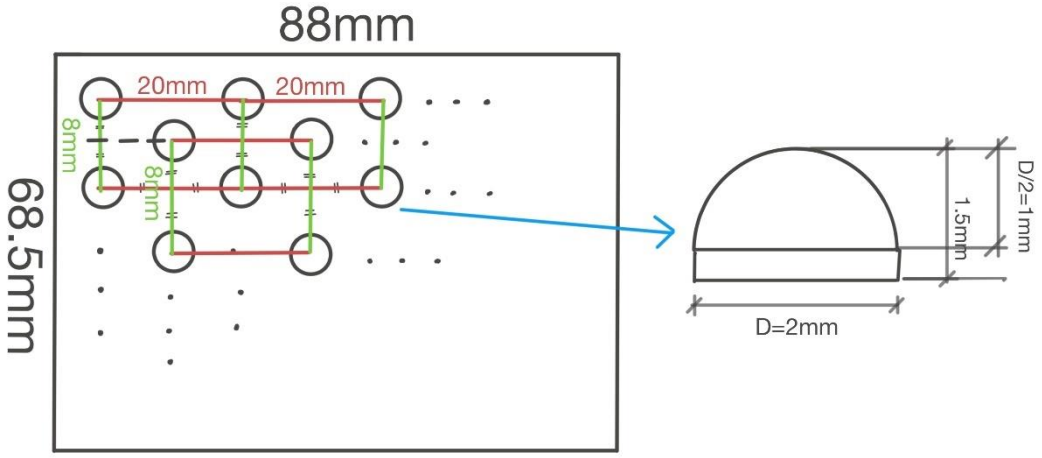

Figure 3.17 - Schematic drawing of the asperity geomembrane model derived from HDPE geomembrane.

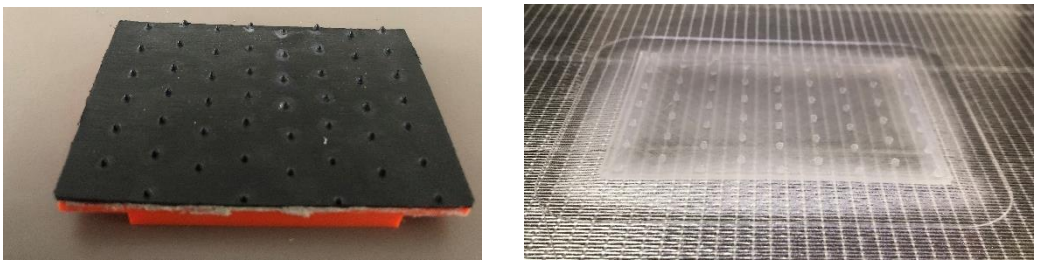

(a) (b)

Figure 3.18 - Side by side comparison of: (a) Reference asperity HDPE geomembrane; (b) PP asperity geomembrane

After the modeling of the replicated HDPE geomembrane, in order to manufacture the PP geomembrane without any significant geometrical defects that might occur due to warping (Bachhar et al., 2020), as explained in the previous chapter of this thesis, a PP tape reinforced with biaxially embedded glass fiber and a removable feature known in the FDM manufacturing literature as “brim” was used. This PP tape was replaced after each batch of production since it was observed that the tape gets weakened under constant stress and the heat of the build plate. Manufacturing parameters used in the PP geomembrane are listed in Table 3.3. A photograph of the

PP geomembrane just after manufacturing seen in Figure 3.19 shows no visible warping in the specimen. Furthermore, asperity heights, including the thickness of geomembrane samples (2 mm) of replicated and PP geomembrane, was measured using a micrometer by taking a sample from each membrane. Forty-four measurements were conducted on each membrane sample. The mean and standard deviation of these measurements can be seen in Table 3.4

Table 3.3 - FDM manufacturing parameters for PP geomembranes

Material	Filament Manufacturer	Layer Height	Printing Temperature	Print Bed Temperature	Print Speed	Infill	Brim Width	Fan Speed	Perimeter Count	Layer Adhesion
PP	BASF	0.2 mm	220	100	80 mm/s	100%	15 mm	20%	2	PP tape (fiber)

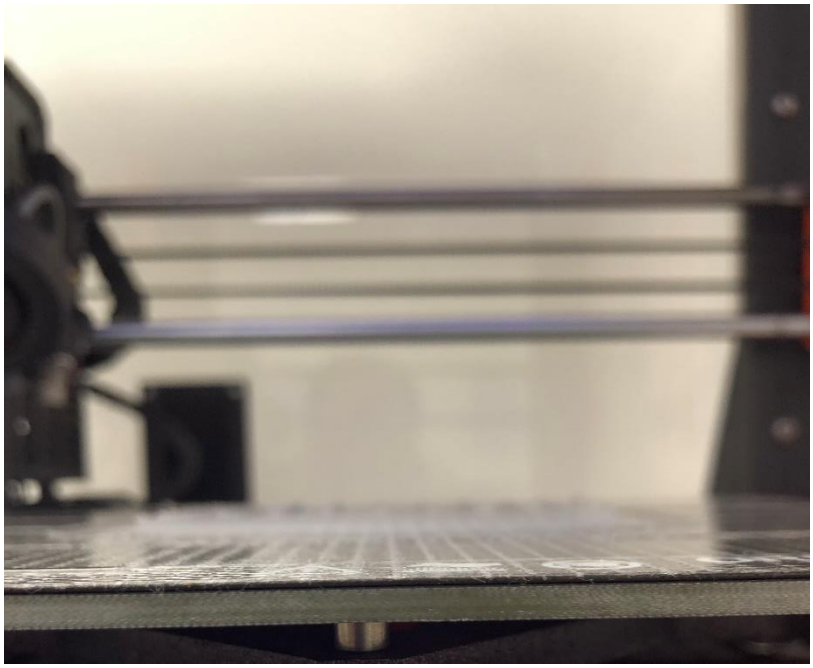

Figure 3.19 - Photograph of PP geomembrane after manufacturing showing no visible signs of warping.

Table 3.4- Mean and standard deviation of asperity height measurements using a micrometer. (Nominal value specified by factory: 1.5 mm)

Specimen Type	**Mean Asperity Height**	**Standard Deviation**
HDPE with asperity	1.415 mm	0.079
FDM manufactured PP	1.347 mm	0.218

After the preparation of geomembrane specimens, all geomembranes were glued to the two-part assembly using a Silyl Modified Polymer (SMP) based glue commercially named Derby One High Tack. Special molds were prepared to enable curing under load to ensure adequate bonding strength is achieved. The following bonding procedure was applied to all geomembranes:

1. The mold was prepared, assembled, and cleaned.
2. The bonding surface of the geomembrane was lightly sanded using 60 grit sanding paper to maximize the surface area.
3. Elastomer foam sheet was placed on the mold so that asperities would not deform under the applied mold clamping load.
4. The glue was applied and distributed using a plastic spatula so that over or under deposition of the glue would not deform the orientation of the surface. (Figure 3.20)
5. The mold was closed and clamped.
6. After 24 hours, molds were unclamped and disassembled. Geomembrane specimens were inspected against any surface damage, glue leak, or orientation change and discarded if necessary.
7. Surfaces were cleaned using isopropyl alcohol.
8. Additionally, geomembranes were stapled to the underlying assembly using metal staplers. Staples carefully placed outside the shear zone. A prepared and placed geomembrane specimen can be seen in Figure 3.21.

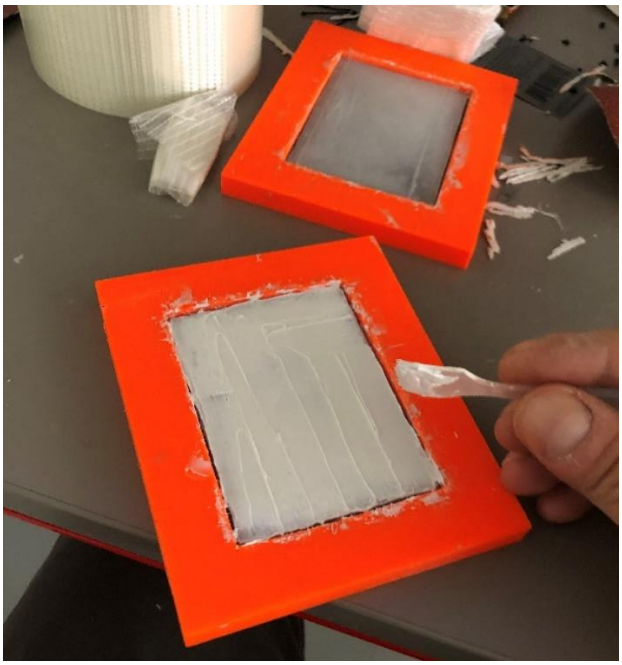

Figure 3.20 - The application of SMP glue to the geomembrane in the molds.

Figure 3.21 - A prepared, smooth HDPE geomembrane specimen placed in the direct shear box.

Direct shear tests were conducted on the 60 x 60 mm square direct shear box device located in the geotechnical engineering laboratory in METU, as seen in Figure 3.22.

Figure 3.22 - Direct shear box device used in tests.

The following testing protocol was followed for the interface direct shear tests:

1. The bottom piece of the two-piece assembly was appropriately fitted to the bottom half of the shear box.
2. The upper piece of the two-piece assembly containing the geomembrane specimen was fitted to the lower piece, makings sure the stamped edge was on the opposite side of the shearing direction and pushed to ensure proper fit to the bottom piece.
3. The upper half of the shear box is placed on top of the membrane and fixed to the lower half using the fixing screws.
4. A pre-determined amount of soil is weighed according to the test (loose/dense, soil type). Soil is carefully deposited on the upper half of the

shear box using a spoon without allowing the soil particles to deposit on top of each other by gravity.

5. The soil surface was leveled using a spatula without causing unnecessary compression to ensure a homogeneous compression was achieved in the next step.
6. The soil was compressed to the desired volume using a fixed height (15 mm inside the upper shear box) compression device. (Figure 3.23)

Figure 3.23 - Compression of the soil to the desired volume using a fixed height compression device.

7. The ribbed plate, porous stone, and top cap were placed on top of the soil. Gap screws were tightened until a slight resistance was felt, indicating screws are touching the lower half of the shear box.
8. The shear rate of the shearing device was calibrated to be 0.4 mm/minute using the gear mechanism on the device.

9. The whole shear box assembly was placed on the shearing device, and roller bearings were controlled, ensuring free movement in the horizontal direction. (Figure 3.24)

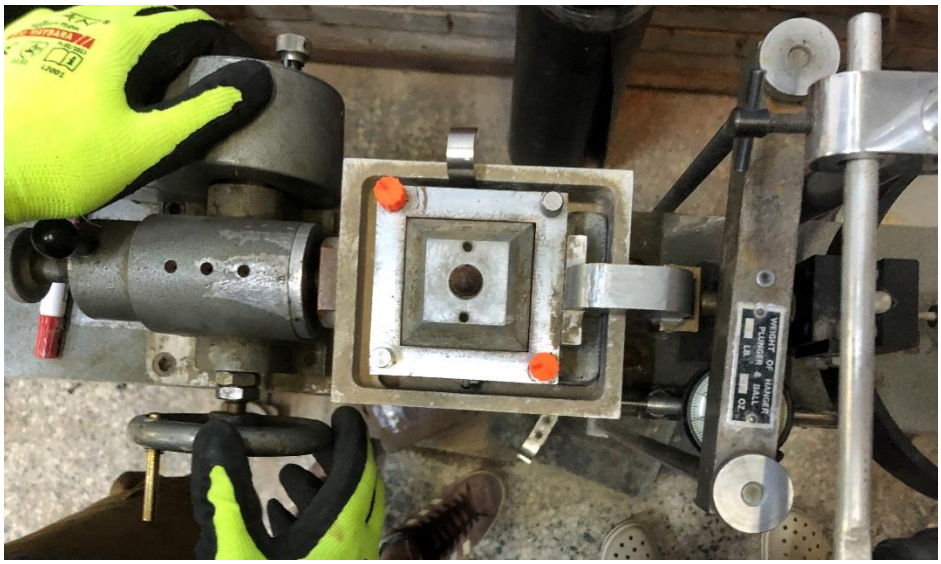

Figure 3.24 - Assembled and placed shear box assembly to the shearing device.

10. Necessary normal load transfer equipment is loaded on top of the shear box. No leverage system was used for 20 kPa loading, while a 1 to 5 leverage system was used for 100 and 200 kPa loadings. It should be noted that while the normal load transferred by the weight of this equipment is included in the normal load calculations, the vertical deformation caused by this equipment is neglected.
11. A vertical deformation gauge was placed on top of the load transfer equipment, zero position of the gap screws were marked and, fixing screws were loosened.
12. Vertical deformation gauge was zeroed, and the load was applied using pre-determined weight sets. (Figure 3.25)
13. Gap screws were turned in clockwise direction until 2.5 rotations were achieved, opening a gap of 2 mm between the soil and the geomembrane.

This gap distance was to be higher than the nominal asperity height of 1.5 mm to make sure the shear box would not block the shear zone by colliding with the asperities. Gap screws were turned back in counterclockwise direction at least 2.5 rotations to ensuring that they do not affect the shear zone. The shear force and horizontal displacement gauges were zeroed after this step.

14. The shearing was initiated after waiting for 5 minutes to ensure all of the initial settlement of soil was completed. Vertical displacement before the shear was recorded, and the horizontal displacement gauge was zeroed until an increase in the shear force gauge was recorded.
15. Data was collected manually by reading the gauges for each 0.127 mm horizontal deformation between 0 and 2.54 mm deformation. Gauges were read for each 0.254 mm horizontal deformation between 2.54 and 5.08 mm deformation.
16. All tests were stopped when the horizontal deformation value reached 5.08 mm.

Figure 3.25 - Placement of leverage mechanism and pre-determined weight sets to the shearing device.

CHAPTER 4

RESULTS & DISCUSSIONS

In this chapter, the results of the tests detailed in the previous chapter will be presented and discussed, starting with the tensile strength tests previously discussed in Chapter 3.2, followed by a justification regarding the use of PP as an HDPE replicant for the interface tests. Afterward, the interface shear test results will be presented, and a detailed discussion using these data will be held

4.1 Tensile Strenght Test Results

In order to determine the FDM additive manufacturing material to replicate commercially available HDPE geomembrane, 40 specimens were tested under tensile load as detailed in Chapter 3.2. It should be noted that the initial modulus of elasticity was calculated as a secant modulus corresponding to %1 axial strain, yield strength calculated as the maximum tensile stress and, elongation at yield was calculated as the corresponding deformation at the maximum tensile load. Figure 4.1 shows the tensile behavior of all specimens on a tensile stress vs. axial strain plot. In this plot, green, gray, blue, yellow, red, and orange lines show the tensile stress behavior of PLA, ABS, re-PETG, smooth HDPE, PP, and asperity HDPE, respectively.

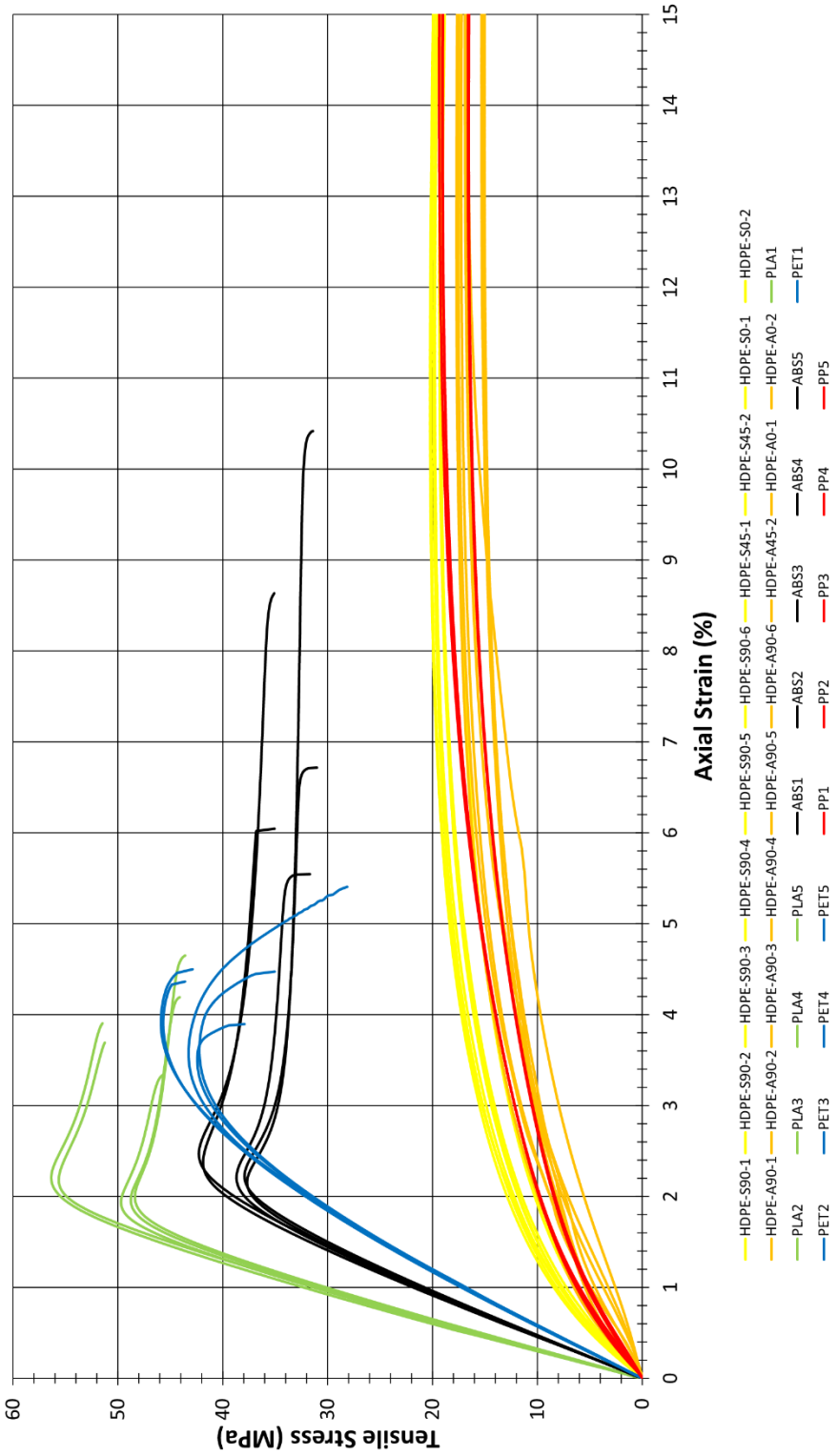

Figure 4.1 – Tensile Stress vs. Axial Strain plot for all tests.

Figure 4.2 shows the tensile stress vs. axial xtrain plot for all HDPE specimens. In this figure, dashed lines represent the HDPE specimens with asperities while solid lines represent HDPE specimens with smooth surfaces. Red lines in this figure shows specimens that were loaded using 5mm/min while all other specimens were loaded using 50mm/min load rate. Blue and green curves in this figure represent samples cut out oriented to be at a 45 and 0 degree angle to the extrusion direction, respectively. Figure 4.3 and Figure 4.4 shows the Average Initial Youngs Modulus, Average Yield Strenght and Average Elongation at Yield values for smooth and asperity HDPE sample sets respectively. It is evident by looking at these figures:

- With increasing loading rate, initial modulus of elasticity, and yield strength increases for both HDPE specimens with asperity and smooth.

- Regardless of cutting orientation, HDPE specimens with asperities have a lower initial modulus of elasticity and yield strength compared to smooth HDPE specimens. Specimens with asperities were also observed to deform more compared to smooth specimens before yielding. These effects could be attributed to manufacturing method related deformations already present in the specimens with asperities.

- Cutting orientation relative to the extrusion direction of the HDPE geomembrane sample also affects the tensile behavior of the specimens for both specimen types. Specimens oriented parallel to the extrusion direction have the least initial elasticity modulus and yield strength, while cutting the specimens toward a perpendicular orientation towards the extrusion direction improves these tensile properties but decreases the elongation at yield. This behavior is also appearing to be related to the inherent deformations and anisotropy already present in the HDPE samples oriented parallel to the extrusion direction caused by the manufacturing method.

- Repeatability of all specimens is shown to be within a reasonable range, especially for the concerning mechanical properties discussed above.

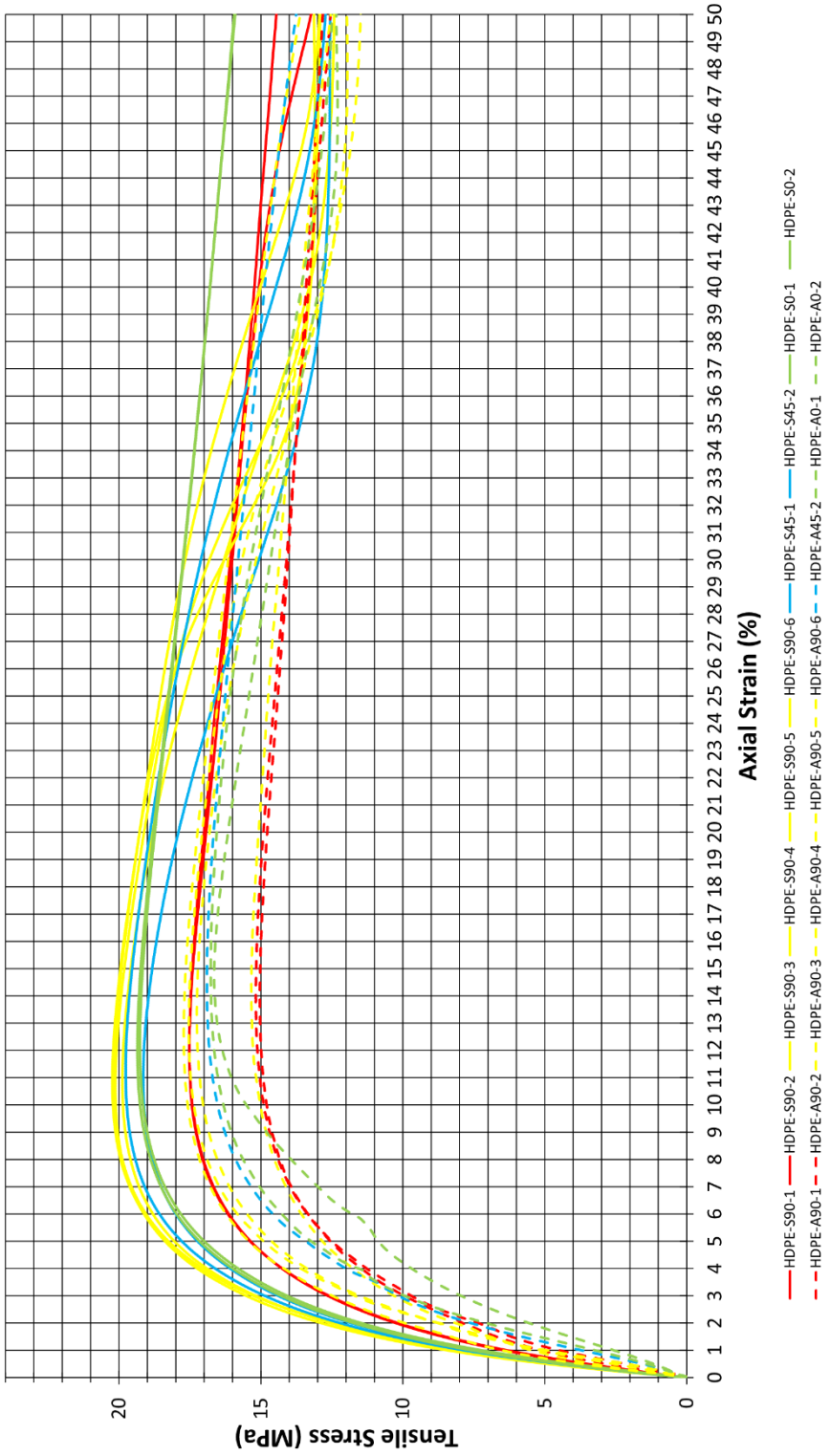

Figure 4.2 – Tensile Load vs. Axial Strain plot for HDPE specimens.

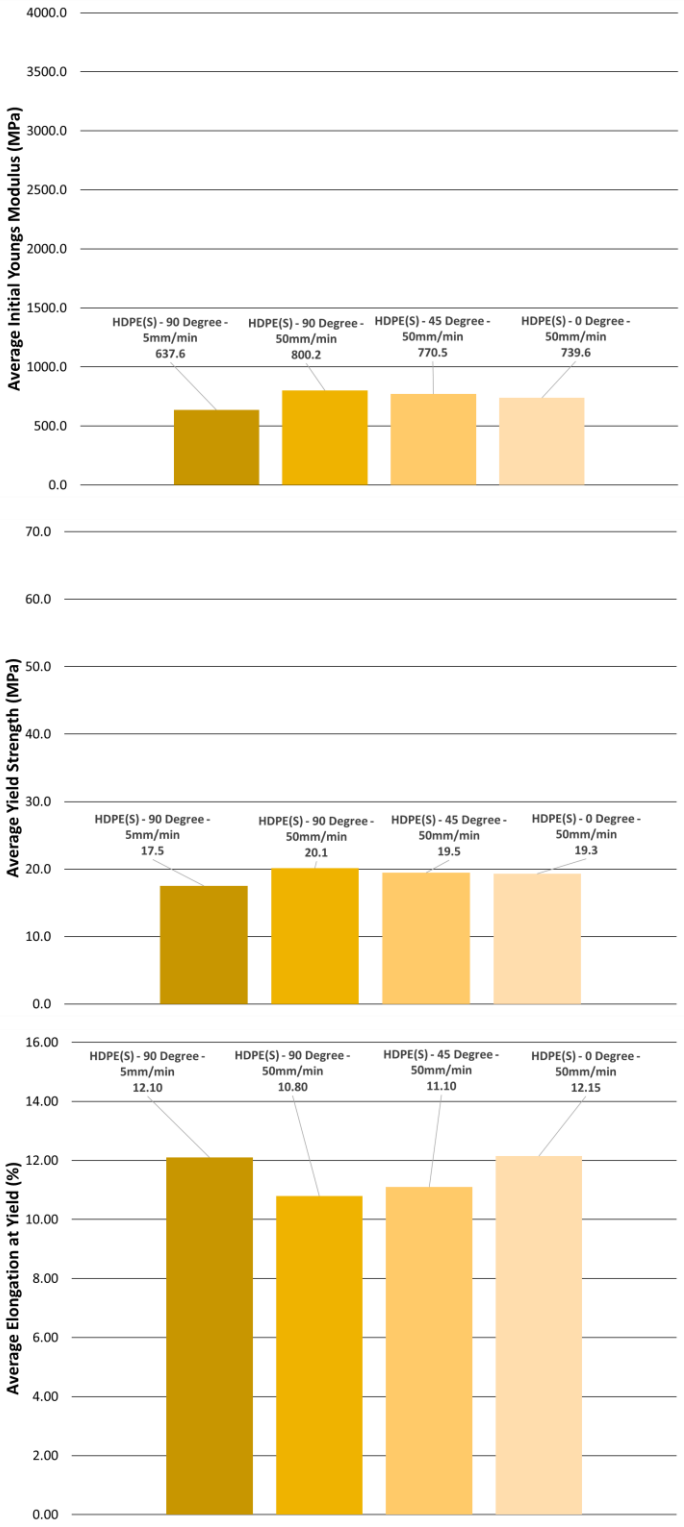

Figure 4.3 – Comparison of smooth HDPE specimens regarding average initial Youngs modulus, average yield strength, and average elongation at yield.

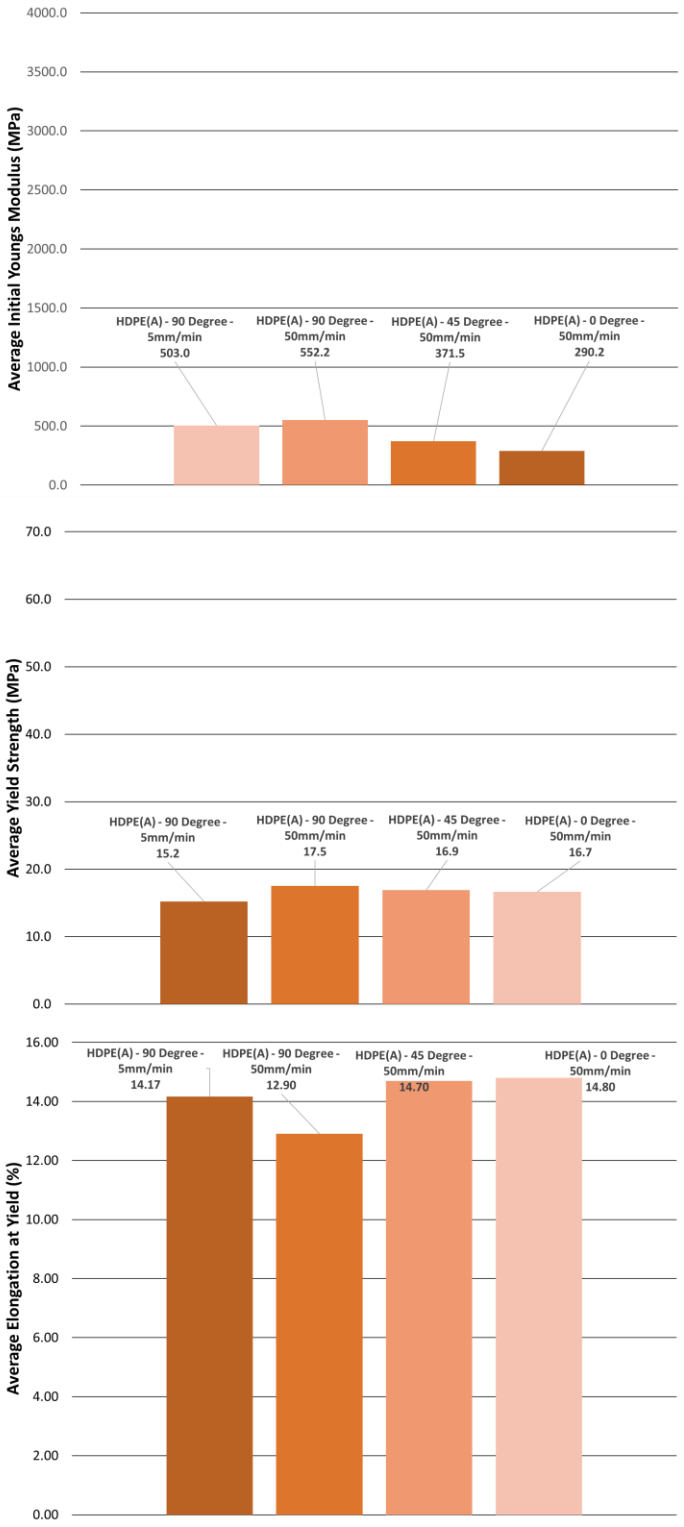

Figure 4.4 - Comparison of asperity HDPE specimens regarding average initial Youngs modulus, average yield strength, and average elongation at yield

Figure 4.5(a) shows the tensile behavior of additively manufactured PLA specimens. PLA is the most common FDM manufacturing material, is also the cheapest and easiest to manufacture with. As discussed in Chapter 2.4 of this thesis, all of the researchers who tried FDM printing in their research used PLA for manufacturing material. That being said, the behavior of this material dramatically differs from other materials. PLA has the greatest tensile yield strength and initial modulus of elasticity. A low elongation at break and yield, coupled with a brittle failure mode, are some characteristics shown by this thermoplastic. For these reasons, while PLA provides great manufacturability, the material properties of this thermoplastic differ significantly compared to thermoplastics commonly used in geosynthetics.

The tensile behavior of additively manufactured ABS specimens is presented in Figure 4.5(b). ABS is another common FDM additive manufacturing material, also used widely in the consumer products industry, therefore also a cheaper alternative compared to other thermoplastics. The behavior of ABS is less stiff than PLA but far greater compared to HDPE. Some deformation after the yield can be seen for the ABS specimens, especially compared to PLA and re-PETG specimens. While the tensile properties of ABS do not fit too well with thermoplastics commonly used in the geosynthetics industry, it should be noted that ABS surfaces could easily be treated with acetone vapor to achieve a much smoother surface. This popular method among hobbyists could prove useful in further studies regarding interface research since surface roughness could be controlled by applying acetone vapor to the surface.

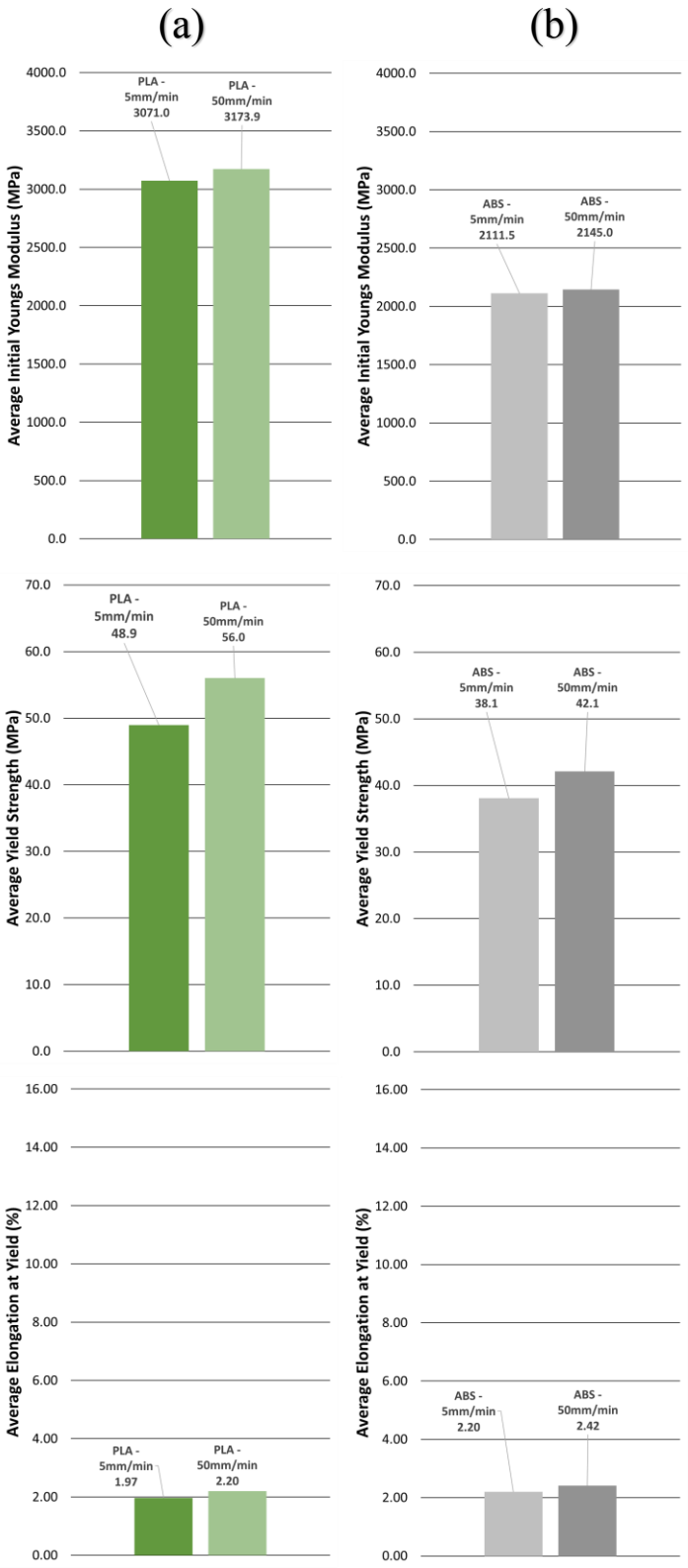

Figure 4.5 - Comparison of (a) PLA, (b) ABS specimens regarding average initial Youngs modulus, average yield strength, and average elongation at yield

Figure 4.6(a) shows the tensile behavior of additively manufactured recycled PETG specimens. This material is shown to have the lowest initial modulus of elasticity among the common FDM manufacturing materials, namely PLA, ABS, and re-PETG. The failure mode showed brittleness, which is attributed to the recycled nature of this material. Also, having the second-highest tensile yield strength while having a lower modulus enables this material to have some deformability. This property is desirable in some assemblies or mechanical parts and is the most common use of PETG in FDM manufacturing. For this reason, for the two-part assembly utilized in direct shear tests discussed in Chapter 3.2 of this thesis, PETG material was used.

In terms of initial modulus of elasticity, E0, tensile yield strength, σy, and elongation at yield, εy, PLA, ABS, and re-PETG thermoplastics behave considerably different from HDPE and PP thermoplastics. Figure 4.6(b) shows the tensile behavior of additively manufactured PP specimens. An unmistakable resemblance between HDPE and PP samples in terms of all three properties can be seen. Similar tensile behavior of these materials can also be seen in the post-test photographs of all specimens in Figure 4.7. This resemblance is attributed to both polymers being in the same sub-group of polymers known as polyolefins (Mihaies & Olaru, 2000). Therefore, PP was selected as the material to be used in the interface direct shear tests in order to represent the behavior of HDPE.

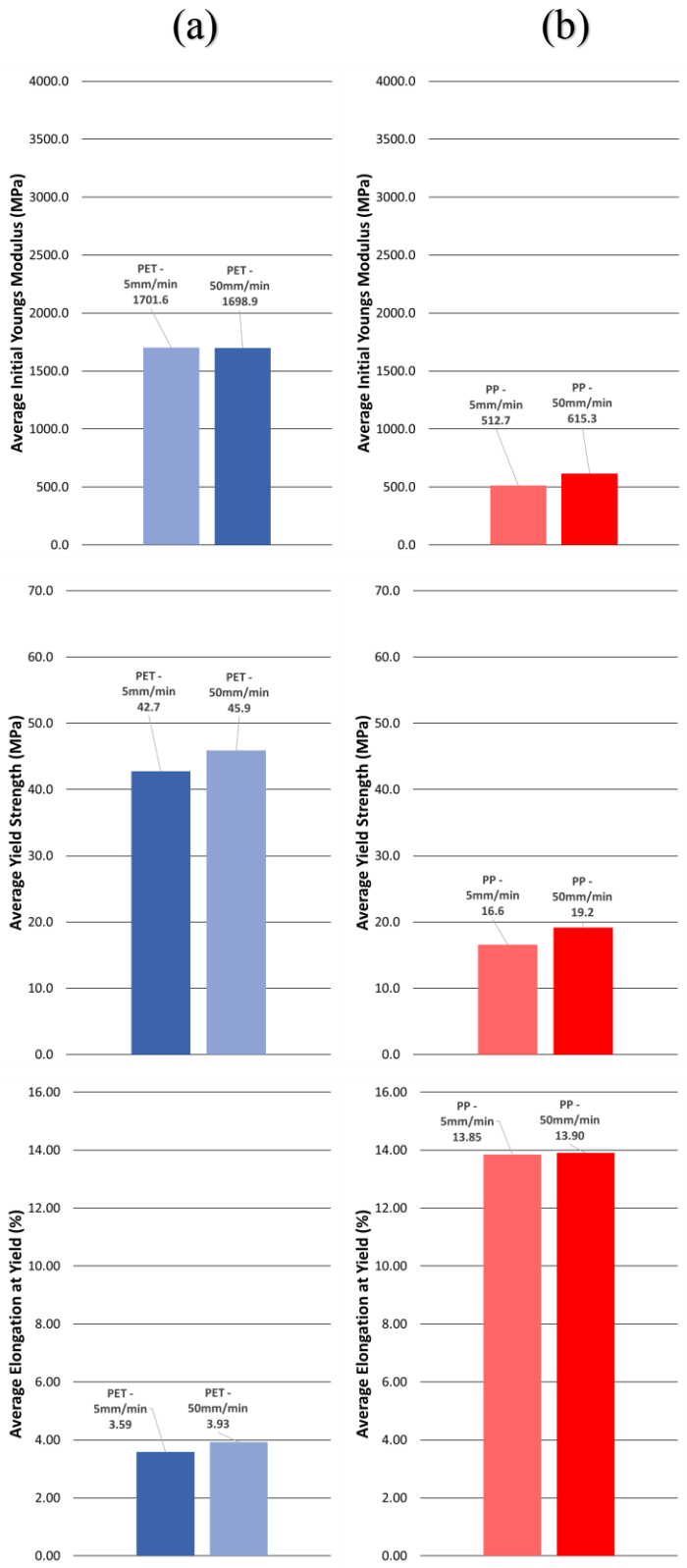

Figure 4.6 - Comparison of (a) re-PETG, (b) PP specimens regarding average initial Youngs modulus, average yield strength, and average elongation at yield

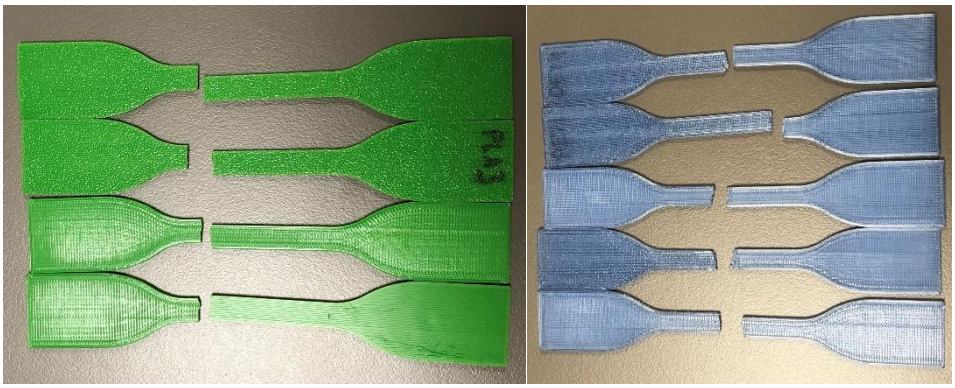

(a) (b)

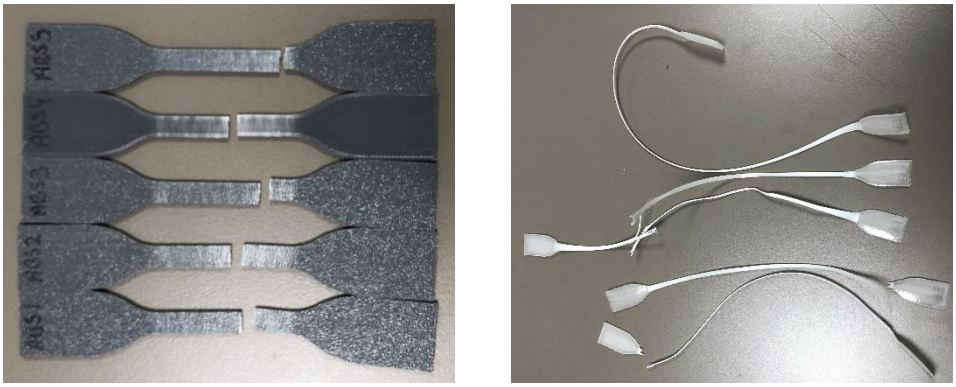

(c) (d)

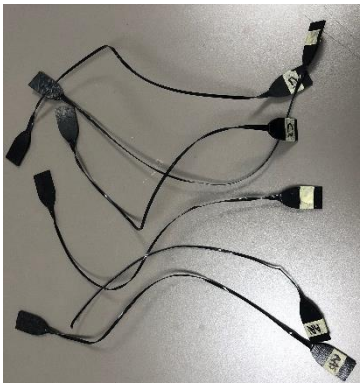

(e)

Figure 4.7 – Photographs of tensile test specimens after the test for (a)PLA, (b) re-PETG, (c) ABS, (d) PP, (e) HDPE

4.2 Interface Shear Test Results

For the evaluation of the replicability of PP geomembranes compared to HDPE geomembranes, two types of geomembrane specimens for PP and HDPE were prepared, as explained in Chapter 3.3. Using three different soil mixtures and two different soil densities for each soil mixture, direct shear tests were conducted using a 60 x 60 mm direct shear box. In this chapter, the results of these tests will be presented and discussed. It should be noted that vertical displacement vs. horizontal displacement plots of these tests is inconclusive due to small amounts of soil loss from the interface due to generated 2 mm gap between soil and geomembranes to prevent asperity collision and are shared in Appendix A.

Shear stress vs. horizontal displacement plots coupled with their related Mohr-Coulomb failure envelopes and friction coefficient vs. normal load plots are reported. Friction coefficients were calculated as:

$$\frac{\tau_u}{\sigma_n} = tan\delta \tag{4.1}$$

Where, σ_n is normal load, τ_u is the ultimate shear stress and, δ is the interface friction angle.

To compare HDPE and FDM manufactured PP, a series of indexes and a ratio is developed. Smooth Similarity(SS) and Asperity Similarity(AS) indexes quantify the difference between Efficiency values by mapping the data range to 0-100 interval and calculates the similarity between HDPE and PP tested under same conditions. Therefore, while a similarity value of 100% represents a perfect replication, 0% represents the minimum theoretical similarity. On the other hand, to assess and compare the implicit improvement provided by the asperities for HDPE and PP Improvement Ratio(IP) and Improvement Similarity(IS) is developed. IP quantifies ratio of the improvement to the Efficiency value of the smooth geomembrane. This

ratio is compared between HDPE and PP by calculating the IS value which follows the same mathematical logic as SS and AS. The formulations behind SS, AS, IS and IR are as follows:

$$Improvement\ Ratio(IR) = \frac{E_{asperity}}{E_{smooth}} \tag{4.2}$$

$$Improvement\ Similarity(IS) = 100 - \left(100 \times \frac{|IR_{HDPE} - IR_{PP}|}{MAX(IR_{HDPE}, IR_{PP})}\right) \tag{4.3}$$

$$Asperity\ Similarity(AS) = 100 - \left(100 \times \frac{\left|E_{asperity,HDPE} - E_{asperity,PP}\right|}{MAX\left(E_{asperity,HDPE}, E_{asperity,PP}\right)}\right) \tag{4.4}$$

$$Smooth\ Similarity(SS) = 100 - \left(100 \times \frac{\left|E_{smooth,HDPE} - E_{smooth,PP}\right|}{MAX\left(E_{smooth,HDPE}, E_{smooth,PP}\right)}\right) \tag{4.5}$$

Where E is the efficiency of the interface calculated using equation 2.2

4.2.1 Smooth Geomembrane Interface Shear Test Results

The result of smooth geomembrane tests using HDPE and PP geomembrane specimens are presented for each soil type as follows.

Figure 4.8, Figure 4.9, Figure 4.10 and Table 4.1 shows and compares the interface shear behavior of commercially available smooth HDPE geomembranes to FDM manufactured PP geomembranes interfaced with loose and dense soil conditions of Soil A. Peak shear stress values and a no cohesion assumption(zero-intercept) was used for assessment. By looking at these results, the decrease followed by an increase

of friction coefficient with increasing normal load for the dense soil vs. smooth HDPE geomembrane suggests raking starts to dominate after 100 kPa. The fact that all friction coefficient values of the smooth PP interface with no apparent contribution of raking due to the linearity of curves in Figure 4.9 suggests the surface roughness is the dominant mechanism for smooth PP interface. The increased effect of surface roughness is expected for FDM manufactured parts caused by the micro valleys and hills generated due to the manufacturing method. It can be seen that, especially for the dense condition of Soil A, this effect becomes much more pronounced leading to a poor performance in replication. By calculating the index SS as seen in equation 4.5, an 84.51% and 84.83% similarity for loose and dense conditions, respectively, is achieved in replication for this interface type. A comparison and overview related to the performance of Soil A is made in the following chapters.

Table 4.1 - Interface friction angle, efficiency and smooth similarity values for smooth geomembrane - soil A tests.

Interface Type	Soil A(Loose) - HDPE(Smooth)	Soil A(Loose) - PP(Smooth)	Soil A(Dense) - HDPE(Smooth)	Soil A(Dense) - PP(Smooth)
Interface Friction Angle (°)	25.3	29.2	27.7	31.7
Efficiency(%)	74	88	68	80
Smooth Similarity(%)	84.51		84.83	

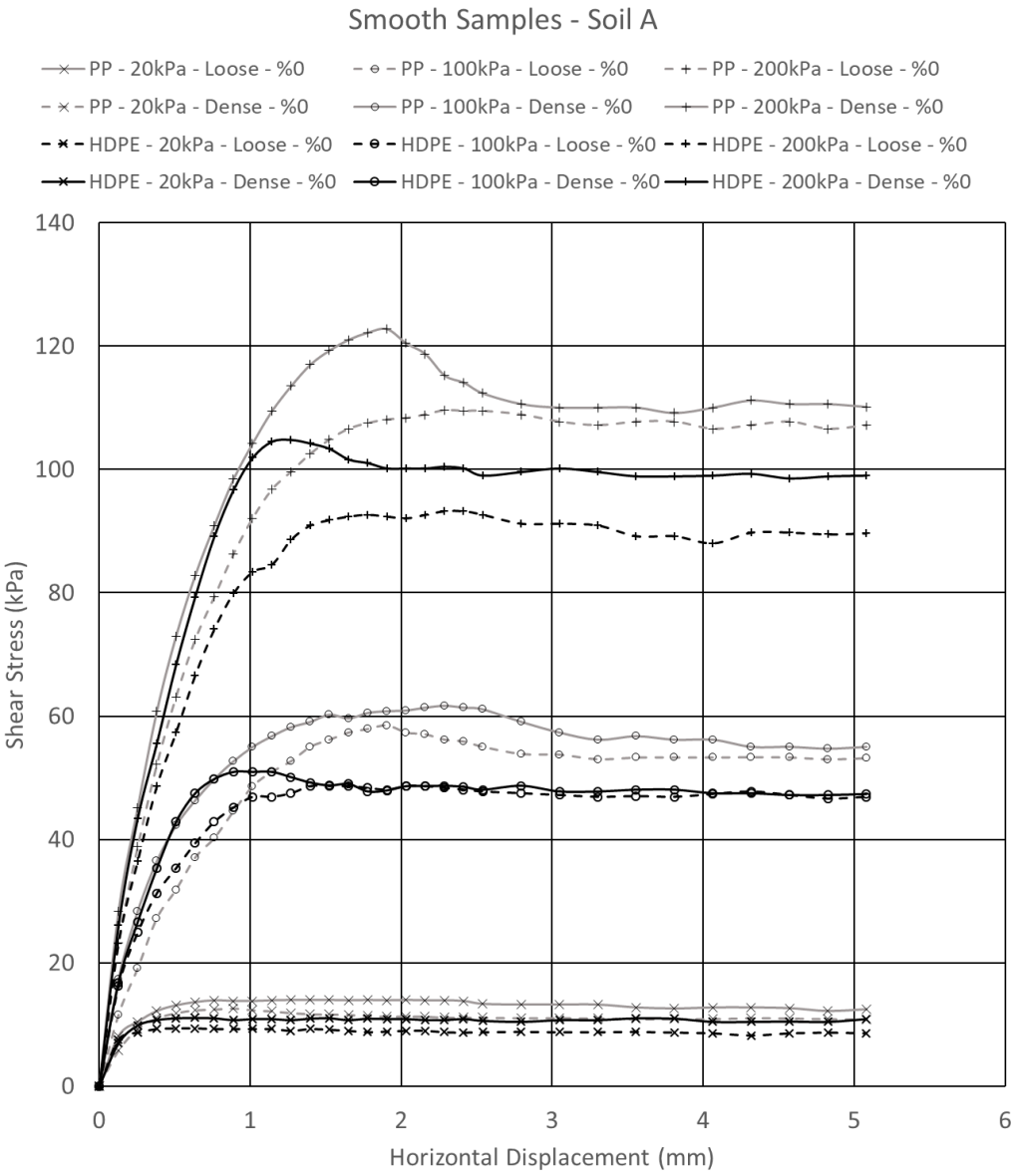

Figure 4.8 – Shear Stress vs. Horizontal Displacement curves of direct shear tests performed on smooth HDPE and PP geomembranes interfaced with soil A.

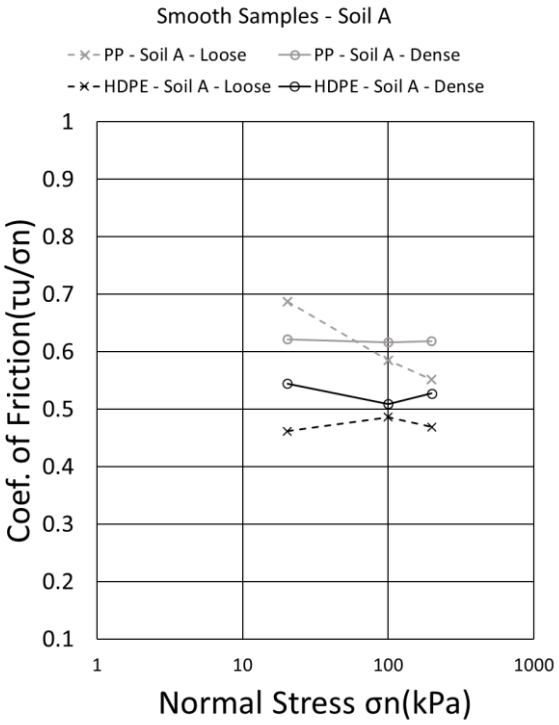

Figure 4.9 – Coefficient of friction vs. Normal Stress curves plotted using peak shear strength parameters of direct shear test for smooth HDPE and PP geomembranes interfaced with soil A.

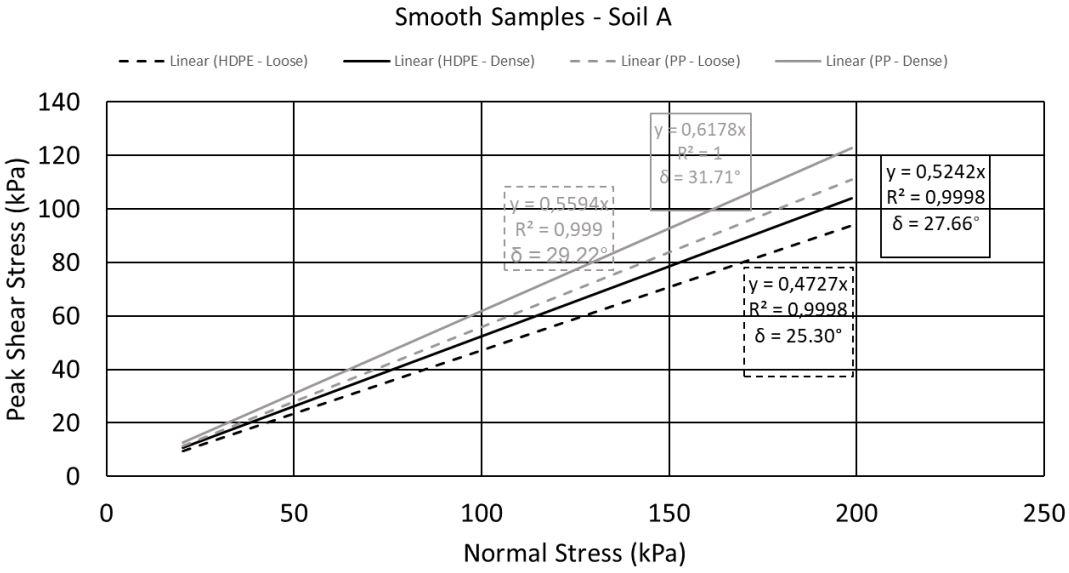

Figure 4.10 – Mohr – Coulomb failure envelopes of the direct shear tests performed on smooth HDPE and PP geomembranes interfaced with soil A.

Figure 4.11, Figure 4.12, Figure 4.13 and Table 4.2 shows and compares the interface shear behavior of commercially available smooth HDPE geomembranes to FDM manufactured PP geomembranes interfaced with loose and dense soil conditions of Soil B. Peak shear stress values and a no cohesion assumption(zero-intercept) was used for assessment. While some difference between HDPE and PP specimens, especially in dense soil conditions, increased similarity with the increase in fines content can be seen compared to Soil A. For both dense and loose soil conditions, the characteristic bi-linear curve of the raking mechanism can be seen in the PP specimen, while this behavior is only apparent in the dense soil condition for the HDPE specimen. Although an in-depth analysis should be performed to define the micro-mechanisms behind this behavior, it is evident that the increase of fine particles in the soil matrix compensates the lack of raking behavior that was observed in PP specimens coupled with Soil A. For this interface type, the SS index was calculated to achieve 89.78% and 94.92% similarity of replication for loose and dense soil conditions.

Table 4.2 - Interface friction angle, efficiency and smooth similarity values for smooth geomembrane - soil B tests.

Interface Type	Soil B(Loose) - HDPE(Smooth)	Soil B(Loose) - PP(Smooth)	Soil B(Dense) - HDPE(Smooth)	Soil B(Dense) - PP(Smooth)
Interface Friction Angle (°)	27.7	30.4	31.6	33.0
Efficiency(%)	77	86	64	67
Smooth Similarity(%)	89.78		94.92	

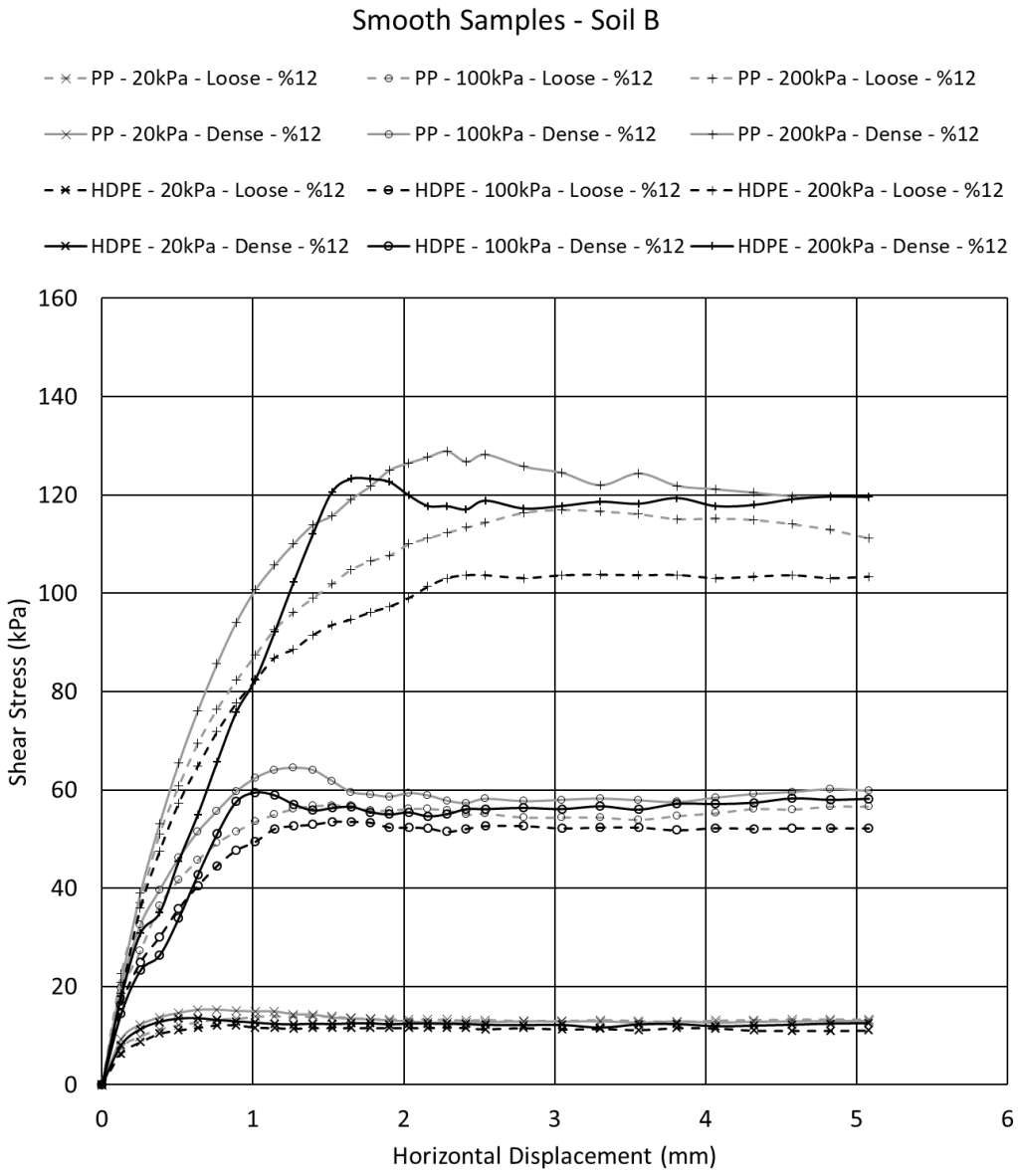

Figure 4.11 - Shear Stress vs. Horizontal Displacement curves of direct shear tests performed on smooth HDPE and PP geomembranes interfaced with soil B

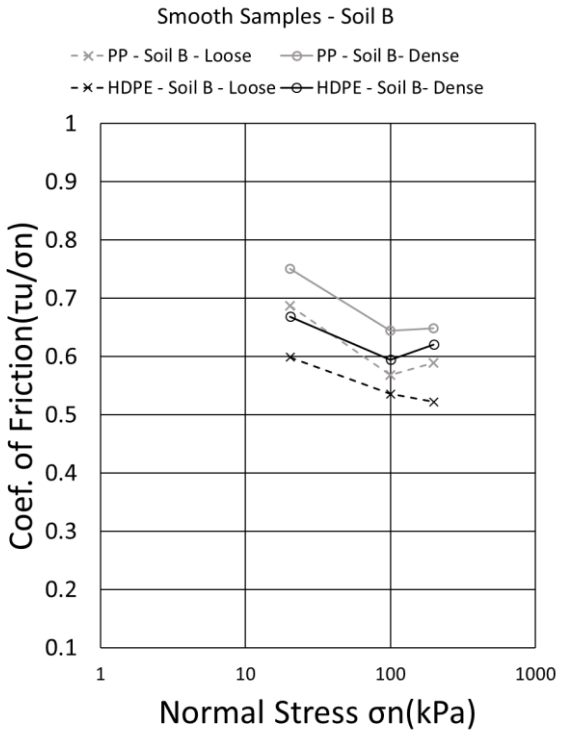

Figure 4.12 - Coefficient of friction vs. Normal Stress curves plotted using peak shear strength parameters of direct shear test for smooth HDPE and PP geomembranes interfaced with soil B.

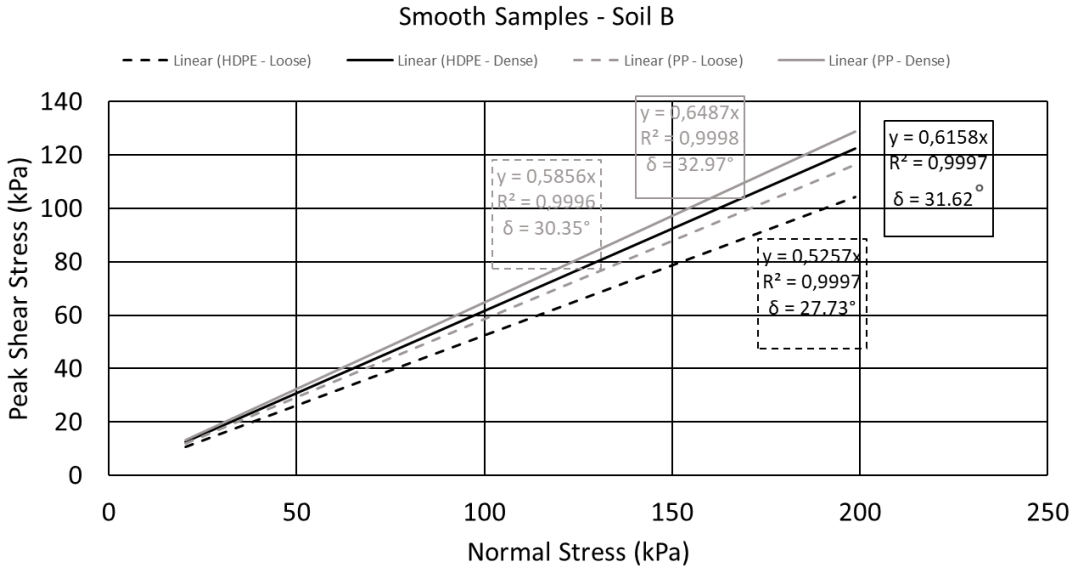

Figure 4.13 - Mohr – Coulomb failure envelopes of the direct shear tests performed on smooth HDPE and PP geomembranes interfaced with soil B.

Figure 4.14, Figure 4.15, Figure 4.16 and Table 4.3 shows and compares the interface shear behavior of commercially available smooth HDPE geomembranes to FDM manufactured PP geomembranes interfaced with loose and dense soil conditions of Soil C. Peak shear stress values and a no cohesion assumption(zero-intercept) was used for assessment. For both HDPE and PP specimens interfaced with Soil C, loose soil condition yields greater friction coefficient values compared to dense condition. With increased normal load, similar values in the coefficient of friction were maintained between loose and dense conditions of the soil. An exceptional jump of the coefficient of friction was observed in the dense soil condition on HDPE specimen under 200kPa normal load that might indicate a raking. Overall, this differentiation of shear behavior under 200kPa for both conditions of the same interface could be seen by analyzing the shear stress vs. horizontal displacement plots. Considering the increased bi-particle composition of Soil C compared to soils A and B, it might be argued that on higher normal load values, sand particles begin to dominate the soil matrix in terms of interface interaction. SS index values of 96.72% and 99.65% similarity of replication for loose and dense soil conditions suggest this behavior is replicated for both HDPE and PP specimens.

Table 4.3 - Interface friction angle, efficiency and smooth similarity values for smooth geomembrane - soil C tests.

Interface Type	Soil C(Loose) - HDPE(Smooth)	Soil C(Loose) - PP(Smooth)	Soil C(Dense) - HDPE(Smooth)	Soil C(Dense) - PP(Smooth)
Interface Friction Angle (°)	30.9	31.8	32.3	32.4
Efficiency(%)	86	89	67	68
Smooth Similarity(%)	96.72		99.65	

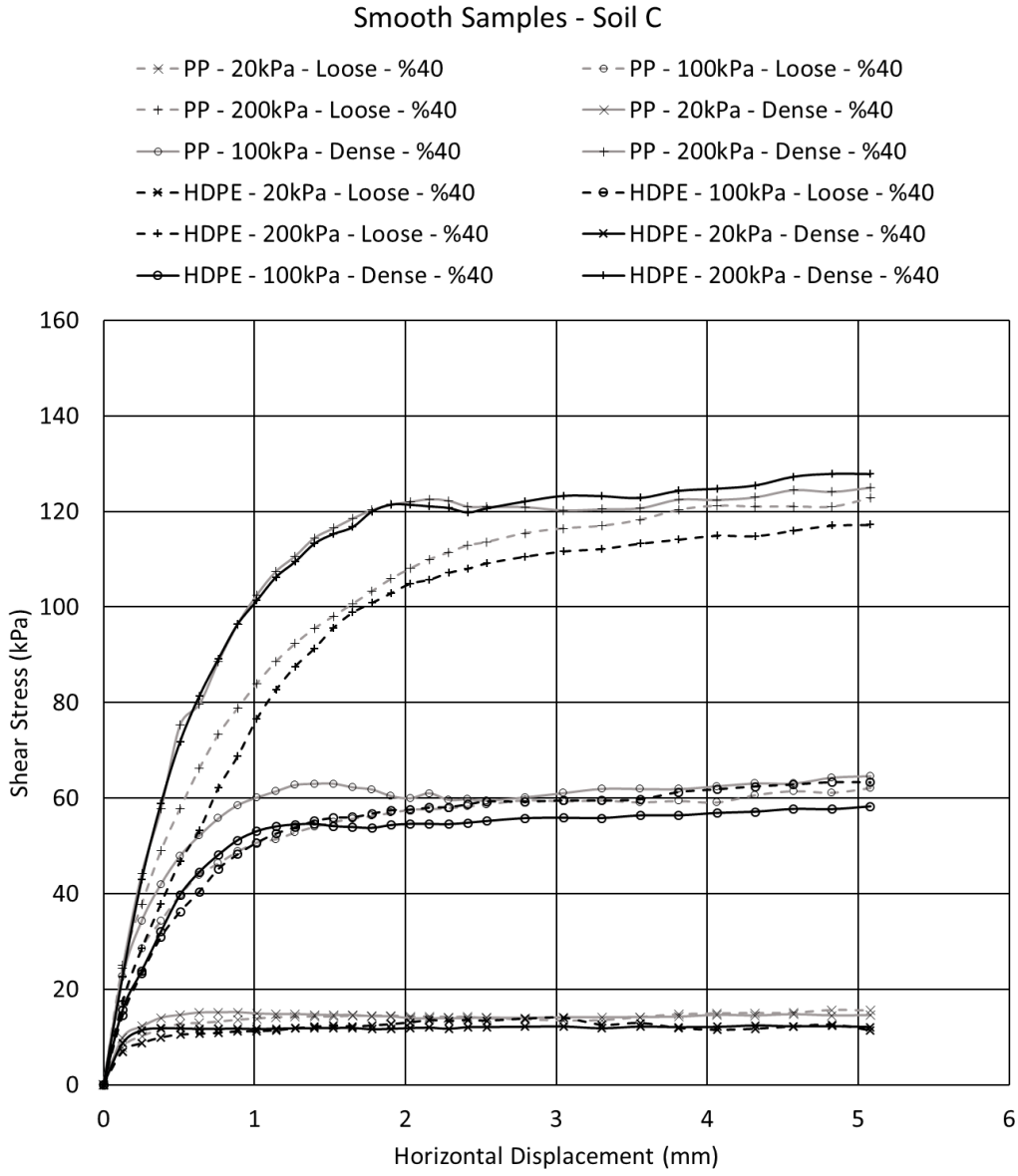

Figure 4.14 - Shear Stress vs. Horizontal Displacement curves of direct shear tests performed on smooth HDPE and PP geomembranes interfaced with soil C.

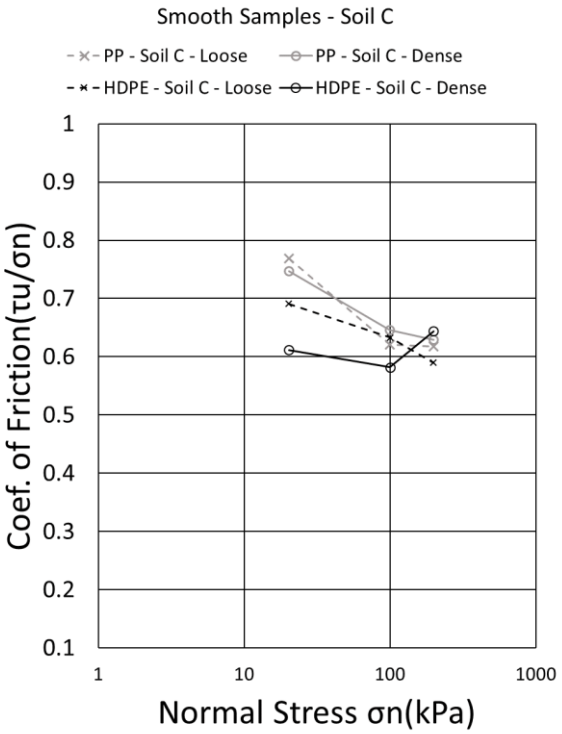

Figure 4.15 - Coefficient of friction vs. Normal Stress curves plotted using peak shear strength parameters of direct shear test for smooth HDPE and PP geomembranes interfaced with soil C.

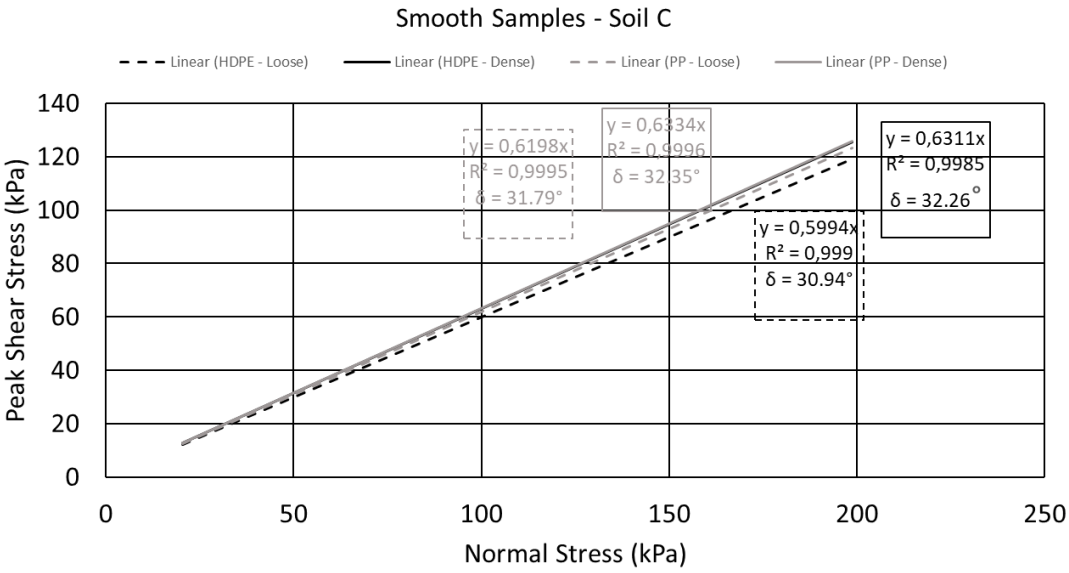

Figure 4.16 - Mohr – Coulomb failure envelopes of the direct shear tests performed on smooth HDPE and PP geomembranes interfaced with soil C.

4.2.2 Asperity Geomembrane Interface Shear Test Results

The result of asperity geomembrane tests using HDPE and PP geomembrane specimens are presented for each soil type as follows.

Figure 4.17, Figure 4.18, Figure 4.19 and Table 4.4 shows and compares the interface shear behavior of commercially available asperity HDPE geomembranes to FDM manufactured PP geomembranes interfaced with loose and dense soil conditions of Soil A. Peak shear stress values and a no cohesion assumption(zero-intercept) was used for assessment. Shear stress vs. horizontal displacement plots shows a similar behavior between HDPE and PP specimens under 20kPa and 100kPa normal loads while PP specimen shows an inflated peak shear stress for dense soil condition and a constant stress region for loose condition specimen under 200kPa normal load. The irregular behavior of this interface type was also noted in the repeatability section of Chapter 3.2. These dissimilarities in the shear behavior attenuate and converge with increasing horizontal displacement, resulting in similar post-peak behavior compared to HDPE specimens. On the other hand, comparing the shear behavior of other tests using Soil A near-exact replication could be argued. Considering the aforementioned irregularity, this argument is supported by AS index values showing 99.52% and 90.86% similarity between HDPE and PP specimens for loose and dense soil conditions, respectively.

Table 4.4 - Interface friction angle, efficiency and smooth similarity values for asperity geomembrane - soil A tests.

Interface Type	Soil A(Loose) - HDPE(Asperity)	Soil A(Loose) - PP(Asperity)	Soil A(Dense) - HDPE(Asperity)	Soil A(Dense) - PP(Asperity)
Interface Friction Angle (°)	30.6	30.7	30.6	33.1
Efficiency(%)	93	93	77	80
Asperity Similarity(%)	99.52		90.86	

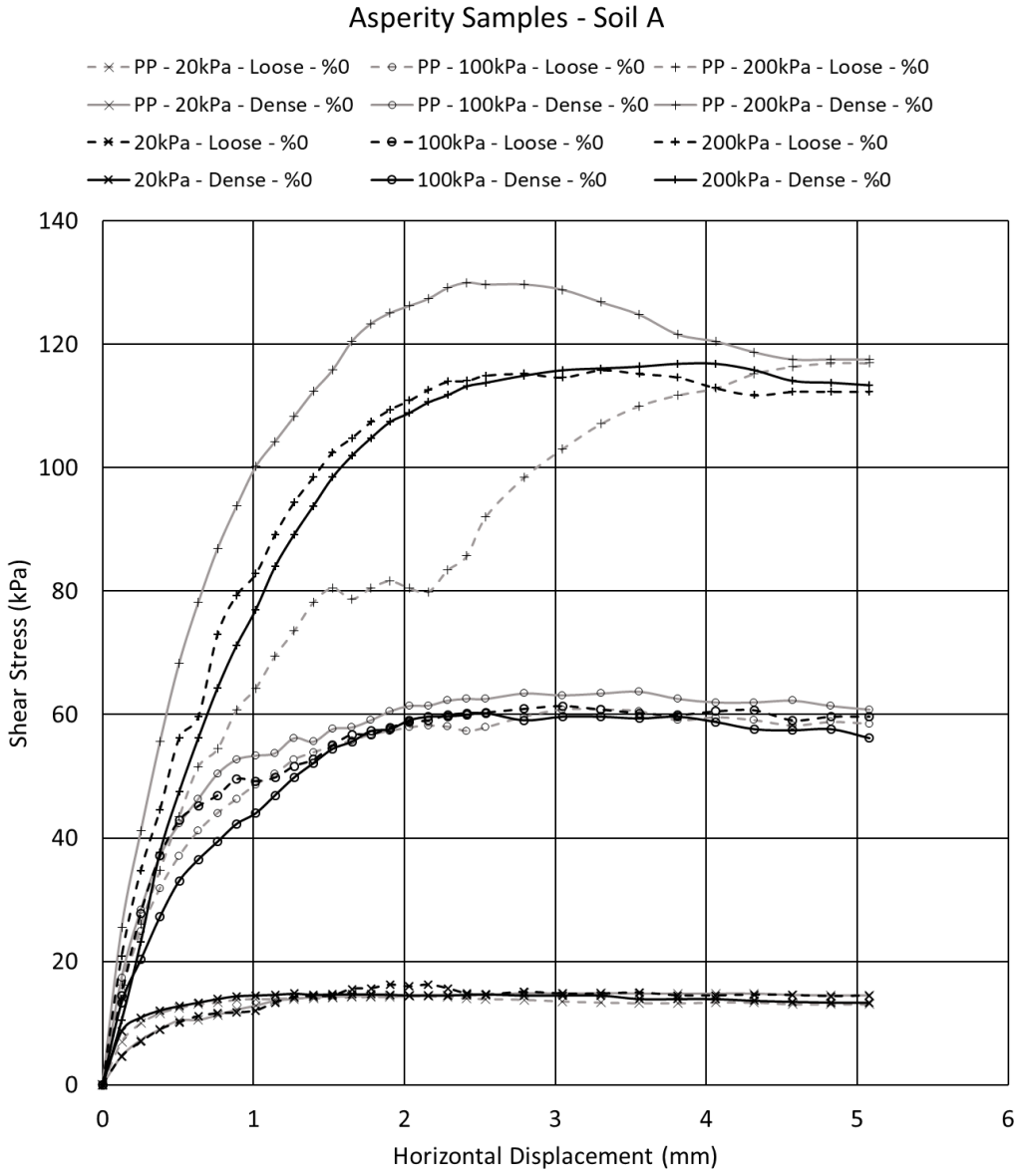

Figure 4.17 - Shear Stress vs. Horizontal Displacement curves of direct shear tests performed on asperity HDPE and PP geomembranes interfaced with soil A.

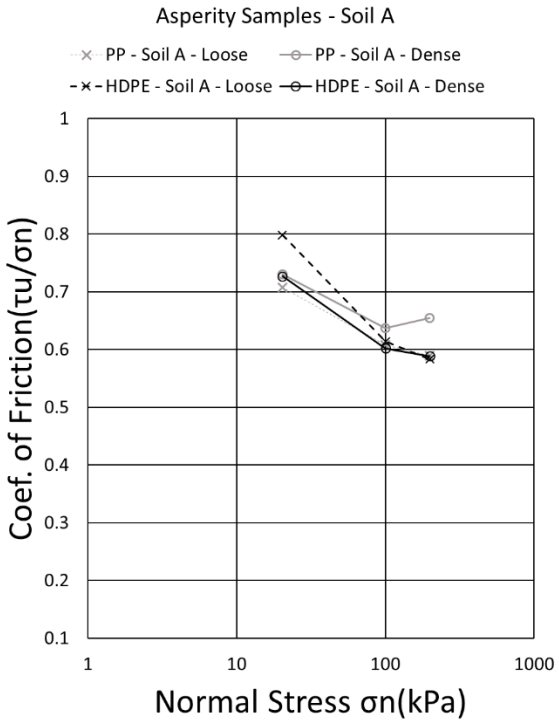

Figure 4.18 - Coefficient of friction vs. Normal Stress curves plotted using peak shear strength parameters of direct shear test for asperity HDPE and PP geomembranes interfaced with soil A.

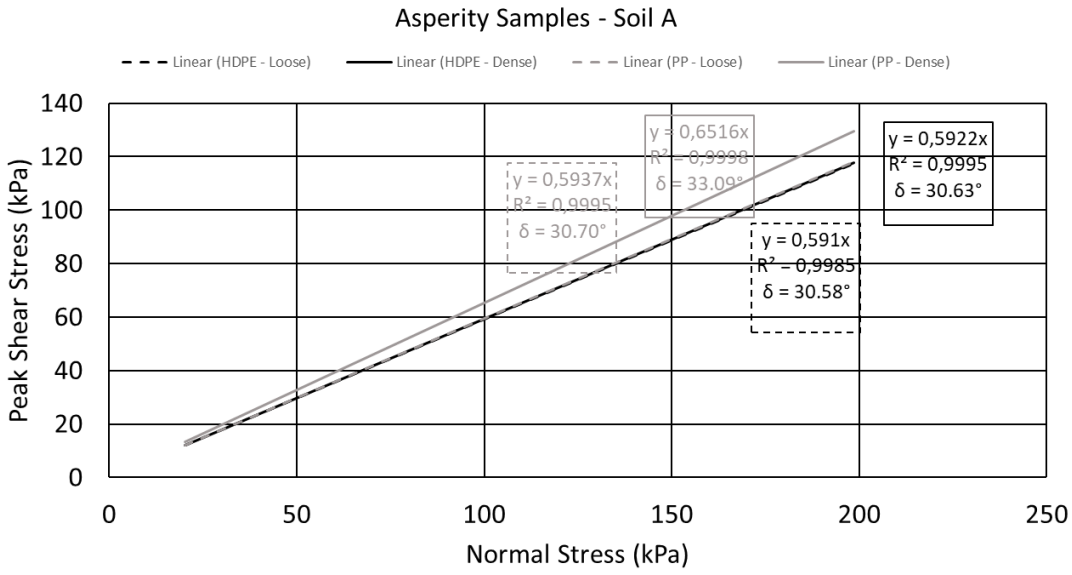

Figure 4.19 - Mohr – Coulomb failure envelopes of the direct shear tests performed on asperity HDPE and PP geomembranes interfaced with soil A.

Figure 4.20, Figure 4.21, Figure 4.22 and Table 4.5 shows and compares the interface shear behavior of commercially available asperity HDPE geomembranes to FDM manufactured PP geomembranes interfaced with loose and dense soil conditions of Soil B. Peak shear stress values and a no cohesion assumption(zero-intercept) was used for assessment. It can be seen in the plots that the density of soil B affects the shear behavior more compared to soils A and C. Shear stress vs. horizontal displacement and coefficient of friction plots looks almost identical between HDPE and PP specimens with the exception of loose soil condition under 200 kPa. Only for PP loose soil condition 200 kPa specimen, an increase in the coefficient of friction is observed. Comparing with smooth HDPE and PP specimens of the same soil type, a similar but upshifted behavior could also be seen. AS of 90.24% and 98.59% similarity between HDPE and PP specimens is reported for loose and dense soil conditions, respectively.

Table 4.5 - Interface friction angle, efficiency and smooth similarity values for asperity geomembrane - soil B tests.

Interface Type	Soil B(Loose) - HDPE(Asperity)	Soil B(Loose) - PP(Asperity)	Soil B(Dense) - HDPE(Asperity)	Soil B(Dense) - PP(Asperity)
Interface Friction Angle (°)	30.2	32.8	34.2	34.5
Efficiency(%)	85	95	70	71
Asperity Similarity(%)	90.24		98.59	

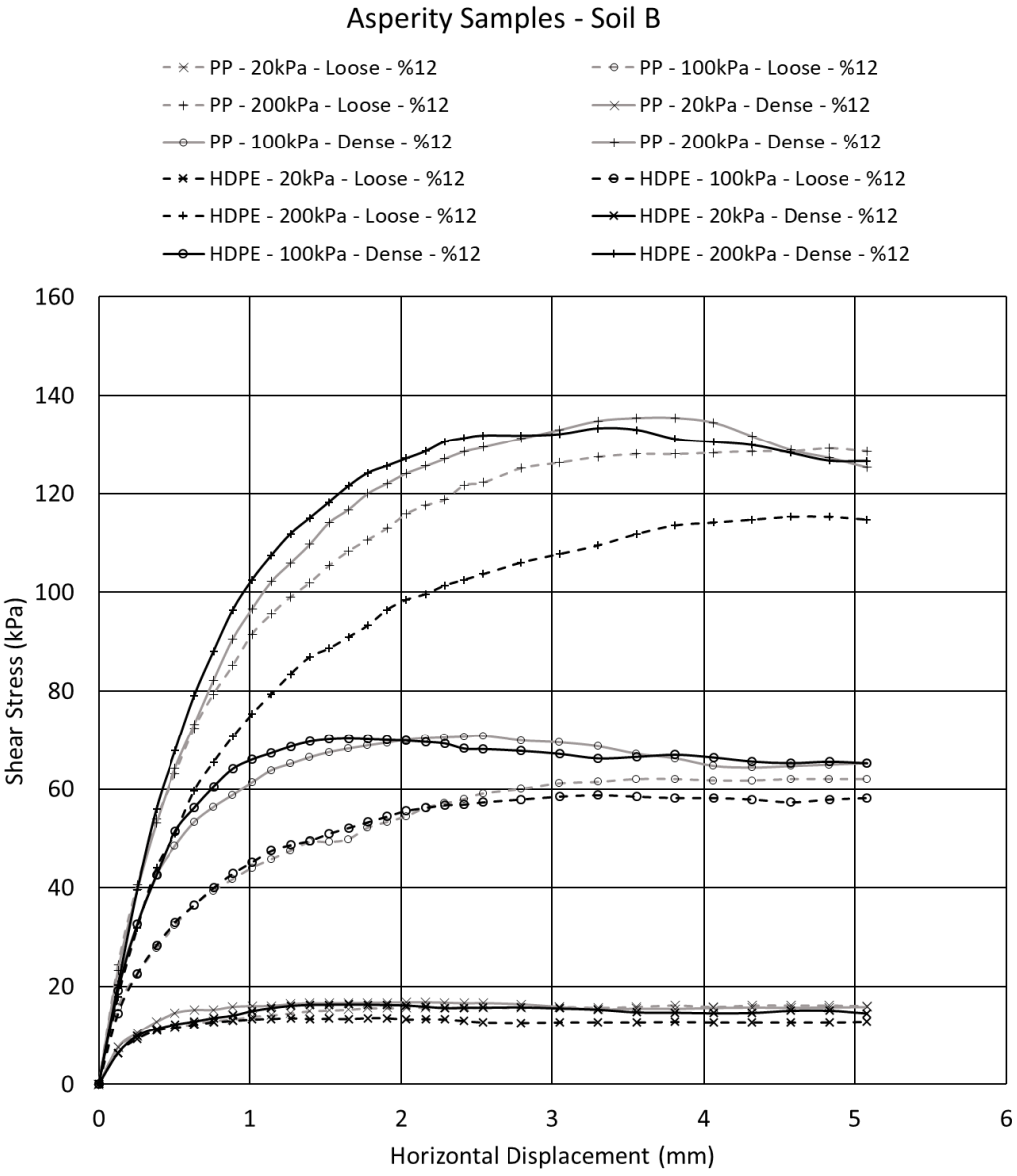

Figure 4.20 - Shear Stress vs. Horizontal Displacement curves of direct shear tests performed on asperity HDPE and PP geomembranes interfaced with soil B

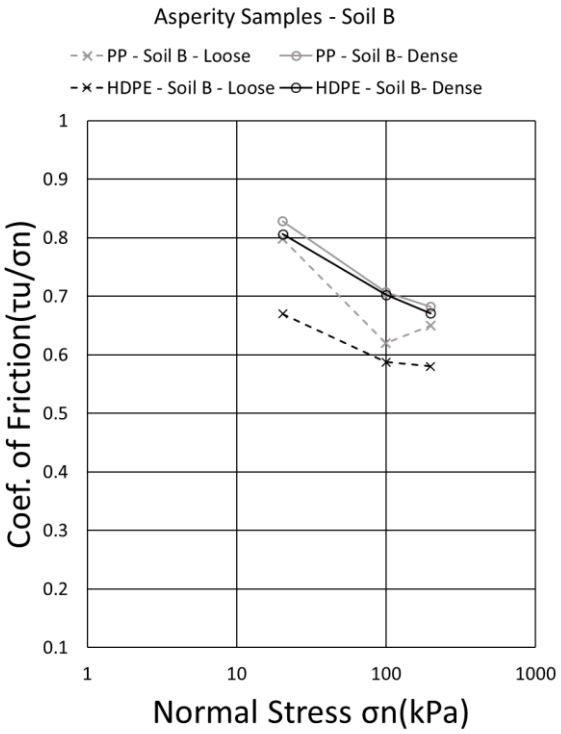

Figure 4.21 - Coefficient of friction vs. Normal Stress curves plotted using peak shear strength parameters of direct shear test for asperity HDPE and PP geomembranes interfaced with soil B.

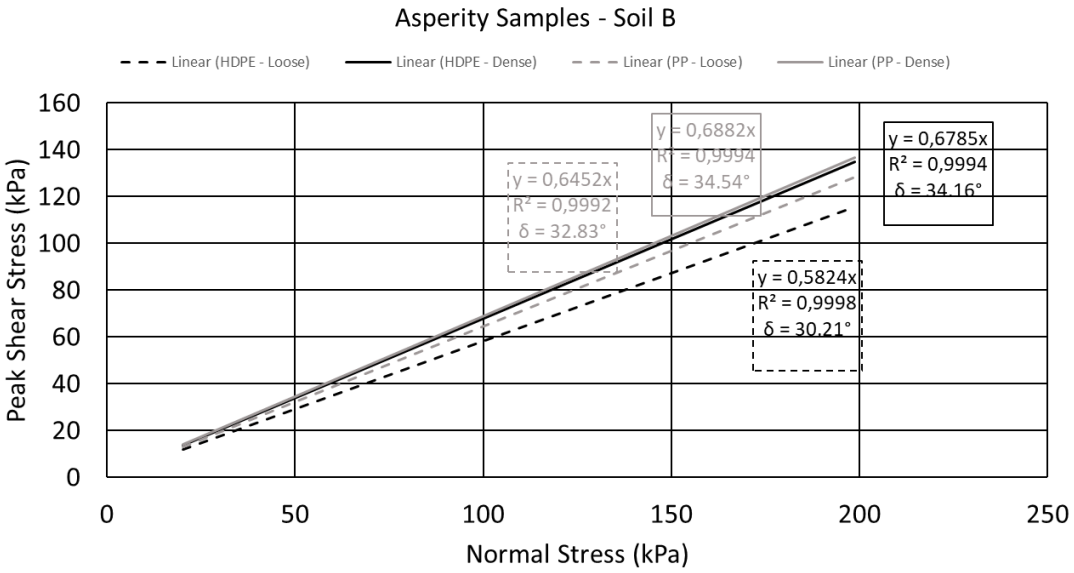

Figure 4.22 - Mohr – Coulomb failure envelopes of the direct shear tests performed on asperity HDPE and PP geomembranes interfaced with soil B.

Figure 4.23, Figure 4.24, Figure 4.25 and Table 4.6 shows and compares the interface shear behavior of commercially available asperity HDPE geomembranes to FDM manufactured PP geomembranes interfaced with loose and dense soil conditions of Soil C. Peak shear stress values and a no cohesion assumption(zero-intercept) was used for assessment. Similar shear behavior can be observed in shear stress vs. horizontal displacement and coefficient of friction plots. A minor increase in the peak shear strength with the increase in density of HDPE specimens for 100kPa and 200kPa tests is observed. No effect of soil density was observed for the PP specimens, as seen in both plots. Overall, for this soil type, PP replicated HDPE geomembranes for both soil densities better compared to soils A and B. The AS for this soil type is calculated to be 94.86% and 98.70% similarity between HDPE and PP specimens.

Table 4.6 - Interface friction angle, efficiency and smooth similarity values for asperity geomembrane - soil C tests.

Interface Type	Soil C(Loose) - HDPE(Asperity)	Soil C(Loose) - PP(Asperity)	Soil C(Dense) - HDPE(Asperity)	Soil C(Dense) - PP(Asperity)
Interface Friction Angle (°)	33.8	35.2	34.3	34.6
Efficiency(%)	96	101	73	74
Asperity Similarity(%)	94.86		98.70	

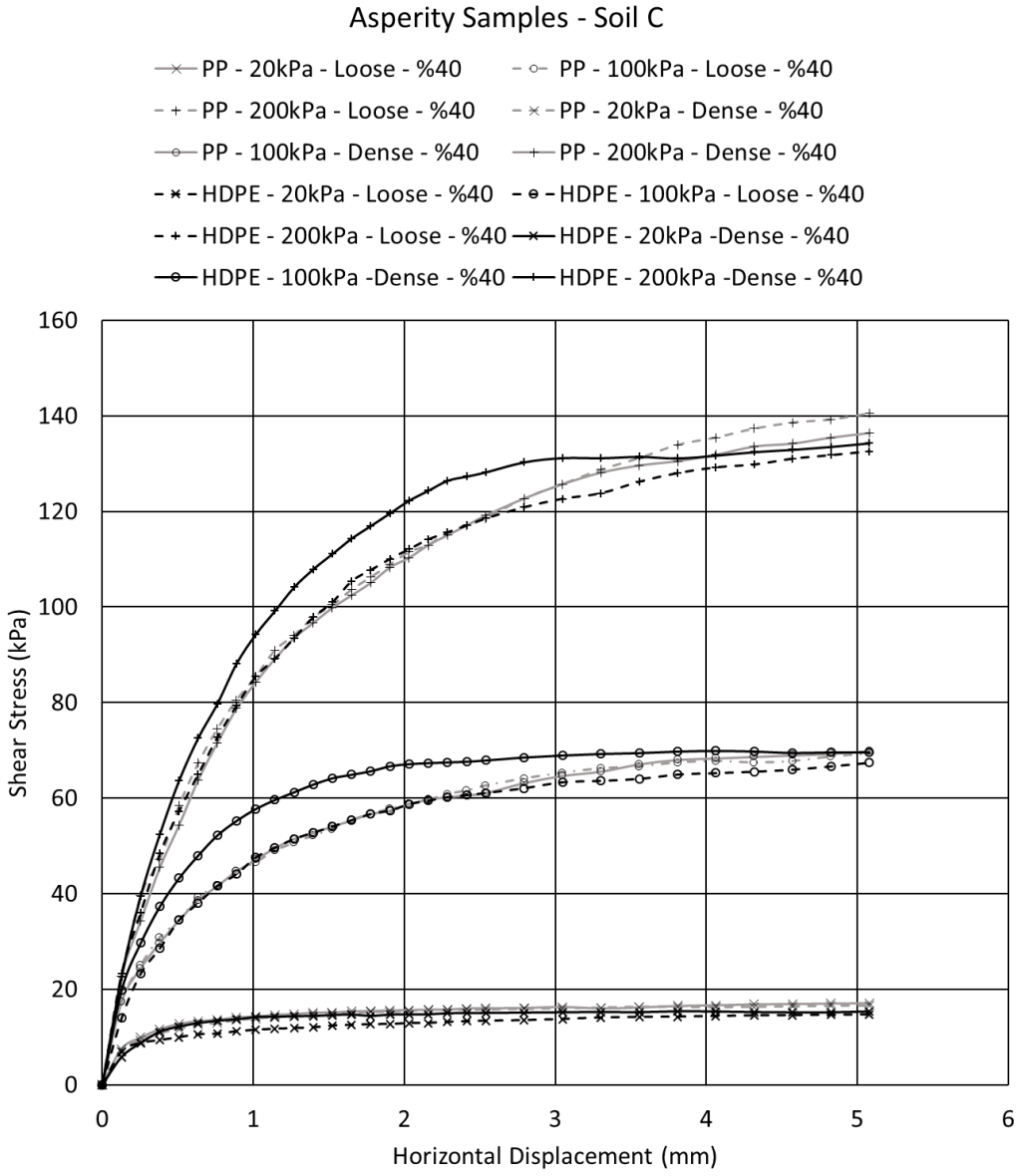

Figure 4.23 - Shear Stress vs. Horizontal Displacement curves of direct shear tests performed on asperity HDPE and PP geomembranes interfaced with soil C

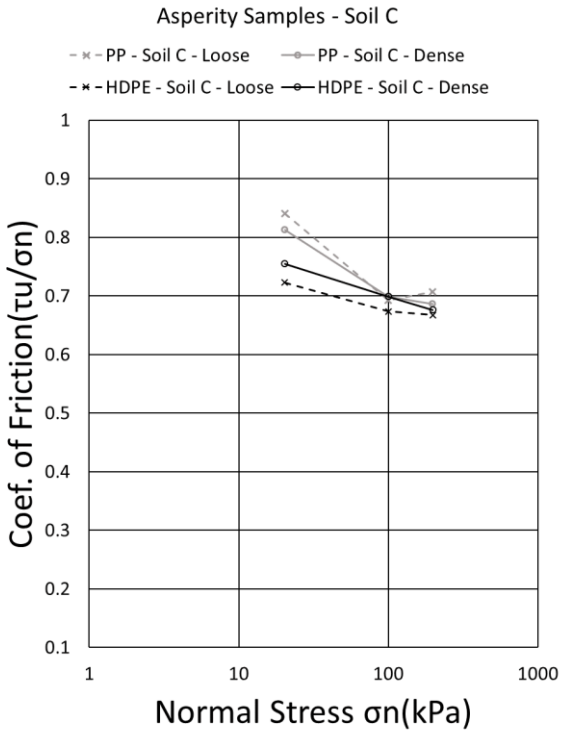

Figure 4.24 - Coefficient of friction vs. Normal Stress curves plotted using peak shear strength parameters of direct shear test for asperity HDPE and PP geomembranes interfaced with soil C.

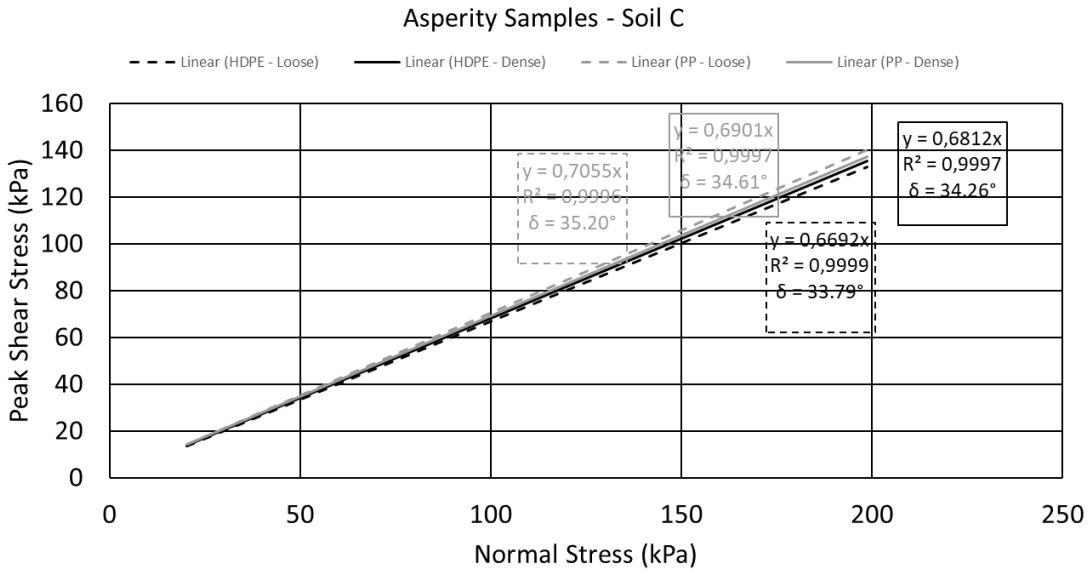

Figure 4.25 - Mohr – Coulomb failure envelopes of the direct shear tests performed on asperity HDPE and PP geomembranes interfaced with soil B.

4.2.3 Cross-Comparison and Overview

Table 4.7 shows the calculated similarity indexes, efficiencies, and improvement ratios of tested geomembrane specimens for Soil A, B, and C. Figure 2.6 compares and sorts the soil and interface types in a descending order of similarity values. An overall view to the replication performance of soil types is presented in this manner. In terms of this overall performance interfaces involving Soil A proved to be the least similar interface type especially for smooth geomembranes. While interfaces with asperities yield higher similarity values for Soil A, this difference between smooth and asperity similarities for Soil A causes a lower performance in terms of improvement similarity. On the other hand, soils B and C performed better in terms of replication of both asperity and smooth geomembrane interface types as seen in the similarity values, therefore FDM manufactured PP is promising for the use in replication and improving studies of geomembrane and geomembrane asperity studies for soils . The inadequate replication performance of Soil A which is a sand with a sub-angular particle shape coupled with an FDM manufactured PP could be attributed to the micro mechanisms and faults especially involved in FDM manufactured smooth geomembranes. An in depth study related to this interface type is needed to fully understand the shear behavior. Future work recommendations in the following chapter addresses possible causes that needs further study including poor surface roughness generated by FDM technique, particle shape, material and loading conditions.

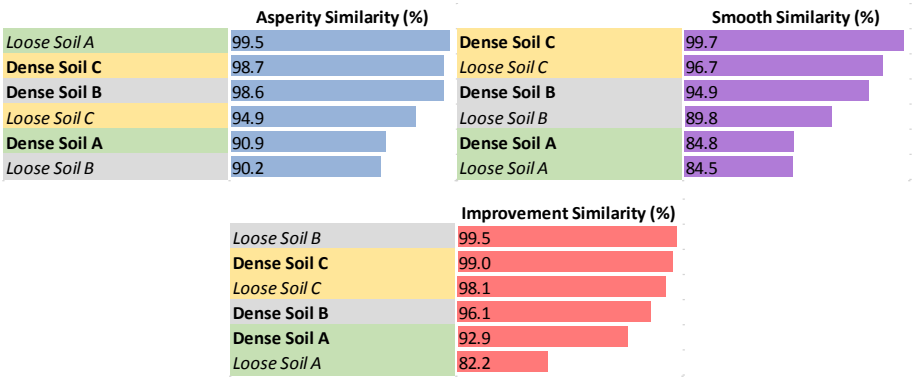

Figure 4.26 – Similarity index values for all soil types.

Table 4.7 - Calculated similarity indexes, efficiencies, and improvement ratios of tested geomembrane specimens for (a) Soil A; (b) Soil B; (c) Soil C

a)

	Loose Soil A - PP(S)	Loose Soil A - PP(A)	Loose Soil A - HDPE(S)	Loose Soil A - HDPE(A)	Dense Soil A - PP(S)	Dense Soil A - PP(A)	Dense Soil A - HDPE(S)	Dense Soil A - HDPE(A)
Internal Friction Angle (°)	32.54				37.71			
Interface Friction Angle (°)	29.22	30.7	25.3	30.58	31.71	33.09	27.66	30.63
Efficiency	0.88	0.93	0.74	0.93	0.80	0.84	0.68	0.77
Improvement Ratio	1.06		1.25		1.05		1.13	
Improvement Similarity (%)	82.23				92.89			
Asperity Similarity (%)	99.52				90.86			
Smooth Similarity (%)	84.51				84.83			

b)

	Loose Soil B - PP(S)	Loose Soil B - PP(A)	Loose Soil B - HDPE(S)	Loose Soil B - HDPE(A)	Dense Soil B - PP(S)	Dense Soil B - PP(A)	Dense Soil B - HDPE(S)	Dense Soil B - HDPE(A)
Internal Friction Angle (°)	34.27				44.05			
Interface Friction Angle (°)	30.35	32.83	27.73	30.21	32.97	34.54	31.62	34.16
Efficiency	0.86	0.95	0.77	0.85	0.67	0.71	0.64	0.70
Improvement Ratio	1.10		1.11		1.06		1.10	
Improvement Similarity (%)	99.48				96.13			
Asperity Similarity (%)	90.24				98.59			
Smooth Similarity (%)	89.78				94.92			

c)

	Loose Soil C - PP(S)	Loose Soil C - PP(A)	Loose Soil C - HDPE(S)	Loose Soil C - HDPE(A)	Dense Soil C - PP(S)	Dense Soil C - PP(A)	Dense Soil C - HDPE(S)	Dense Soil C - HDPE(A)
Internal Friction Angle (°)	34.9				43.1			
Interface Friction Angle (°)	31.79	35.2	30.94	33.79	32.35	34.61	32.26	34.26
Efficiency	0.89	1.01	0.86	0.96	0.68	0.74	0.67	0.73
Improvement Ratio	1.14		1.12		1.09		1.08	
Improvement Similarity (%)	98.08				99.04			
Asperity Similarity (%)	94.86				98.70			
Smooth Similarity (%)	96.72				99.65			

CHAPTER 5

SUMMARY & CONCLUSIONS

In this study, a brief literature review on geosynthetics and novel geosynthetics emphasizing the importance and necessity of innovation in the geosynthetics field is presented. Essential literature on soil – interface mechanism studies are also reviewed and emphasized. Additive manufacturing, especially the Fused Deposition Modelling (FDM) technique, is briefly explained, followed by a state of the art analysis on the applications of additive manufacturing in the geotechnical engineering and geosynthetics field is reported. By reviewing the literature, it is observed that further study for the use of FDM additive manufacturing, which is a simple, efficient and cheap technique compared to other additive manufacturing techniques, in the replication of HDPE geosynthetic interfaces is an area that is both promising and unexplored due to difficulties regarding manufacturing practices concerning relevant materials such as HDPE and PP. For this purpose, using four different FDM manufactured materials, three of which are commonly used in the FDM manufacturing field, namely; PLA, ABS and re-PETG, and a more challenging but essential FDM material, PP was selected to be compared in tensile strength test with smooth and asperity HDPE geomembrane samples.

As a result of the comparison in terms of tensile strength, FDM manufactured PP material is observed to behave very similarly in tensile properties to HDPE samples. It was also observed that HDPE geomembranes lose some of their tensile strength during extrusion and application of asperities. This similar behavior in tensile strength behavior between PP and HDPE samples implied promising results could be achieved using PP as an HDPE replicant in geomembrane - soil interface shear tests. For this purpose, 72 60 x 60 mm direct shear tests were conducted. Half of

these tests are conducted on factory manufactured, benchmark HDPE geomembranes with smooth and asperity surface compositions, while the other half are conducted on FDM manufactured PP geomembrane specimens 3D modeled after the benchmark HDPE geomembranes. For these interface tests, three different soil mixtures are prepared with increasing fines content using Çine sand, which is sub-angular sand and non-plastic silt. These three soil mixtures were also prepared in the shear box assembly using two different soil densities for each soil mixture. To simplify the comparison of the similarity between HDPE and PP specimens, three comparison indexes are calculated, namely, Asperity Similarity(AS), Smooth Similarity(SS), and Improvement Similarity(IS). As a result of these tests, while PP showed promising and comparable results in replication of HDPE samples for all soil mixtures interfaced with geomembranes with asperities, some amount of deviation is observed in soil mixture A, which consists only of sub-angular Çine sand, interfaced with smooth PP geomembrane especially under higher normal loads. This deviation is attributed to the elevated effect of the raking mechanism provided by sub-angular sand coupled with the rougher surface profile that is a known characteristic defect of FDM manufactured parts. While no comparable data could be found in the literature, a previous study was conducted on Çine sand using the same density values that are interfaced with PLA and ABS specimens(Uragan & Huvaj, 2018). By looking at the results of that study, PLA specimens compare excellently in terms of SS with values of 98.67% and 97.05% for loose and dense specimens, respectively. This similarity is argued to be caused by the absence of raking but increased sliding resistance caused by the increased roughness caused by the FDM technique of the PLA specimens compared to HDPE specimens. Further research is needed to fully understand the behavior of soil and FDM manufactured interfaces.

For future research, the following research objectives could be pursued;

- The surface treatment of FDM manufactured geomembrane prototypes and the effects on interface shear properties.
- Replication of asperity geomembranes using FDM materials other than PP. Such as PA, TPU, PLA, ABS, etc.
- Effect of higher normal loads on the interface properties of PP geomembranes, especially interfaced with sands of different angularities.
- The replicability of different asperity types using PP and the potential effects on the similarity index AS.

REFERENCES

Adamidis, O., Alber, S., & Anastasopoulos, I. 2020. Assessment of Three-Dimensional Printing of Granular Media for Geotechnical Applications. Geotechnical Testing Journal, 43(3), 641–659. https://doi.org/10.1520/GTJ20180259

Agerschou, H. A. 1961. Synthetic material filters in coastal protection. Journal of the Waterways and Harbors Division, 87(1), 111–124.

Alsoufi, M., & El-Sayed, A. 2017. Warping Deformation of Desktop 3D Printed Parts Manufactured by Open Source Fused Deposition Modeling (FDM) System. International Journal of Mechanical & Mechatronics Engineering, 17, 7–16.

Amurane, I., Zhang, M., Li, T., & Jiang, H. 2019. Optimization of 3D printed geocells based on numerical simulation and experimental investigation. IOP Conference Series: Earth and Environmental Science, 233, 32043. https://doi.org/10.1088/1755-1315/233/3/032043

Arab, M. G., Maher, O., Emran, A., Omar, M., Marwan, N., & Osama, B. 2020. Bio-Inspired 3D-Printed Honeycomb for Soil Reinforcement. In *Geo-Congress 2020* (pp. 262–271). https://doi.org/doi:10.1061/9780784482834.029

ASTM International. 2004. *D3080-04 Standard Test Method for Direct Shear Test of Soils Under Consolidated Drained Conditions*. ASTM International. https://doi.org/https://doi.org/10.1520/D3080-04

ASTM International. 2015. *ISO/ASTM52900-15 Standard Terminology for Additive Manufacturing – General Principles – Terminology*. ASTM International. https://doi.org/https://doi.org/10.1520/ISOASTM52900-15

ASTM International. 2017. D6913/D6913M-17 Standard Test Methods for Particle-Size Distribution (Gradation) of Soils Using Sieve Analysis. In *ASTM International, West Conshohocken, PA,* (Vol. 04, Issue Reapproved 2009). ASTM International. https://doi.org/https://doi.org/10.1520/D6913_D6913M-

17

ASTM International. 2018. ASTM D4439-18 Standard Terminology for Geosynthetics. https://doi.org/https://doi.org/10.1520/D4439-18

ASTM International. 2020a. *ASTM Volume 04.13 Geosynthetics*.

ASTM International. 2020b. *D6693/D6693M-20 Standard Test Method for Determining Tensile Properties of Nonreinforced Polyethylene and Nonreinforced Flexible Polypropylene Geomembranes.* ASTM International. https://doi.org/https://doi.org/10.1520/D6693_D6693M-20

Bachhar, N., Gudadhe, A., Kumar, A., Andrade, P., & Kumaraswamy, G. 2020. 3D printing of semicrystalline polypropylene: towards eliminating warpage of printed objects. Bulletin of Materials Science, 43(1), 171. https://doi.org/10.1007/s12034-020-02097-4

Bikas, H., Stavropoulos, P., & Chryssolouris, G. 2016. Additive manufacturing methods and modelling approaches: a critical review. The International Journal of Advanced Manufacturing Technology, 83(1–4), 389–405.

Blond, E., Boyle, S., Ferrara, M., Herlin, B., Plusquellec, H., Rimoldi, P., & Stark, T. 2019. Applications of Geosynthetics to Irrigation, Drainage and Agriculture. Irrigation and Drainage, 68(1), 67–83. https://doi.org/10.1002/ird.2300

Briscoe, B. J. 1992. Friction of Organic Polymers. In I. L. Singer & H. M. Pollock (Eds.), *Fundamentals of Friction: Macroscopic and Microscopic Processes* (pp. 167–182). Springer Netherlands. https://doi.org/10.1007/978-94-011-2811-7_9

Carneiro, O. S., Silva, A. F., & Gomes, R. 2015. Fused deposition modeling with polypropylene. Materials & Design, 83, 768–776. https://doi.org/https://doi.org/10.1016/j.matdes.2015.06.053

Chong, S., Pan, G.-T., Khalid, M., Yang, T. C.-K., Hung, S.-T., & Huang, C.-M. 2017. Physical Characterization and Pre-assessment of Recycled High-Density Polyethylene as 3D Printing Material. Journal of Polymers and the

Environment, 25(2), 136–145. https://doi.org/10.1007/s10924-016-0793-4

Dove, J. E., & Frost, J. D. 1999. Peak Friction Behaviour of Smooth Geomembrane-Particle Inerfaces. Journal of Geotechnical and Geoenvironmental Engineering, *July*, 544–555. https://doi.org/10.1061/(ASCE)1090-0241(1999)125:7(544)

Feligha, M., Hammoud, F., Belachia, M., & Nouaouria, M. S. 2016. Experimental Investigation of Frictional Behavior Between Cohesive Soils and Solid Materials Using Direct Shear Apparatus. Geotechnical and Geological Engineering, 34(2), 567–578. https://doi.org/10.1007/s10706-015-9966-5

Fleming, I. R., Sharma, J. S., & Jogi, M. B. 2006. Shear strength of geomembrane–soil interface under unsaturated conditions. Geotextiles and Geomembranes, 24(5), 274–284. https://doi.org/https://doi.org/10.1016/j.geotexmem.2006.03.009

Fowmes, Gary J, Dixon, N., Zaharescu, A., & Fu, L. 2016. 3D printing of high-strength geosynthetic interfaces. GeoAmericas 2016 Proceedings, 2, 1698–1708.

Fowmes, Gary John, Dixon, N., Fu, L., & Zaharescu, C. A. 2017. Rapid prototyping of geosynthetic interfaces: Investigation of peak strength using direct shear tests. Geotextiles and Geomembranes, 45(6), 674–687. https://doi.org/10.1016/j.geotexmem.2017.08.009

Frost, J. D., DeJong, J. T., & Recalde, M. 2002. Shear failure behavior of granular–continuum interfaces. Engineering Fracture Mechanics, 69(17), 2029–2048. https://doi.org/https://doi.org/10.1016/S0013-7944(02)00075-9

Gilbert, M. 2017. Plastics Materials : Introduction and Historical Development. 1–18. https://doi.org/10.1016/B978-0-323-35824-8.00001-3

Hanaor, D. A. H., Gan, Y., Revay, M., Airey, D. W., & Einav, I. 2016. 3D printable geomaterials. Géotechnique, 66(4), 323–332. https://doi.org/10.1680/jgeot.15.P.034

Hebeler, G L, Frost, J. D., & Myers, A. T. 2005. Quantifying hook and loop

interaction in textured geomembrane–geotextile systems. Geotextiles and Geomembranes, 23(1), 77–105. https://doi.org/https://doi.org/10.1016/j.geotexmem.2004.06.002

Hebeler, Gregory L. 2005. *Multi-scale behavior at geomaterial interfaces*. Georgia Institute of Technology.

Hull, C. W. 1984. *Apparatus for production of three-dimensional objects by stereolithography*.

Jones, C., Lamont-Black, J., Huntley, D., Alder, D., & Glendinning, S. 2017. Electrokinetic geosynthetics: from research to hype to practice. Proceedings of the Institution of Civil Engineers - Civil Engineering, 170(3), 127–134. https://doi.org/10.1680/jcien.16.00039

Jones, J. F. C., & Pugh, C. R. 1998. *Electrokinetic, geosynthetic structure* (Patent No. DE69931662T2).

K., M. J., B., S. R., & Bolton, S. H. 1990. Kettleman Hills Waste Landfill Slope Failure. I: Liner- System Properties. Journal of Geotechnical Engineering, 116(4), 647–668. https://doi.org/10.1061/(ASCE)0733-9410(1990)116:4(647)

Koerner, R. M. 2005. *Designing with Geosynthetics, vol.1* (Fifth Edit).

Kraton Corporation. 2019. *KRATON FG1901 G Technical Data Sheet*.

Mallett, S. D., Matsumura, S., & David Frost, J. 2018. Additive manufacturing and computed tomography of bio-inspired anchorage systems. Géotechnique Letters, 8(3), 219–225. https://doi.org/10.1680/jgele.18.00090

Markou, I. N., & Evangelou, E. D. 2018. Shear Resistance Characteristics of Soil–Geomembrane Interfaces. International Journal of Geosynthetics and Ground Engineering, 4(4), 1–16. https://doi.org/10.1007/s40891-018-0146-6

Martinez, A., & Palumbo, S. 2018. Anisotropic Shear Behavior of Soil-Structure Interfaces: Bio-Inspiration from Snake Skin. In *IFCEE 2018* (pp. 94–104). https://doi.org/doi:10.1061/9780784481592.010

Mihaies, M., & Olaru, A. 2000. Mechanical Properties and Parameters of

Polyolefins. Handbook of Polyolefins, 267.

Miskin, M. Z., & Jaeger, H. M. 2013. Adapting granular materials through artificial evolution. Nature Materials, 12(4), 326–331. https://doi.org/10.1038/nmat3543

Palumbo, S. 2018. *Anisotropic interface shear behavior of granular soil and surfaces biologically-inspired by snakeskin*. University of California, Davis.

Plastics – the Facts 2019. 2019.

Punetha, P., Mohanty, P., & Samanta, M. 2017. Microstructural investigation on mechanical behavior of soil-geosynthetic interface in direct shear test. Geotextiles and Geomembranes, 45(3), 197–210. https://doi.org/10.1016/j.geotexmem.2017.02.001

Schirmeister, C. G., Hees, T., Licht, E. H., & Mülhaupt, R. 2019. 3D printing of high density polyethylene by fused filament fabrication. Additive Manufacturing, 28, 152–159. https://doi.org/https://doi.org/10.1016/j.addma.2019.05.003

Shelton, W. S., & Tyagi, M. J. 2017. *Geogrid made from a coextruded multilayered polymer* (Patent No. WO 2017/062632 AI).

Shukla, S. K. 2012. Fundamentals of geosynthetics. In *Handbook of Geosynthetic Engineering*. https://doi.org/doi:10.1680/hge.41752.001

Simsek, M. C. 2017. *Behavior of Geocell Reinforced Sandy Soils Under Static Load* (Issue December). Middle East Technical University.

Singh, K. 2018. Experimental study to prevent the warping of 3D models in fused deposition modeling. International Journal of Plastics Technology, 22(1), 177–184. https://doi.org/10.1007/s12588-018-9206-y

Spoerk, M., Holzer, C., & Gonzalez-Gutierrez, J. 2020. Material extrusion-based additive manufacturing of polypropylene: A review on how to improve dimensional inaccuracy and warpage. Journal of Applied Polymer Science, 137(12), 48545. https://doi.org/https://doi.org/10.1002/app.48545

Standard Test Methods for Specific Gravity of Soil Solids by Water Pycnometer. n.d.

Stathas, D., Wang, J. P., & Ling, H. I. 2017. Model geogrids and 3D printing. Geotextiles and Geomembranes, 45(6), 688–696. https://doi.org/10.1016/j.geotexmem.2017.07.006

Su, Y. F., Bhattacharya, S., Lee, S. J., Lee, C. H., & Shin, M. 2020. A new interpretation of three-dimensional particle geometry: M-A-V-L. Transportation Geotechnics, 23, 100328. https://doi.org/https://doi.org/10.1016/j.trgeo.2020.100328

Uesugi, M., & Kishida, H. 1986. Frictional Resistance at Yield between Dry Sand and Mild Steel. Soils and Foundations, 26(4), 139–149. https://doi.org/https://doi.org/10.3208/sandf1972.26.4_139

Uragan, S., & Huvaj, N. 2018. Properties and Potential Uses of 3D Printed Geosynthetics. Proceedings of the 17th National Soil Mechanics and Geotechnical Engineering Conferance.

Viswanadham, B. V. S., & König, D. 2004. Studies on scaling and instrumentation of a geogrid. Geotextiles and Geomembranes, 22(5), 307–328. https://doi.org/10.1016/S0266-1144(03)00045-1

Zabielska-Adamska, K. 2006. Shear strength parameters of compacted fly ash–HDPE geomembrane interfaces. Geotextiles and Geomembranes, 24(2), 91–102. https://doi.org/https://doi.org/10.1016/j.geotexmem.2005.11.006

Zettler, T. E., Frost, J. D., & DeJong, J. T. 2000. Shear-Induced Changes in Smooth HDPE Geomembrane Surface Topography. Geosynthetics International, 7(3), 243–267. https://doi.org/10.1680/gein.7.0174

APPENDICES

A. Vertical Displacement vs. Horizontal Displacement Plots of Direct Shear Tests

Smooth HDPE

	20kPa	100kPa	200kPa
Soil A - Loose	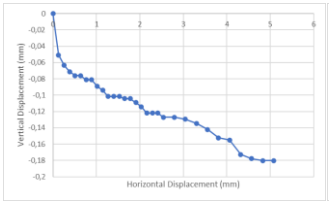	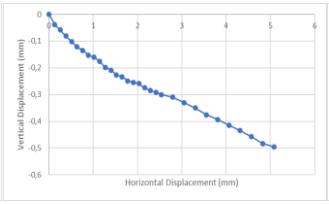	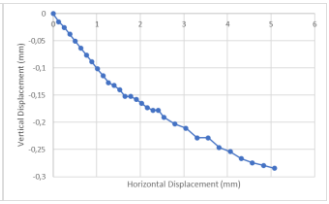
Soil A - Dense	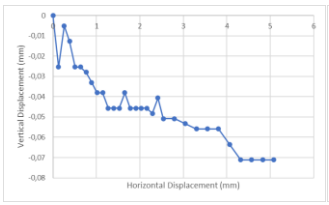	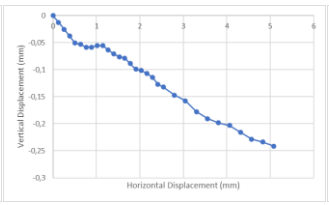	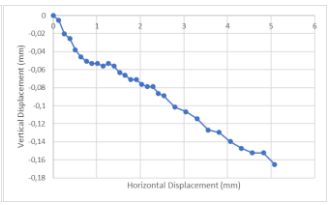
Soil B - Loose	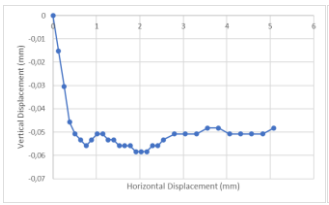	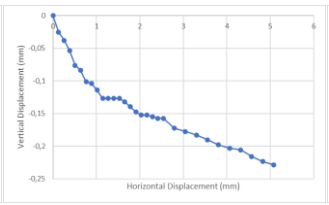	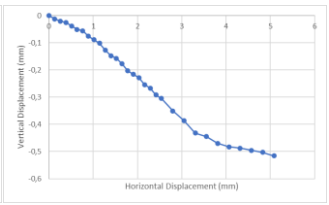
Soil B - Dense	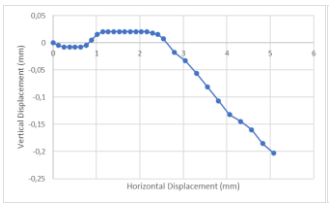	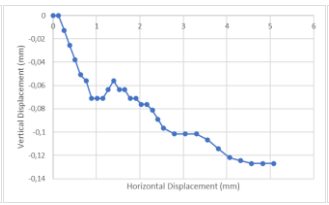	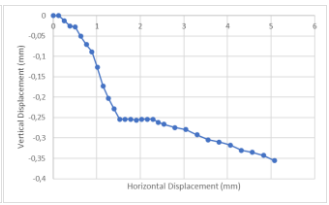
Soil C - Loose	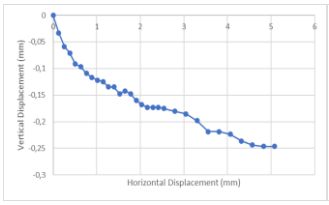	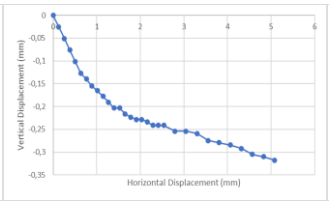	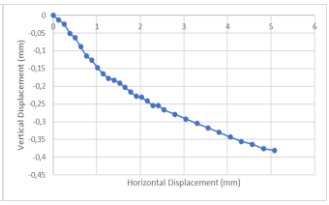
Soil C - Dense	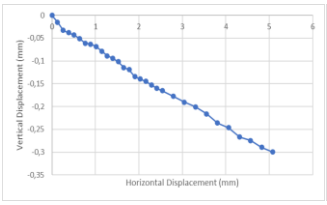	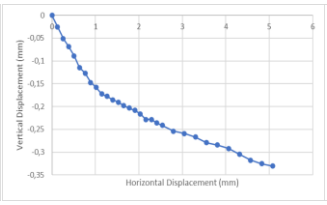	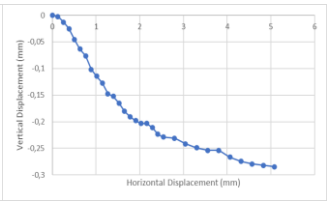

Smooth PP

	20kPa	100kPa	200kPa
Soil A - Loose	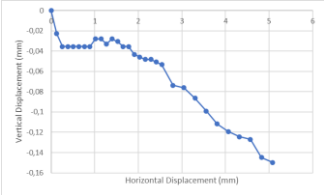	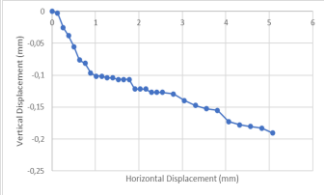	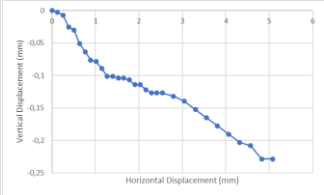
Soil A - Dense	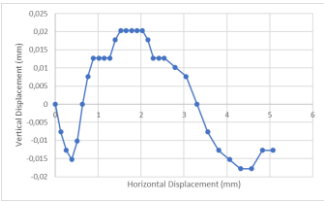	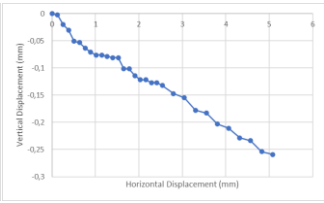	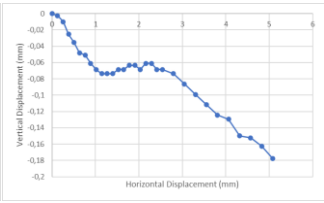
Soil B - Loose	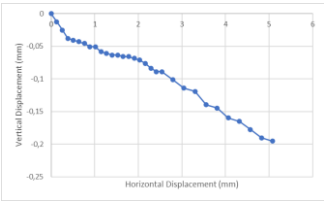	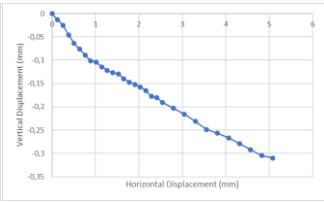	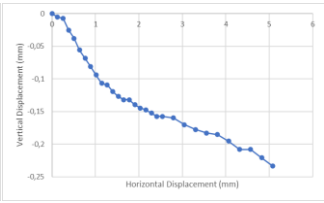
Soil B - Dense	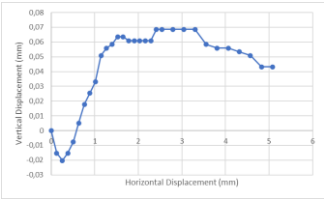	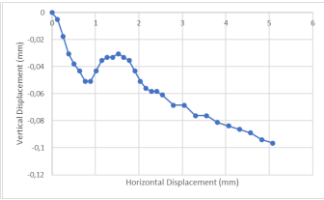	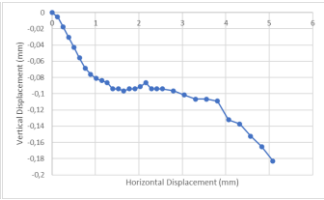
Soil C - Loose	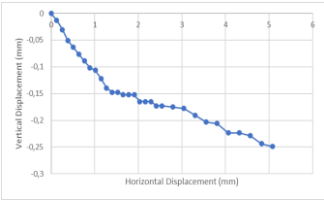	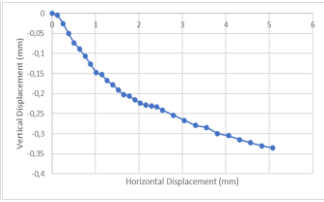	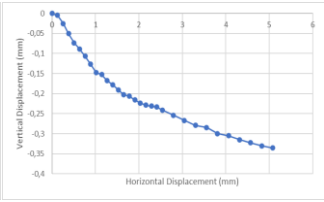
Soil C - Dense	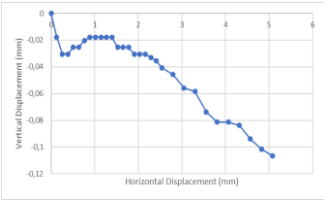	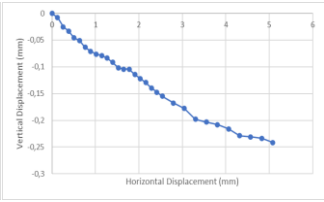	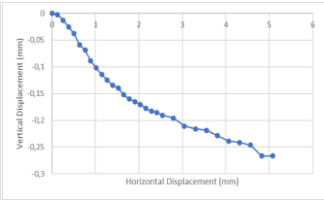

Asperity HDPE

	20kPa	100kPa	200kPa
Soil A - Loose	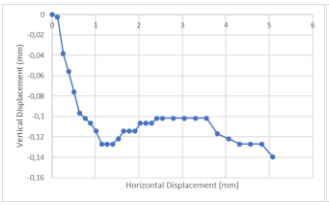	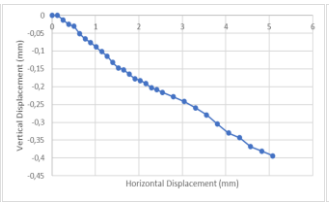	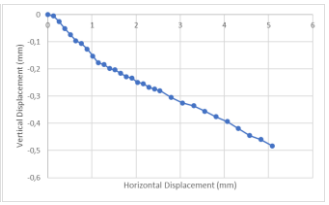
Soil A - Dense	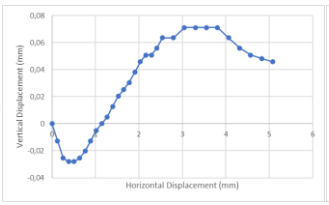	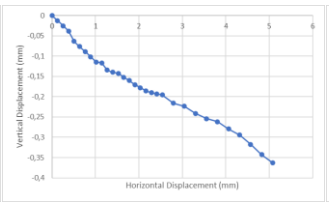	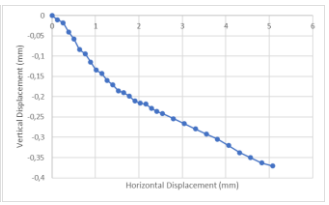
Soil B - Loose	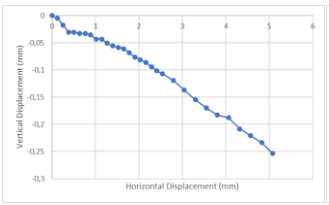	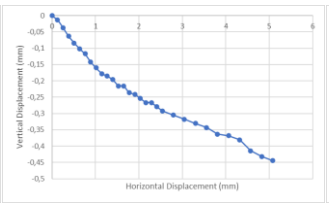	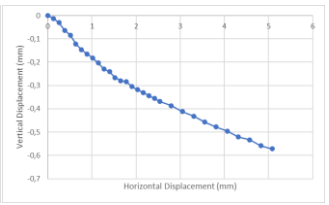
Soil B - Dense	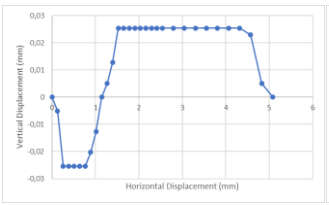	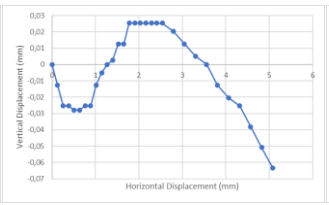	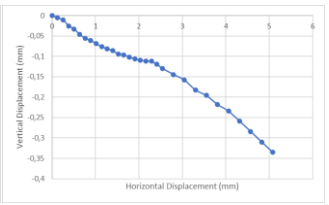
Soil C - Loose	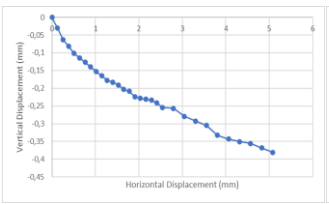	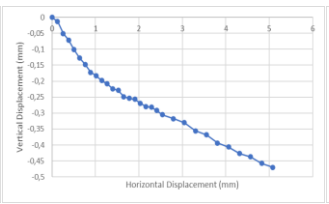	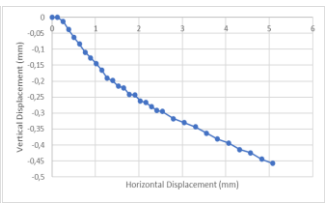
Soil C - Dense	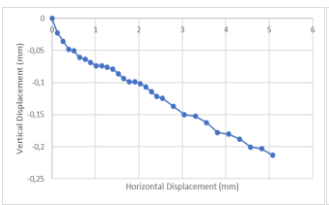	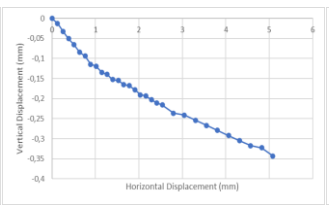	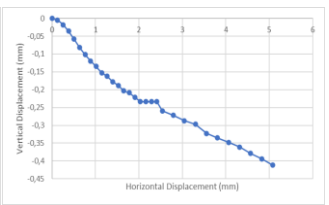

Asperity PP

	20kPa	100kPa	200kPa
Soil A - Loose	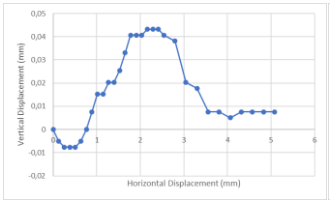	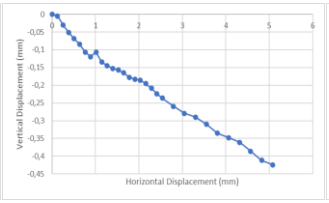	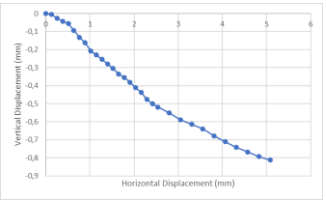
Soil A - Dense	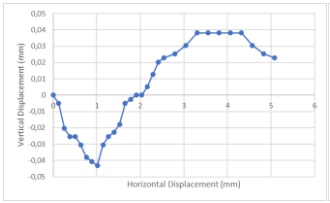	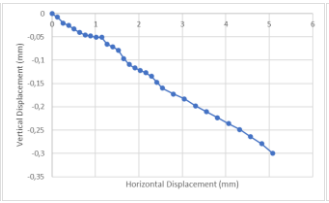	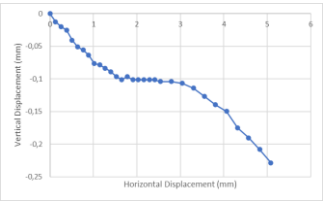
Soil B - Loose	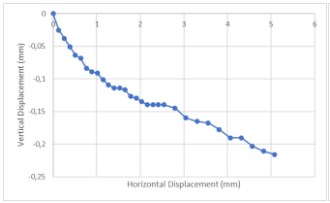	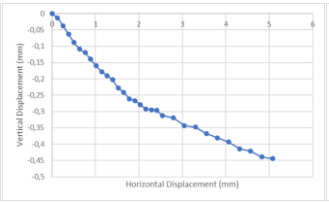	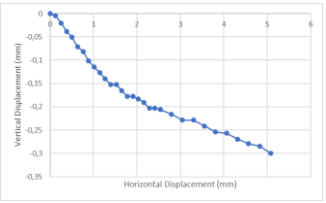
Soil B - Dense	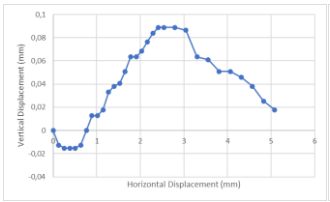	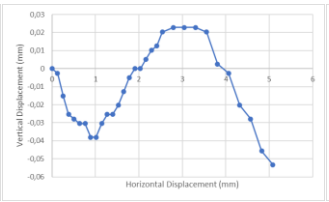	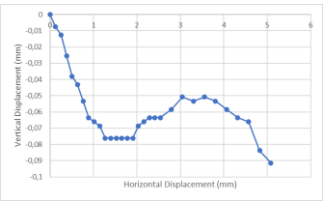
Soil C - Loose	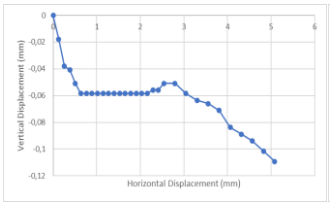	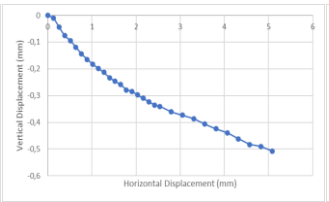	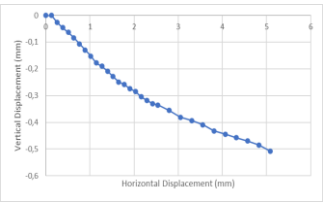
Soil C - Dense